

APPENDIX A : List of published articles

| no. / št. | Scientific article / Znanstveni članek | Journal / Revija | Dostop / Access |
|-----------|--|---|--|
| 1 | B. Fetai, J. Tekavec, M. K. Fras, and A. Lisec, "Inconsistencies in Cadastral Boundary Data – Digitisation and Maintenance," <i>Land</i> , vol. 11, no. 12, p. 2318, Dec. 2022, doi: 10.3390/land11122318 | <i>Land</i> | Licenca odprtega dostopa (Open Access) |
| 2 | B. Fetai, K. Oštir, M. Kosmatin Fras, and A. Lisec, "Extraction of Visible Boundaries for Cadastral Mapping Based on UAV Imagery," <i>Remote Sensing</i> , vol. 11, no. 13, p. 1510, Jun. 2019, doi: 10.3390/rs11131510. | <i>Remote sensing</i> | Licenca odprtega dostopa (Open Access) |
| 3 | B. Fetai, M. Račič, and A. Lisec, "Deep Learning for Detection of Visible Land Boundaries from UAV Imagery," <i>Remote Sensing</i> , vol. 13, no. 11, p. 2077, May 2021, doi: 10.3390/rs13112077. | <i>Remote sensing</i> | Licenca odprtega dostopa (Open Access) |
| 4 | B. Fetai, D. Grigillo, and A. Lisec, "Revising Cadastral Data on Land Boundaries Using Deep Learning in Image-Based Mapping," <i>ISPRS International Journal of Geo-Information</i> , vol. 11, no. 5, p. 298, May 2022, doi: 10.3390/ijgi11050298. | <i>ISPRS International Journal of Geo-Information</i> | Licenca odprtega dostopa (Open Access) |

APPENDIX B : Inconsistencies in cadastral boundary data – digitisation and maintenance

B. Fetai, J. Tekavec, M. K. Fras, and A. Liseč (2022)

Land vol. 11, no. 12, p. 2318

doi: 10.3390/land11122318

Article

Inconsistencies in Cadastral Boundary Data—Digitisation and Maintenance

Bujar Fetai , Jernej Tekavec , Mojca Kosmatin Fras  and Anka Lisec 

Faculty of Civil and Geodetic Engineering, University of Ljubljana, Jamova Cesta 2, 1000 Ljubljana, Slovenia

* Correspondence: bujar.fetai@fgg.uni-lj.si; Tel.: +386-1-4768629

Abstract: Most cadastral systems today are coordinate-based and contain only a weak or no reference to measurements or the origin of the information. In some contexts, this is largely due to the transition of land data management and maintenance from an analogue to a digital environment. This study focuses on analysing the importance of the measurement-based cadastre and the digitisation process in North Macedonia and Slovenia. The survey-based boundary data and their integration into the digital environment were not considered in either case study. The positional differences between the survey-based boundary coordinates and the graphical coordinates of the boundaries are significant. The RMSE(2D) for Trebosh was 48 cm, and the RMSE(2D) for Ivanjševci was 56 cm. Consequently, the differences in location affected the areas of the cadastral parcels, resulting in an RMSE of 26 m² and 23 m² for Trebosh and Ivanjševci, respectively. These differences can be considered as differences within the cadastral boundary data. Therefore, before harmonising the data between the cadastre and the land register, the inconsistencies within the cadastral data should be eliminated first. The differences in the location of cadastral boundaries and parcel area create new challenges in cadastral procedures (formatting of parcels), conflicts in the relocation of boundaries, and impacts on the land market. The solution lies in the way data is maintained, avoiding duplication of attributes or eliminating inconsistencies (after duplication). Both solutions require further modifications of the legal framework for cadastral procedures related to boundary adjustments and data compliance. This study provides a basis for evaluating inconsistencies in cadastral data and highlights the importance of proper source data selection in the digitization process.

Keywords: land; cadastre; cadastral map; surveying; measurement-based; cadastral triangular model



Citation: Fetai, B.; Tekavec, J.; Fras, M.K.; Lisec, A. Inconsistencies in Cadastral Boundary Data—Digitisation and Maintenance. *Land* **2023**, *11*, 2318. <https://doi.org/10.3390/land11122318>

Academic Editor: Hossein Azadi

Received: 7 October 2022

Accepted: 15 December 2022

Published: 17 December 2022

Publisher's Note: MDPI stays neutral with regard to jurisdictional claims in published maps and institutional affiliations.



Copyright: © 2022 by the authors. Licensee MDPI, Basel, Switzerland. This article is an open access article distributed under the terms and conditions of the Creative Commons Attribution (CC BY) license (<https://creativecommons.org/licenses/by/4.0/>).

1. Introduction

The land administration system (LAS) includes two main functions: the cadastre and land registration [1,2]. The cadastre is usually defined as a public inventory of surveyed land boundaries. Land registration defines the associated land rights and the parties involved [3,4]. In recent decades, much attention has been paid to the establishment of a LAS but not to its maintenance [5]. That is, once the relationship between people, rights, and the land was recorded, the procedures for capturing changes to these entities were poorly defined and ill-conceived [6]. Efforts to build LAS focused primarily on countries with low cadastral coverage [7]. However, not much attention was paid to maintaining the system and updating land data, for instance, in countries with complete cadastre [8].

Surveying and mapping techniques have been and are still used differently in different cases. For example, advanced and innovative techniques are being tested and applied mainly in developing countries with low cadastral coverage to establish a LAS [9,10]. These are generally indirect techniques, such as delineating visible land boundaries using remote sensing data, including satellite imagery, and, increasingly, imagery from unmanned aerial vehicles (UAVs) [11–14]. In developed contexts, when countries have full cadastral coverage and registered land rights, there are few case studies reporting on the ability of UAV-based cadastral mapping to update land data and meet accuracy requirements

compared to ground-based methods [15–20]. However, image-based cadastral mapping is not new in these countries. In the 20th century, particularly from 1930 onwards, aerial surveys and photogrammetric mapping methods were used to collect cadastral data in many countries [21,22].

In countries with a long tradition of the so-called parcel-oriented cadastre and a complete cadastre, conventional surveying (e.g., theodolites) and mapping techniques were used, which required high positional accuracy, and cadastral outputs were produced in analogue form. In these cases, the digitization process was initiated in the 1990s and at the beginning of the new century with the digitisation of existing analogue cadastral maps and the computerisation of land records [23]. The digitisation process was followed by the conversion and integration of cadastral data, change of the environment—for example, from computer-aided design (CAD) to geographic information systems (GIS), and harmonisation of cadastral data. Today's cadastral surveying is still ground-based but more advanced, including total stations and receivers of global navigation satellite systems.

The conversion of the cadastre from paper-based to digital data made it possible to better identify inconsistencies between the cadastral data and the land register [24,25]. These discrepancies usually concerned the common attributes of the cadastre and the land register, such as the parcel numbers (updated in the cadastral map but not in the land register, or vice versa) and the differences in the area (the area calculated from the cadastral map differs from the area in the land register document) [24,26]. After digitisation, a harmonisation process was initiated in many countries to eliminate inconsistencies [24]. This process is highly dependent on the cadastral data on boundaries, which was used as input to compare and identify inconsistencies in the land records.

Digitisation also led to a change from a measurement-based cadastre to a coordinate-based cadastre in some countries [27]. The processing of measurement data and the storage of the resulting coordinates corresponds to a coordinate-based cadastre. The measurement-based cadastre uses measurement data as a carrier of metric information [28]. To implement a digital measurement-based cadastre and manage survey data digitally, supporting tools and improving the design of the traditional environment GIS are required [29].

In most cases, the digital ownership layer was created by scanning and vectorising analogue cadastral maps. This raises the question of whether the digitization process was properly carried out in regions where measurement-based cadastral data from fieldwork existed alongside analogue cadastral maps. To get a clear idea of the complexity and quality of cadastral data [30], especially land boundaries, it is necessary to take into account the historical development of the country under consideration [31,32].

This study explores the challenges posed by the digitization process and the complexity of boundary definition in countries with traditional parcel-oriented cadastre. The objective is to identify the inconsistencies in cadastral boundary data, which are mainly caused by the way they are maintained, and to reconsider the process of digitisation. We used the cadastral triangulation model (CTM) [30] as a framework to present and clarify these challenges. It was also used to evaluate the cadastral boundaries and the digitising process. The CTM distinguishes three types of land boundaries, namely physical boundaries, documentary boundaries, and digital spatial boundaries, and which of these should be treated as cadastral or legal boundaries.

The paper is organised as follows: after a description of the research context (Section 1), an overview of the CTM and the selected case studies, including the dataset on land boundaries, and the methodological approach are described (Section 2). The results are then presented and discussed (Section 3). Finally, general statements are made about the CTM and variations, the revised digitization process, the importance of measurement-based data, and inconsistencies in land boundary data (Section 4).

2. Materials and Methods

2.1. Cadastral Triangular Model

The cadastral triangular model (CTM) was formulated and proposed by Grant et al. [33] and can be applied to analyse cadastral systems using cadastral data for land boundaries.

The model consists of four elements: physical boundary, documentary boundary, digital spatial boundary, and legal boundary. The last element is a conceptual element used to clarify and determine which of the previous three elements should be considered formal or cadastral when determining the boundary position in the field.

Physical boundaries are clues to the land boundary in the real physical world. Physical features may be natural features (e.g., land cover), including movable boundaries such as riverbanks, or man-made features such as walls and fences visible on remote sensing imagery. This group also includes boundary markers that may be visible on satellite or aerial imagery. The arrows pointing to the physical boundary (Figure 1) represent the use of information from the documentary records or the digital spatial boundary to either place boundary markers at boundary locations or record and locate existing physical features that represent boundaries (natural boundaries, fences, walls, markers).

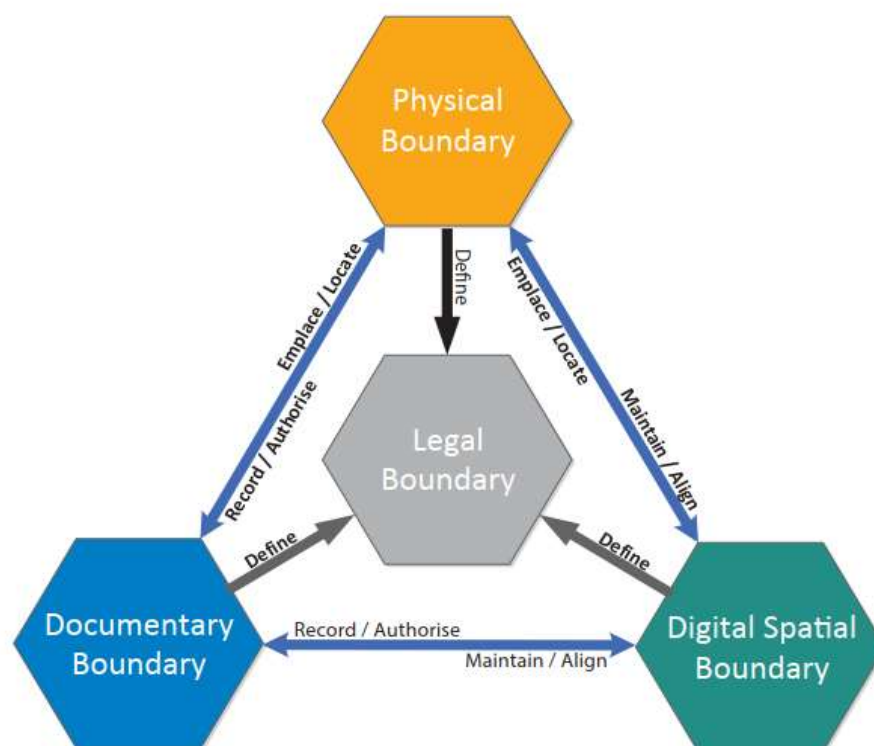


Figure 1. Cadastral Triangular Model (CTM) [33].

A documentary boundary is evidence of a recorded boundary based on documents that are legally backed up by a regulated procedure, such as an adjudication or a cadastral survey. This type of information includes survey measurements, e.g., measurements on boundary markers, offsets to other features, calculated boundary dimensions, etc. It also includes cadastral maps and plans showing the relationships between land boundaries, markers, and other features. The documentary boundary also includes survey plans, field notes, and other documents based on the cadastral survey. The arrows pointing to the documentary boundary (Figure 1) represent the recording and approval of field notes, calculation sheets, reports, and survey plans based on the measurement of boundary stones or other markers and physical features. Paper-based cadastral maps of boundaries are also classified as documentary boundaries.

A digital spatial boundary is a boundary that is stored in a digital spatial database. This database is usually initially created by scanning and georeferencing analogue cadastral maps. The points, lines, and polygons are defined as spatial objects that have coordinates with respect to an official coordinate reference system and the topological relationship between spatial objects is defined. Arrows pointing to the digital spatial boundary (Figure 1) represent the use of documented boundary information or information about the location of physical boundary features (coordinates) to maintain data on spatial objects in the database by adding changed or new boundaries (e.g., subdivisions) and to update and adjust the digital spatial database based on the surveying of physical boundaries using improved measurements.

2.2. Cadastral Boundary Data

Most designs of land administration GIS solutions are characterised by the fact that the position of land boundaries is represented by derived coordinates rather than by original measurements [29]. This approach has also affected the maintenance and management of cadastral data. Many cadastral systems today are coordinate-based and have various, sometimes only a weak reference to measurements or the origin of the information [34].

The LAS of North Macedonia and Slovenia were selected for this study. The selection is justified by the availability of similar cadastral data on land boundaries, which are based on measurements and coincide with the elements of the CTM. Specifically, the focus is on cadastral districts that have field books from land surveying in addition to analogue cadastral maps. In addition to data collection, literature research and interviews with key informants were also conducted.

2.2.1. Measurement-Based Data and Analogue Cadastral Maps

In North Macedonia, the main functions of the LAS are performed by the Agency for Real Estate Cadastre (AREC). In Slovenia, the same functions are performed by two public bodies. The Surveying and Mapping Authority of the Republic of Slovenia (SMA) is responsible for the cadastre, and land registration is carried out at the Supreme Court. Both countries have a complete cadastre, and the maintenance of the cadastre, such as cadastral surveying and the determination of cadastral boundaries, is carried out by private surveying offices [24,35]. In North Macedonia, the Real Estate Cadastre is the public register of registered real estate boundaries (land plots, buildings, parts of buildings), real estate rights and parties involved. The Real Estate Cadastre was created mainly through three types of registrations: systematic, sporadic and conversion [36]. In the latter, the measurement-based cadastral data of boundaries were converted from Land cadastre into Real Estate cadastre through a digitisation process [24]. The Slovenian LAS is very similar. The Slovenian Real Estate Cadastre, introduced in 2022 by merging the former land cadastre and building cadastre [35], includes data on land boundaries, buildings, and parts of buildings. The data on building parts forms the basis for the registration of strata titles in the land registry.

In North Macedonia, the measurement-based cadastral survey (field book known as tacheometric survey) was conducted from 1928–1945. It covered some towns and their surroundings (see Figure 2a, in light grey). The cadastral survey was carried out using the surveying technologies of the time, such as theodolites. During this period, 549 cadastral districts were surveyed. The total surveyed area was about 7000 km², which is almost 30% of the total territory. For the rest of the territory, around 70% of cadastral maps were produced using airborne methods (Figure 2a, in white). From 1950 to 1990, analogue stereo plotters were used to produce analogue cadastral maps. From 1998 to 2005, cadastral maps were produced directly in digital format using stereo instruments SD2000 and SD3000 [36].

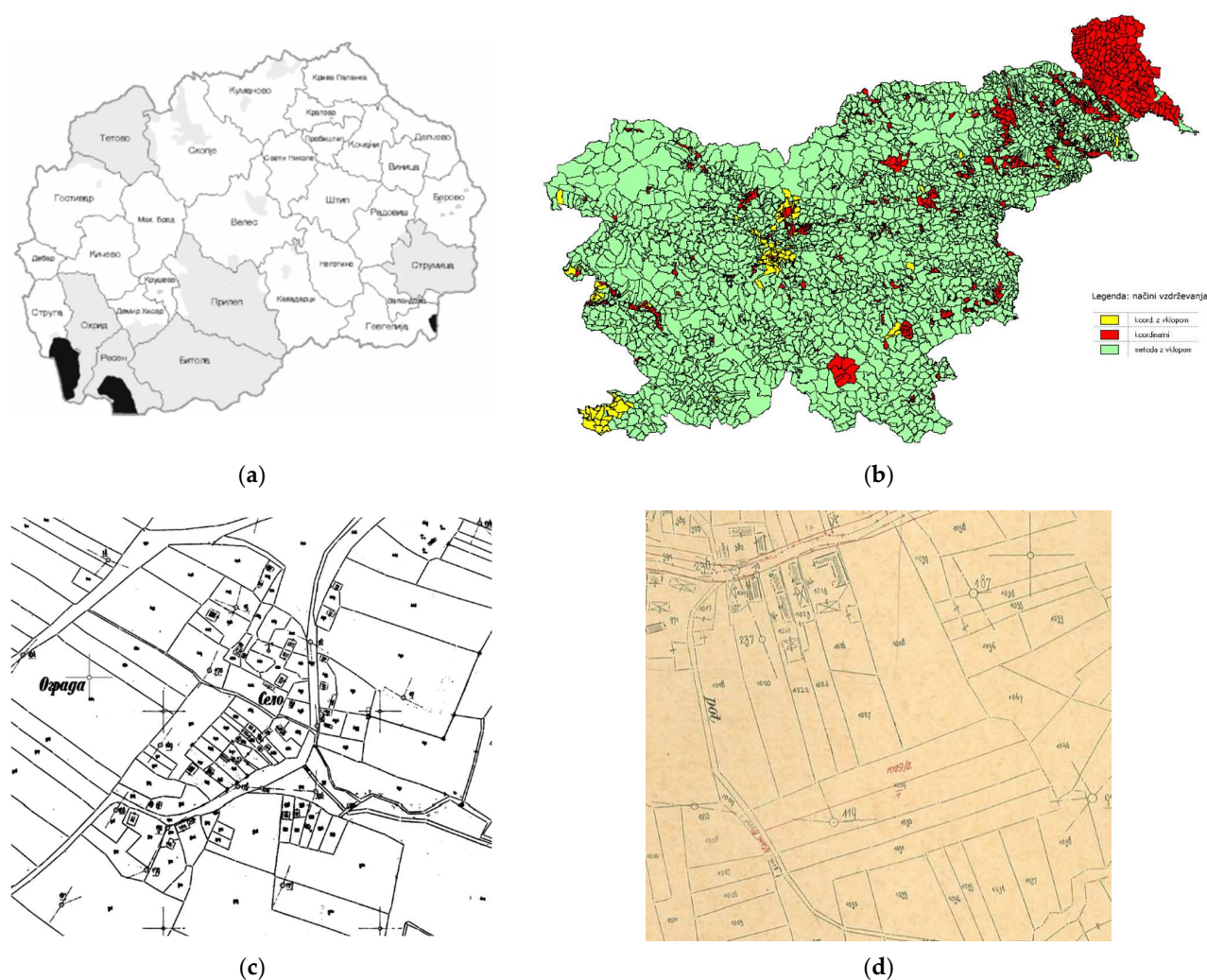


Figure 2. Regions with measurement-based cadastral survey including surveying field books; (a) Cadastral survey in North Macedonia in the period 1928–1945 (grey) [36]. (b) Cadastral survey in Slovenia in the period 1945–1974 and in the period 1975–2005 (red and yellow) [37]; (c) Example of archived/initial cadastral map at 1:2500 scale; (d) Example of working cadastral map at 1:2500 scale.

As far as their origin is concerned, cadastres were established on the territory of present-day Slovenia in the period between the middle of the 18th and 19th centuries. The Theresian cadastre was characterised mainly by the fact that land was not surveyed but only inventoried and assessed in terms of its yield on the basis of the estimated area, soil quality and type of crops. The Josephinian cadastre from the end of the 18th century was characterised mainly by the fact that the land was surveyed using the prescribed surveying instruments (wooden surveying stick, surveying chain, wooden pegs, and wooden posts), but the cadastral maps were not prepared for all inventoried areas. An important role in the introduction of a more stable cadastre was played by the patent of Emperor Franz Joseph I in 1817. Surveying with surveying instruments (surveying table, diometer with ruler, plumb bob, stake-out flags, and target marks) was carried out by trained surveyors, but the maps were drawn directly in the field, and there were only limited numerical data archived in the cadastre—the so-called graphic cadastre. The use of surveying tables was abolished in the 1920s, while the modern polar and orthogonal surveying methods with the required field books had already been introduced at the end of the 20th century [38].

Cadastral surveying of wider areas, e.g., of the whole cadastral district or part of it, based on field books (tacheometry) was carried out partly already before 1945, but more

massively in the period 1945–1974, when the new coordinate system D48/GK was introduced [39]. Systematic cadastral surveying and maintenance of cadastral data continued on the basis of the legislation from 1974 until 2000; however, with the new legislation in 2000, systematic land surveying of larger areas was no longer supported by the state; there have been only a few projects in the last two decades, except for land consolidation, which has also contributed to higher coverage of quality cadastral data. Consequently, the land cover with the so-called numerical cadastre is still very limited in Slovenia [37,40]. Systematic land surveying was conducted in urban areas and the north-eastern part of the country covering approximately 12% of the territory (Figure 2b, red and yellow) [37]. This was and still is reflected in the method of updating cadastral maps, i.e., in the areas with the new cadastral land survey, the measurement-based method is used for updating maps while in the areas of the old graphic cadastre concerning its origin maps are updated using some geometric and positional adjustments [39].

In North Macedonia and Slovenia, the map of the first cadastral survey is called the “archived map” (Figure 2c). Boundary updates for all cadastral-related events (e.g., subdivisions, land consolidation) were drawn on a cadastral map called a “working map” (Figure 2d), which was a copy of the archived cadastral map. Cadastral boundaries were mapped mostly at a scale of 1:2500. In urban areas, scales of 1:500 and 1:1000 have also been used, while the land boundaries in mountainous areas were mapped at a scale of 1:5000.

In both cases, all cadastral maps were accompanied by field books detailing the measurements of each cadastral boundary point (Figure 3). In addition, special geodetic reference networks were designed for the surveyed parts, using the network points as station/orientation points from which the survey (direction, distance) of each boundary point was made. These networks are very dense and accurate as they are connected to the national trigonometric network. The network points are often situated underground (30–40 cm deep) and are still available nowadays. If a control point is damaged or lost, the next control points are located at a distance of about 150–200 m (Figure 2c,d).

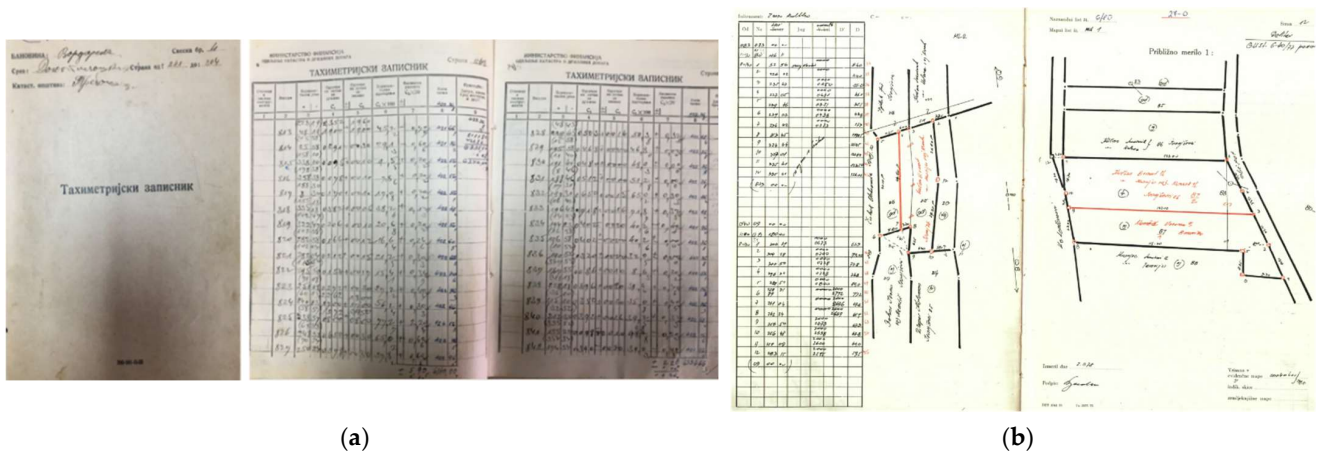


Figure 3. (a,b) Surveying field books; (a) Surveying field book from initial cadastral survey—North Macedonia; (b) Surveying field books in process of cadastral maintenance—Slovenia.

Field books represent a measurement-based cadastral survey, and the derived data on land boundaries based on CTM can be categorised as documentary boundaries.

2.2.2. Digital Cadastral Data—Process of Digitisation

In countries with complete cadastral coverage, the most common method of creating digital cadastral maps, i.e., the land boundary data layer, is to scan and vectorise boundaries from analogue cadastral maps. This was selected in North Macedonia and Slovenia as a suitable method for extracting boundary features in vector format. However, the cadastral measurements from the field books were not considered in the digital conversion,

although the analogue cadastral maps were derived from the measurements archived in the field books.

The digitisation of analogue cadastral maps was essentially done in a three-steps process: (1) analogue cadastral maps were scanned, (2) georeferenced, and (3) vectorised (Figure 4). This approach introduced additional geometric errors in each of these three steps. In addition, there is a mapping error due to the map scale. The field books, on the other hand, may only contain errors from surveying.

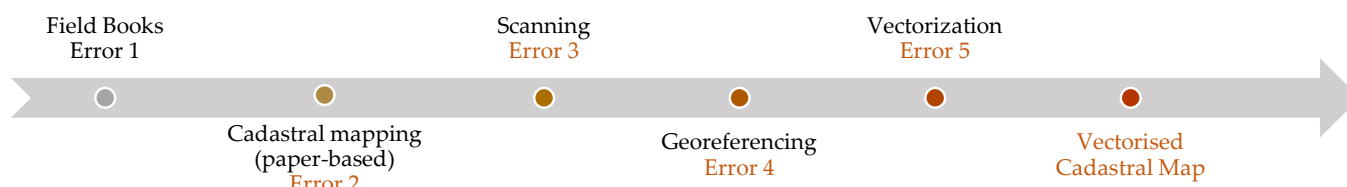


Figure 4. Digitisation of analogue cadastral maps in North Macedonia and Slovenia. Field books with measurement data were not considered in this process.

This approach resulted in all cadastral features being in vector format and initially maintained in the file system. Later they were converted to coordinate-based GIS platforms and stored in cadastral spatial databases. Field books containing surveying measurements were not integrated into such a GIS platform, nor was the coordinate-based GIS established by calculating coordinates from surveying measurements.

In addition, the separate maintenance of two databases, the cadastral spatial database and the land registry database, resulted in numerous inconsistencies between the two databases, such as a cadastral parcel being updated (divided) in the administrative part but not in the graphical part, mismatch on numeration of cadastral parcels, inconsistencies in the data on cadastral parcel area (one data on parcel area in the land title certificate, another data on parcel area in the graphical part) etc. [24,25]. These inconsistencies were one more reason to start harmonising process between the two databases. The harmonisation was based on vectorised land boundaries in both cases.

Vectorised cadastral boundaries are categorised as digital spatial boundaries according to the CTM.

2.3. Study Areas—Inconsistencies in Cadastral Boundary Data

Two cadastral districts (municipalities), one from North Macedonia and one from Slovenia, were selected to identify the inconsistencies in the boundary data and to revise the digitisation process. The cadastral districts of Trebosh and Ivanjševci were selected for North Macedonia and Slovenia, respectively (Figure 5). Trebosh is located in the north-western part of North Macedonia and has an area of 446 hectares. Ivanjševci is located in the north-eastern part of Slovenia and has an area of 235 hectares.

The data collection included cadastral survey measurement data such as tacheometric reports, official georeferenced cadastral maps (used in the vectorisation process), vectorised cadastral boundaries, and official coordinates of the geodetic network from which the points of the boundaries were surveyed (Figure 5). Data were collected from local cadastral offices and e-portals of both countries [41,42].

A comparative method was used to analyse the digitisation and location differences between the two data layers (measurement-based and vectorised data). First, the coordinates of the boundary points were calculated from the field books/tacheometric reports. Second, the parcel boundaries were plotted considering the calculated coordinates from the tacheometry, which are in the formal state coordinate system. Then, the cadastral boundaries constructed from the tacheometric reports were compared with the vectorised land boundaries.

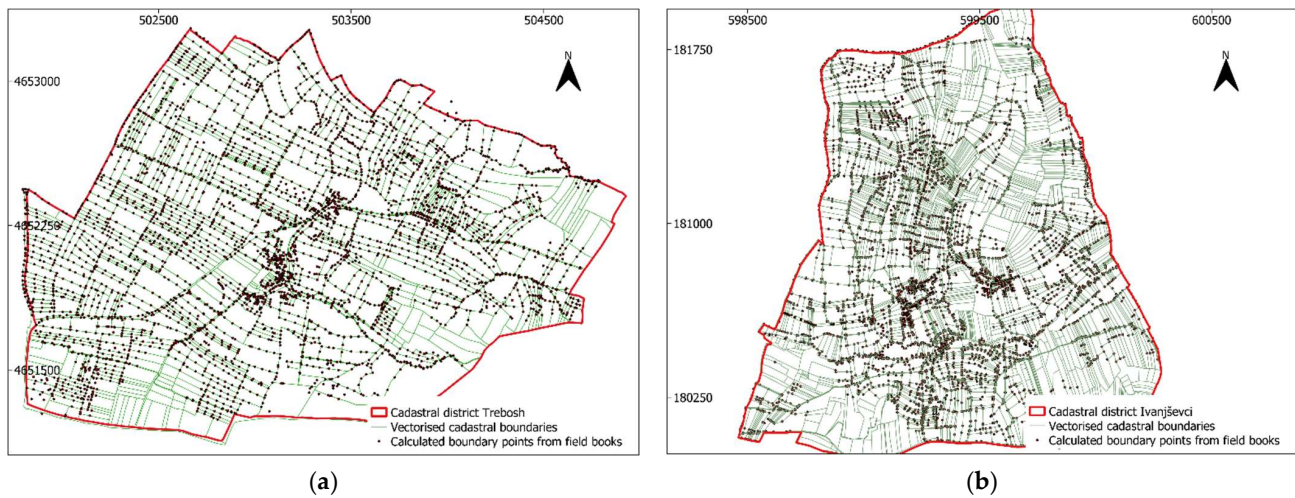


Figure 5. Calculated coordinates of land boundary points from field books overlaid on vectorised land boundaries; (a) Cadastral district of Trebosh, North Macedonia; (b) Cadastral district Ivanjševci, Slovenia.

Positioning accuracy was assessed as root mean square error (RMSE). The value of RMSE is usually calculated using a series of control measurements (coordinate values from an independent source with higher accuracy for identical points). In this study, the boundary coordinates obtained from the field book data were considered as ground truth, while the coordinates obtained from the vectorised boundaries were considered as measured values. In addition to calculating the differences in east and north directions, another distance-based analysis was performed. Moreover, after the parcel boundaries were constructed based on field books, the area differences between the parcels between the two layers were assessed.

3. Results and Discussions

3.1. Cadastral Boundary Data in Pre-Digitisation Phase

The focus of this study has been on cadastral districts with measurement-based data on land boundaries along with analogue cadastral maps, i.e., the cadastral districts where ground-based cadastral surveying was conducted in the past century. Observation of the selected case studies, namely the cadastral districts of Trebosh and Ivanjševci, showed that the situation in the pre-digitisation period was clearer in terms of legal or cadastral boundaries. For example, during the adjudication (static model), survey-based data on physical boundaries were recorded and stored in field books. Analogue cadastral maps were created from the cadastral measurements to allow for more efficient data management and keep the geometric and positional accuracy derived from the quality of surveying. The field books, together with the analogue cadastral maps, formed the documentary boundary that also defined the legal/cadastral boundary (Figure 6a).

While the cadastre was maintained, survey data on new land boundaries continued to be recorded in the field books and changes were mapped on paper-based cadastral maps. In the event of boundary disputes or missing boundary markers, data from the field books were used to locate the physical boundary on site.

Discrepancies between the physical boundaries and the documentary boundaries occurred when the documentary boundaries were incorrect or outdated (Figure 6b). The errors may have occurred during the cadastral survey, resulting in discrepancies in the location of the boundary. The outdatedness was usually caused by man-made informal changes of boundaries in the field or by natural changes such as riverbanks, and the time factor of these types of obsolescence gave some precedence to the physical boundaries so that in the case of disputes or other land-related legal events, they were considered legitimate because they had been in use for so long.

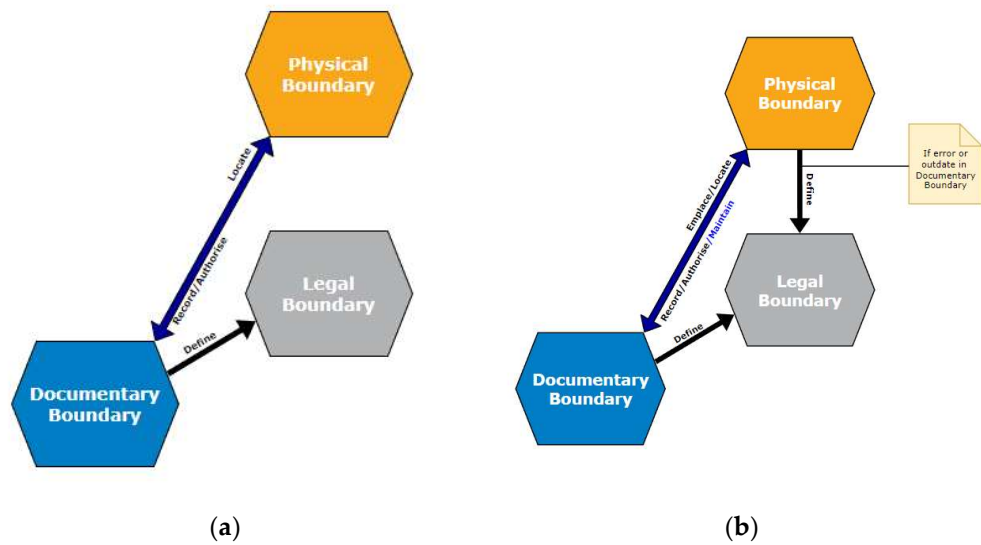


Figure 6. Evaluation of land boundaries and inconsistencies based on cadastral triangular model (CTM); (a) CTM for static model in pre-digitisation period; (b) CTM for dynamic model/maintenance in pre-digitisation period.

3.2. Digitising Cadastral Boundary Data—Revised

In both cases, i.e., North Macedonia and Slovenia, analogue cadastral maps were used as the main input for the digitisation process. The georeferenced maps were vectorised, but the measurement data were not taken into account. On the contrary, the coordinates of the boundary points were to be calculated from the field books to avoid errors caused additionally by the scanning, georeferencing and vectorisation of the analogue cadastral maps. The scanned and georeferenced cadastral maps (in raster format) served as a background and were used as a guide to linking the calculated coordinates of the boundary points more efficiently. The digitisation process carried out in practice is shown in Figure 7a. The revised digitisation approach based on the CTM is shown in Figure 7b, and the workflow is reproduced in Figure 8.

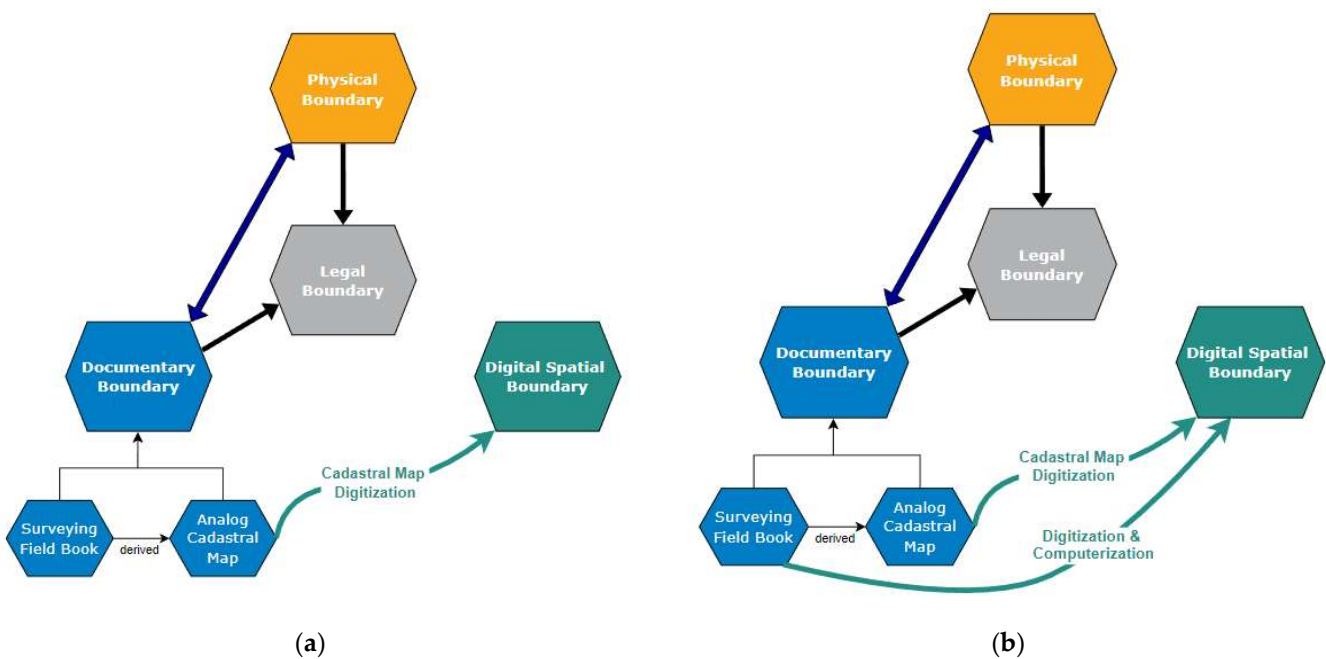


Figure 7. (a) The process of digitisation conducted in North Macedonia and Slovenia based on CTM; (b) Revised process of digitisation based on CTM by considering surveying field books.

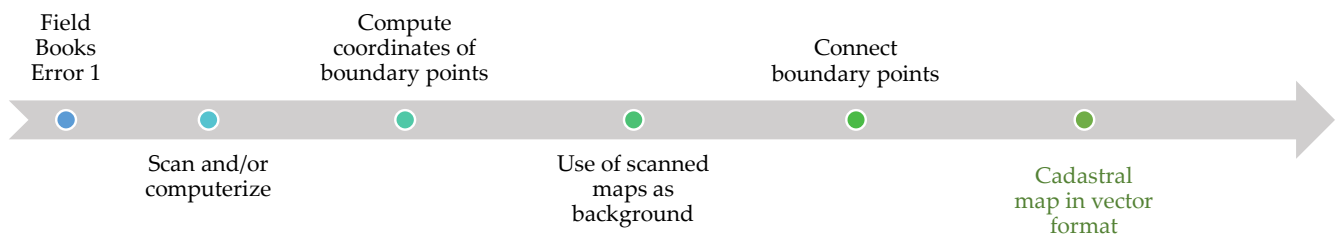


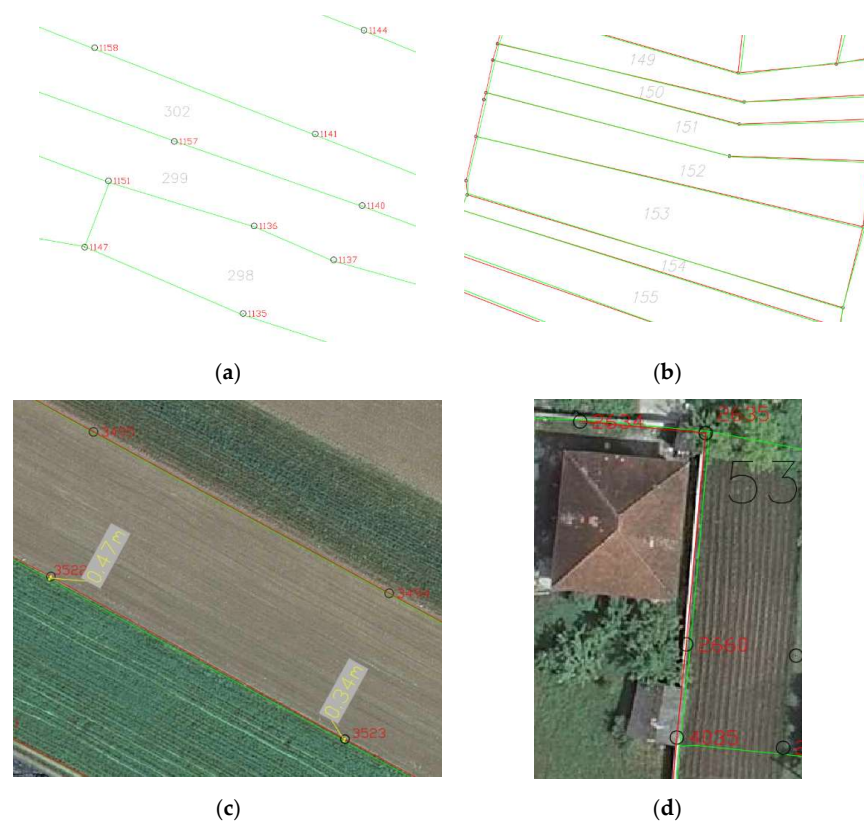
Figure 8. Workflow steps of revised digitisation process by respecting the importance of surveying field books.

The revised digitisation workflow still contains systematic errors from the cadastral surveying. In addition, errors can occur due to the computerisation of numerical surveying data or calculations. However, human errors can be easily detected and corrected in most cases. In contrast, the errors that occurred during the vectorisation of analogue cadastral maps cannot be simply traced or avoided (Figure 4).

3.3. Identification of Inconsistencies in Cadastral Boundary Data

The proposed digitisation approach can be applied to both coordinate-based GIS and measurement-based GIS if it supports the storage and visualisation of scanned and/or computerised field books. In this study, a coordinate-based approach was used as the aim was to identify inconsistencies between the two layers of land boundaries.

Once the boundary points were imported and compared to the vectorised boundaries, inconsistencies in the position of the boundary points were also detectable by visual interpretation. Some examples of such inconsistencies are shown in Figure 9.



In addition to the visual analysis, an additional statistical analysis was performed. The differences in easting and northing of parcel boundary points are shown in Figure 10a,b.

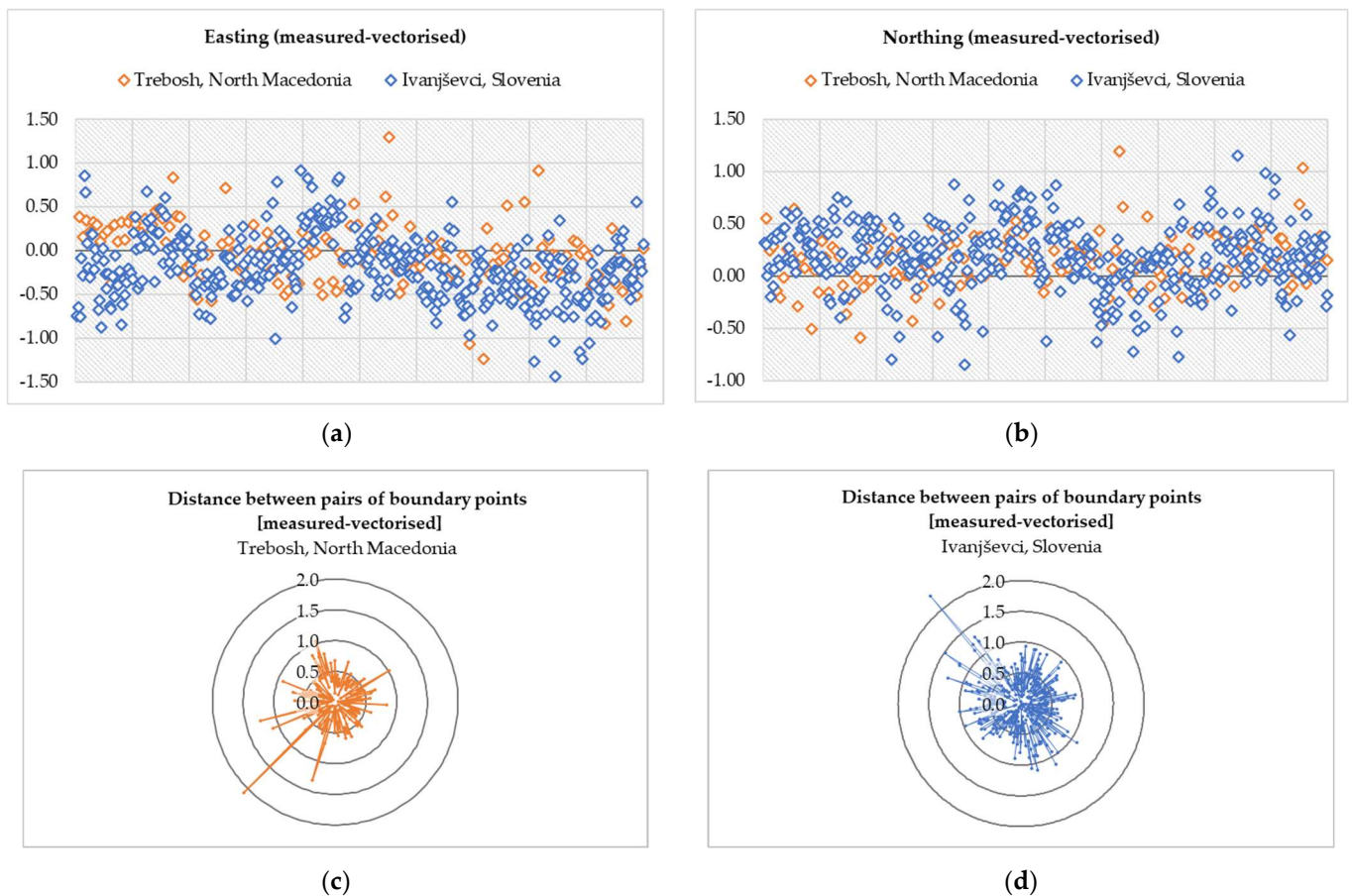


Figure 10. (a,b) Coordinate differences (easting and northing) for boundary points in cadastral district Trebosh, North Macedonia, and (c,d) distance—based analysis between pairs of boundary points calculated from measurements and obtained from vectorisation.

Positional analysis was performed by calculating the RMSE and distances between identical boundary points from two spatial data layers (Figure 10c,d). The boundary points from the two layers had the same IDs, and a list of coordinate pairs was created to conduct the analysis. The differences in the boundary positions are listed in Table 1. Furthermore, an area-based analysis was performed by calculating the RMSE, and the minimum, mean, and maximum area differences. The area differences are shown in Table 2.

The results showed similar differences between the measurement-based and vectorised coordinates of the selected case studies. The horizontal RMSE was 0.48 m and 0.56 m for Trebosh and Ivanjševci, respectively. The distance-based differences yielded a mean of 0.40 m for Trebosh and 0.49 m for Ivanjševci. However, in some cases, the distance between the measurement-based coordinates and the vectorised coordinates resulted in a difference of more than 2 m (Table 1).

These types of differences in boundary data can be categorised as discrepancies between the measurement-based (or documentary) boundaries and the digital spatial boundaries. Simply put, discrepancies within cadastral data about boundaries. The selection of cadastral data for determining or staking land boundaries in the field should be considered critical. This has primarily to do with the certainty and confidence that the surveyor has in the cadastral data. In addition to the computable coordinates, the survey data provide additional spatial or metric information to locate the position of the boundary in the field, which brings confidence when staking boundary points [28,34].

Table 1. Positional accuracy of boundary points—documentary boundaries compared to digital spatial boundaries.

| Cadastral District | RMSE (x) | RMSE (y) | RMSE (2D) | min Δ (D) | mean Δ (D) | max Δ (D) |
|--------------------------|----------|----------|-----------|------------------|-------------------|------------------|
| Trebosh, North Macedonia | 0.38 m | 0.29 m | 0.48 m | 0.05 m | 0.40 m | 2.10 m |
| Ivanjševci, Slovenia | 0.43 m | 0.36 m | 0.56 m | 0.01 m | 0.49 m | 2.29 m |

Δ difference.

Table 2. Differences of land parcel areas—documentary boundaries compared to digital spatial boundaries.

| Cadastral District | RMSE (Area) | min Δ (Area) | mean Δ (Area) | max Δ (Area) | Average Parcel (Area) |
|--------------------------|---------------------|---------------------|----------------------|---------------------|-----------------------|
| Trebosh, North Macedonia | 25.9 m ² | 1 m ² | 18.7 m ² | 81.1 m ² | 2955.8 m ² |
| Ivanjševci, Slovenia | 22.8 m ² | 1 m ² | 17.4 m ² | 77.4 m ² | 1252.4 m ² |

Δ difference.

Having only the coordinates of boundary points does not seem to be sufficient to locate the boundary in the field with certainty since there is no additional information or metric relationships to other spatial objects or geodetic points. The main advantage of a measurement-based system over a coordinate-based system is the ease of updating and improving accuracy over time due to the existence and value of measurements that are independent of other measurements [28,29,34]. For this reason, documentary boundaries are preferable for determining cadastral boundaries or relocating boundary points [33].

Consequently, the differences in boundary lines resulted in differences in the area of the plots. The area differences resulted in an RMSE of 26 m² for Trebosh and an RMSE of 23 m² for Ivanjševci, corresponding to average plot sizes of 2956 m² and 1252 m², respectively. However, the differences in area are not directly related to plot size. They are mainly related to the mapping scale, the shape of the plot, and the mapping skills of the operator. Sometimes the differences were larger for smaller plots; for example, a difference of 23 m² was registered for a plot of 933 m² and 8 m² for a plot of 2788 m². The mean area difference for Trebosh was 19 m², and for Ivanjševci, 17 m² (Table 2).

The area is one of the most important units in the cadastre and especially in the land market [1,43]. Usually, prices for land are set per square meter. Thus, the question of which data should be considered relevant in the digitization process, namely the documentary or the vectorised, affects the cadastral procedures and the legal documents. It also affects the harmonization process between the attributes of the cadastre and the land registration.

For example, in the case of North Macedonia, the area is one of the attributes indicated in the land registration. In the harmonization of attributes between the cadastre and the land registry, vectorised cadastral boundaries were considered relevant, which resulted in a change of the areas in the land title certificates [24]. In addition, many cadastral boundaries were determined using documentary data on boundaries (prior to digitization), and these differences, in post digitizing phase, pose an additional challenge when formatting parcels, e.g., in subdivision procedures, i.e., half of the parcel from documentary data does not correspond to half of the vectorised parcel.

In Slovenia, the situation is different; the area is part of the cadastre and is not shown in the land title certificate. Therefore, during land formatting or harmonization, no additional changes need to be made in the land register or the land title certificates related to this area. Moreover, it offers the possibility of using both documentary and digital spatial boundaries (even if created by vectorising) as a sporadic process. The emplacement of land boundaries continues to be done with documentary boundaries case by case, where alignments are applied to digital spatial boundaries without complication regarding the changes in the area of land parcels.

As a rule, there are inconsistencies between cadastral and land registry data [24,25], mainly due to unclear definitions of attributes or duplication of attributes. Cadastral data, together with attributes generated from geometry, should be part of the cadastre and not

duplicated in the land registry [3]. For this reason, many harmonization processes have been performed to eliminate such inconsistencies. The harmonization process requires data in digital format, namely vector format. However, before harmonisation, or more precisely during digitization, the inconsistencies between the cadastral data themselves should be systematically avoided.

3.4. Cadastral Boundary Data in Post-Digitisation Period

The digitisation approach has also affected the maintenance of cadastral data on land boundaries. In land surveying practice, determining the location of the parcel boundary and recording the land boundary data involves on-site measurements. Digitisation has led to changes in surveying technologies and methods, and it seems that the conventional approach to surveying is no longer a precondition for practising surveying, especially in the land administration domain.

In the case of North Macedonia, after establishing digital data the emplacement of boundary marks is done using digital spatial boundary coordinates. This approach is generally less common, considering that other evidence, such as documentary boundary, is available and more reliable. Prior to digitisation in areas where measurement-based cadastre was established, all cadastral procedures, including the emplacement of boundary points or to locate existing physical features that represent boundaries, were done using the field book data, i.e., through documentary boundary (Figure 11). Thus, once digital spatial boundaries were available, documentary boundaries are no longer used and maintained (Figure 12a).



Figure 11. Example of differences in the location of boundary points: (red) calculated coordinates from the survey data; (green) coordinates from the vectorised cadastral map.

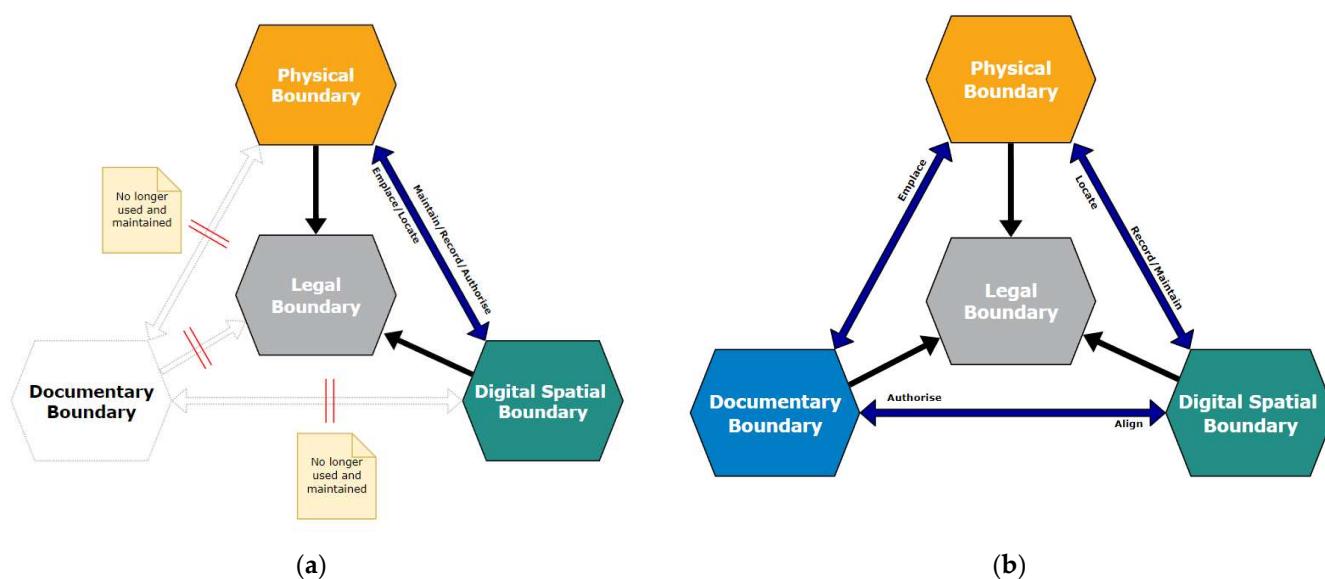


Figure 12. Evaluation of land boundaries and inconsistencies based on cadastral triangular model (CTM) in the post-digitisation phase; (a) CTM for North Macedonia in the pre-digitisation period; (b) CTM for Slovenia in the post-digitisation period.

The Slovenian approach to post-digitisation is far too different. Although digital spatial boundaries have been created from analogue cadastral maps, even in the areas with high-quality survey data in field books, the emplacement of boundaries in the field still relies on documentary boundary records. In this case, the surveyor must refer to the records of documentary evidence and calculate the coordinates of the boundary points from the measurements. This approach is used only sporadically and on a case-by-case basis. Once the documentary boundary is determined onsite, the necessary alignments are made to the digital spatial boundary.

In the case of a new boundary, e.g., subdivision, the physical features representing the boundary are surveyed and considered as documentary as well as digital spatial boundaries. The newly surveyed boundaries, namely documentary boundaries, are stored in digital format in the form of surveying reports. In addition, these new records are used to reallocate the boundary in place if needed.

In both cases, North Macedonia and Slovenia, the new boundaries are surveyed using ground-based techniques, including total stations and GNSS receivers. The application of indirect-mapping techniques falls outside the scope of cadastral surveying and is usually used for other surveying purposes.

3.5. CTM for Indirect-Mapping Techniques—Fit for Purpose

The current CTM, as proposed by Grant et al. [33], may be considered more appropriate for developed countries that have a long cadastral history and where ground-based surveying techniques were used, with the original cadastral output being on paper. This is primarily because digital spatial boundaries were created by digitising documentary boundaries in analogue format (Figure 7a).

For developing countries adopting a digital cadastre, this approach should be revised since no digitization process is required. Today, survey data and cadastral maps are directly available in digital format, and documentary boundaries may also be digital. However, the content of documentary boundaries is strongly dependent on surveying and mapping techniques that are applied and used.

For example, the Fit-for-purpose initiative [7] suggests using indirect mapping techniques instead of ground-based ones. In this sense, UAV-based cadastral mapping is increasingly being used to implement cadastres in countries with little or no cadastral coverage. In indirect mapping techniques, the documentary boundaries for land parcels

may be in the form of photo sketches with additional survey data or reports, such as line dimensions of the land parcel or other objects visible in the image, sensor characteristics, flight parameters, image accuracy, ground sampling distance, etc. However, the need for documentary boundaries depends on the purpose of the application and the required positional accuracy. Namely, Fit-for-purpose can be only introduced digital spatial boundaries by delineating land boundaries from remote sensing imagery, while digital documentary boundaries can be optional (Figure 13a).

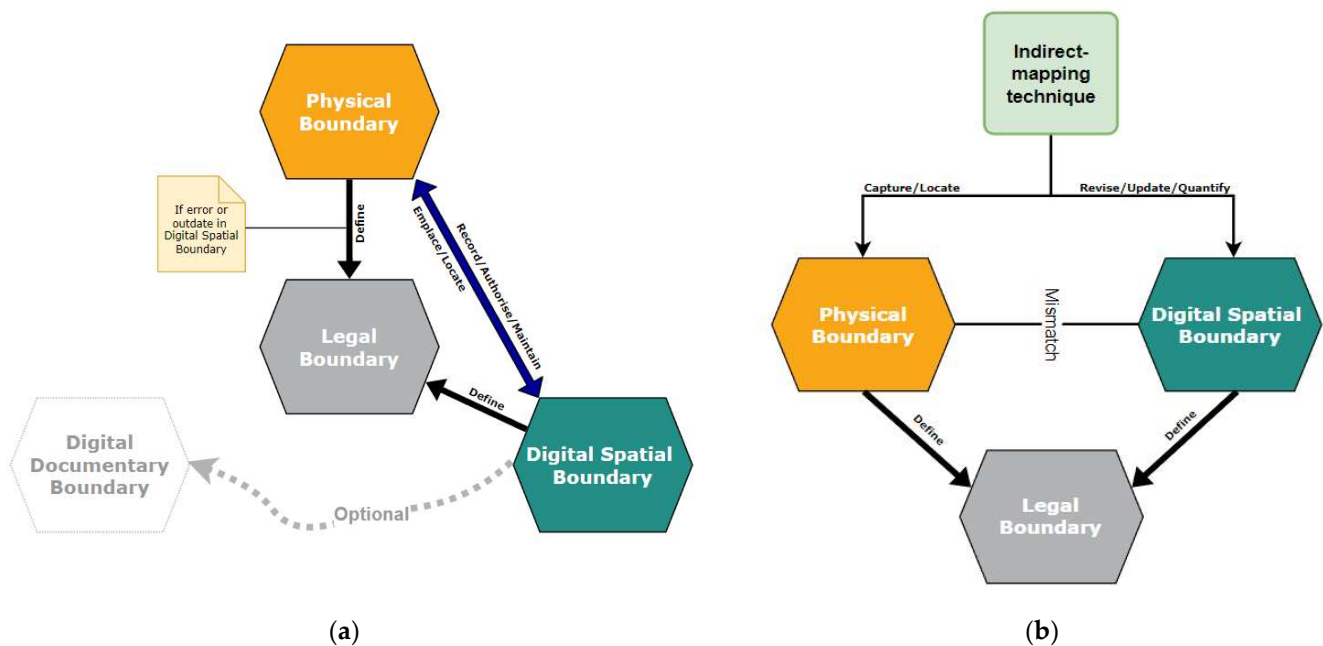


Figure 13. Land boundaries and inconsistencies based on cadastral triangular model (CTM) for digital indirect-mapping techniques; (a) CTM for Fit-for-purpose and countries with no or low cadastral coverage; (b) Fit-for-purpose maintenance for countries with complete cadastre based on indirect-mapping techniques and CTM.

In more developed contexts that have full cadastral coverage, the maintenance of cadastral boundaries is usually done with ground-based techniques. The application of UAV-based cadastral mapping is very limited—there are few case studies on updating and evaluating the accuracy and compliance [18,44]. The main challenge in this context is the maintenance of cadastral data over land boundaries [6]. The changes in physical boundaries that cadastres attempt to map are complex and dynamic [30], and underestimating the dynamics of human-land relationships leads to outdated cadastral maps. In other words, this leads to inconsistencies between physical and cadastral boundaries—both digital spatial and documentary. An automated approach is needed to identify areas that need to be updated or where there is a discrepancy between physical and cadastral boundaries.

In cadastral applications, UAVs have shown great potential for mapping urban and rural areas. In addition, UAVs provide a fast, accurate, and flexible system for data collection. This is mainly due to the good visibility of physical boundaries (artificial or natural) in a UAV orthoimage [45]. Recent developments show that delineating visible physical boundaries can be automated using various image processing algorithms, computer vision, and machine learning methods, including deep learning [46].

Automatic detection of physical boundaries using remote sensing imagery, especially UAV imagery (since it is more accurate and flexible), opens new possibilities for countries with a complete cadastre. The approach can be used for maintenance purposes in the form of automatic revision of existing cadastral maps to automatically identify areas where discrepancies exist. Detected visible physical boundaries can be used as preliminary digital spatial boundaries that can later be manually aligned using UAV imagery or resurveyed

using ground-based techniques, where documentary boundaries can be determined and reconciled with the digital spatial boundaries. For this reason, digital documentary boundaries are not emphasised as a special type of boundary. The approach can be classified as fit-for-purpose maintenance for countries with complete cadastres and can be expressed by the CTM (Figure 13b).

This study examined measurement-based data in North Macedonia and Slovenia, which are very similar in content and form. However, different countries or cadastral systems may have different approaches to the storage, content, and format of such data. Approaches may include measurements at boundary markers, offsets to other features, calculated boundary dimensions, etc. They may also include survey plans, field notes, and other documents based on cadastral surveys. The type of information and the surveying and mapping technique used can affect the accuracy of the land boundary positions and, consequently, the digitisation process.

4. Conclusions

Observations and analysis focused on identifying inconsistencies in cadastral boundary data resulting from digitisation. Specifically, the focus was on what cadastral boundary data were used as input during digitisation.

In the two selected case studies, one in North Macedonia and one in Slovenia, mainly analogue cadastral maps were used as input. The differences between the coordinates calculated from the measurements and those obtained from the vector representation were considerable, yielding a horizontal RMSE of 0.48 m for Trebosh and 0.56 m for Ivanjševci. Consequently, the area differences resulted in an RMSE of 26 m² for Trebosh and an RMSE of 23 m² for Ivanjševci. These differences can be considered a discrepancy in the cadastral data on land boundaries. The differences between the cadastral boundary data are due to digitisation, which introduces additional errors through scanning, georeferencing, and vectorization of analogue cadastral maps. The use of measurement-based data, i.e., the calculation and import of coordinates directly in digital format, avoids these errors. Moreover, it should be emphasised that in the pre-digitization phase, the situation regarding discrepancies was clearer; basically, discrepancies existed only in the case of errors or outdated documentary boundaries. Therefore, it should be pointed up that before harmonising the cadastral data with the land registry data, harmonisation within the cadastral data is first required, or duplication of cadastral attributes should be avoided. Removing the area information from the land registry extracts makes the maintenance of the cadastral boundary data more flexible by avoiding complications or changes that are required in the legal data.

In the case of North Macedonia, the documentary boundary data are not used or maintained after the digitisation of the cadastral maps. Since in the pre-digitisation phase, the cadastral boundaries were defined and relocated as documentary boundaries, the current approach (defining digital spatial boundaries as masters) leads to new obligations when relocating the same boundaries or formatting land plots or other cadastral procedures—due to the different location of the boundaries and the different area of the land plots. In the case of Slovenia, although the documentary boundary data was deemed irrelevant during the digitisation process, it was still retained, and in the event of a boundary relocation, the documentary boundary data is calculated and staked in the field. This represents a sporadic approach to matching and integrating documentary boundaries into the digital spatial database. For this reason, countries that have survey data should use it as a data source for digitisation.

The content of the documentary boundaries depends on the surveying and mapping techniques used. Countries with complete cadastres in the past and today mostly use ground-based techniques, while countries with low cadastral coverage use more innovative approaches, such as indirect mapping techniques. In view of this, the current CTM is more suitable for countries that have a long cadastral tradition and where paper cadastral maps exist. This is mainly because the digital spatial boundaries within the model are derived

11. Luo, X.; Bennett, R.; Koeva, M.; Lemmen, C.; Quadros, N. Quantifying the Overlap between Cadastral and Visual Boundaries: A Case Study from Vanuatu. *Urban Sci.* **2017**, *1*, 32. [CrossRef]
12. Babawuro, U.; Zou, B. Satellite Imagery Cadastral Features Extractions using Image Processing Algorithms: A Viable Option for Cadastral Science. *IJCSI Int. J. Comput. Sci. Issues* **2012**, *9*, 30–38.
13. Crommelinck, S.; Bennett, R.; Gerke, M.; Nex, F.; Yang, M.; Vosselman, G. Review of Automatic Feature Extraction from High-Resolution Optical Sensor Data for UAV-Based Cadastral Mapping. *Remote Sens.* **2016**, *8*, 689. [CrossRef]
14. Casiano Flores, C.; Tan, E.; Crompvoets, J. Governance assessment of UAV implementation in Kenyan land administration system. *Technol. Soc.* **2021**, *66*, 101664. [CrossRef]
15. Stöcker, C.; Bennett, R.; Nex, F.; Gerke, M.; Zevenbergen, J. Review of the Current State of UAV Regulations. *Remote Sens.* **2017**, *9*, 459. [CrossRef]
16. Koeva, M.; Muneza, M.; Gevaert, C.; Gerke, M.; Nex, F. Using UAVs for map creation and updating. A case study in Rwanda. *Surv. Rev.* **2018**, *50*, 312–325. [CrossRef]
17. Stöcker, C.; Bennett, R.; Koeva, M.; Nex, F.; Zevenbergen, J. Scaling up UAVs for land administration: Towards the plateau of productivity. *Land Use Policy* **2022**, *114*, 105930. [CrossRef]
18. Manyok, M.; Theiler, P.; Steudler, D.; Eisenbeiss, H. Unmanned Aerial Vehicle in Cadastral Applications. *Int. Arch. Photogramm. Remote Sens. Spat. Inf. Sci.* **2011**, XXXVIII-1/C22, 57–62. [CrossRef]
19. Rijdsdijk, M.; van Hinsbergh, W.H.M.; Witteveen, W.; ten Buuren, G.H.M.; Schakelaar, G.A.; Poppinga, G.; van Persie, M.; Ladiges, R. Unmanned Aerial Systems in the process of Juridical verification of Cadastral border. *Int. Arch. Photogramm. Remote Sens. Spat. Inf. Sci.* **2013**, XL-1/W2, 325–331. [CrossRef]
20. Mesas-Carrascosa, F.J.; Notario-García, M.D.; Meroño de Larriva, José Emilio; Sánchez de la Orden, Manuel; García-Ferrer Porras, A. Validation of measurements of land plot area using UAV imagery. *Int. J. Appl. Earth Obs. Geoinf.* **2014**, *33*, 270–279. [CrossRef]
21. Bennett, R.M.; Koeva, M.; Asiama, K. Review of Remote Sensing for Land Administration: Origins, Debates, and Selected Cases. *Remote Sens.* **2021**, *13*, 4198. [CrossRef]
22. Chen, J.; Dowman, I.; Li, S.; Li, Z.; Madden, M.; Mills, J.; Paparoditis, N.; Rottensteiner, F.; Sester, M.; Toth, C.; et al. Information from imagery: ISPRS scientific vision and research agenda. *ISPRS J. Photogramm. Remote Sens.* **2016**, *115*, 3–21. [CrossRef]
23. Potsiou, C.; Volakakis, M.; Doublidis, P. Hellenic cadastre: State of the art experience, proposals and future strategies. *Comput. Environ. Urban Syst.* **2001**, *25*, 445–476. [CrossRef]
24. Fetai, B. Analysing the Effects of Merging Land Registration and Cadastre. Master's Thesis, ITC Faculty of Geo-information Science and Earth Observation, University of Twente, Enschede, The Netherlands, 2015.
25. Roić, M.; Križanović, J.; Pivac, D. An Approach to Resolve Inconsistencies of Data in the Cadastre. *Land* **2021**, *10*, 70. [CrossRef]
26. Yildiz, U.; Gürel, M.; Kocaman, S. State liability and uncertainty perception on cadastral parcel area registry in Turkey. *Land Use Policy* **2022**, *116*, 106075. [CrossRef]
27. Ferlan, M.; Šumrada, R.; Čeh, M.; Lisec, A. Načini vzpostavitve digitalnih katastrskih načrtov v primerljivih državah = Approaches to the establishment of digital cadastral maps in comparable countries. *Geod. Vestn.* **2011**, *55*, 235–256. [CrossRef]
28. Buyong, T.B.; Kuhn, W.; Frank, A.U. A Conceptual Model of Measurement-Based Multipurpose Cadastral Systems. *J. Urban Reg. Inf. Syst. Assoc. URISA* **3** **1991**, *2*, 35–49.
29. Navratil, G.; Franz, M.; Pontikakis, E. Measurement-based GIS Revisited. In Proceedings of the 7th AGILE Conference on Geographic Information Science, Heraklio, Greece, 29 April–1 May 2004.
30. Navratil, G. Cadastral Boundaries: Benefits of Complexity. *URISA J.* **2011**, *23*. ISBN 1045-8077. Available online: https://www.researchgate.net/publication/228777713_Cadastral_Boundaries_Benefits_of_Complexity (accessed on 10 November 2022).
31. Lisec, A.; Navratil, G. The Austrian land cadastre: From the earliest beginnings to the modern land information system. *Geod. Vestn.* **2014**, *58*, 482–516. [CrossRef]
32. Pivac, D.; Roić, M.; Križanović, J.; Paar, R. Availability of Historical Cadastral Data. *Land* **2021**, *10*, 917. [CrossRef]
33. Grant, D.; Enemark, S.; Zevenbergen, J.; Mitchell, D.; McCamley, G. The Cadastral triangular model. *Land Use Policy* **2020**, *97*, 104758. [CrossRef]
34. Goodchild, M.F. Measurement-based GIS. In *Spatial Data Quality*, 1st ed.; Shi, W., Fisher, P.F., Goodchild, M.F., Eds.; Taylor and Francis: New York, NY, USA, 2002; p. 13. ISBN 97804292196100.
35. Drobež, P.; Grigillo, D.; Lisec, A.; Kosmatin Fras, M. Remote sensing data as a potential source for establishment of the 3D cadastre in Slovenia. *Geod. Vestn.* **2016**, *60*, 392–422. [CrossRef]
36. Fetai, J. Развојот на катастарот во Република Македонија = The Development of Cadastre in Republic of Macedonia. Master's Thesis, Ss. Cyril and Methodius University in Skopje, Faculty of Civil Engineering, Skopje, North Macedonia, 2009.
37. Kovačič, M.; Jevšnik, D.; Gnilšek, J.; Avgustinčič, V.; Novak, P.; Bovha, D.; Urh, J.; Kuhar, M.; Tanko, D.; Martinuč-Brajnik, J. *Priprava Finančno Orednotenega Programa Izboljšave Podatkov Zemljiškega Katastra in Testiranje Metod Poenostavljenih Novih Izmer*; GZD: Celje, Slovenia, 2005.
38. Petek, T. Cadastral Template 2.0-Slovenia. Available online: <http://cadastraltemplate.org/slovenia.php> (accessed on 15 September 2022).

39. Triglav, J. *Katastrske Izmere V Prekmurju-Zgodovinski Zapisi = Cadastral Measurements in Prekmurje-Historical Notes*; Geodetski Vestnik: Ljubljana, Slovenia, 2021; Available online: https://www.geodetski-vestnik.com/arhiv/65/4/gv65-4_triglav.pdf (accessed on 5 September 2022).
40. Triglav, J. *POzor: Zk-Točke Z Upravnim Statusom 5 = Attention: Lc Points with Administrative Status 5*; Geodetski Vestnik: Ljubljana, Slovenia, 2022; Available online: https://www.geodetski-vestnik.com/arhiv/66/2/280-288_Triglav.pdf (accessed on 5 September 2022).
41. Agency for Real Estate Cadastre. OneStopShopPortal (OSSP). Available online: <https://oss.katastar.gov.mk/OSSP/> (accessed on 15 September 2022).
42. The Surveying; Mapping Authority of the Republic of Slovenia. e-Surveying Data. Available online: <https://egp.gu.gov.si/egp/?lang=en> (accessed on 17 January 2022).
43. Zevenbergen, J.; Frank, A.; Stubkjaer, E. *Real Property Transactions. Procedures, Transaction Costs and Models: Procedures, Transaction Costs and Models*; IOS Press: Amsterdam, The Netherlands, 2008; ISBN 9781607501565.
44. Puniach, E.; Bieda, A.; Ćwiakala, P.; Kwartnik-Pruc, A.; Parzych, P. Use of Unmanned Aerial Vehicles (UAVs) for Updating Farmland Cadastral Data in Areas Subject to Landslides. *IJGI* **2018**, *7*, 331. [[CrossRef](#)]
45. Kohli, D.; Bennett, R.; Lemmen, C.; Morales, A.; Pinheiro, A.; Zevenbergen, J. A Quantitative Comparison of Completely Visible Cadastral Parcels Using Satellite Images: A Step towards Automation. In Proceedings of the FIG Working Week 2017, Helsinki, Finland, 29 May–2 June 2017; pp. 1–14.
46. Crommelinck; Koeva; Yang; Vosselman. Application of Deep Learning for Delineation of Visible Cadastral Boundaries from Remote Sensing Imagery. *Remote Sens.* **2019**, *11*, 2505. [[CrossRef](#)]

APPENDIX C : Extraction of Visible Boundaries for Cadastral Mapping Based on UAV Imagery

B. Fetai, K. Oštir, M. Kosmatin Fras, and A. Liseč (2019)

Remote sensing vol. 11, no. 13, p. 1510

doi: 10.3390/rs11131510

Article

Extraction of Visible Boundaries for Cadastral Mapping Based on UAV Imagery

Bujar Fetai ^{*}, Krištof Oštir , Mojca Kosmatin Fras and Anka Lisec 

Faculty of Civil and Geodetic Engineering, University of Ljubljana, Jamova cesta 2, 1000 Ljubljana, Slovenia

^{*} Correspondence: bujar.fetai@fgg.uni-lj.si; Tel.: +386-1-476-8560

Received: 8 May 2019; Accepted: 24 June 2019; Published: 26 June 2019



Abstract: In order to transcend the challenge of accelerating the establishment of cadastres and to efficiently maintain them once established, innovative, and automated cadastral mapping techniques are needed. The focus of the research is on the use of high-resolution optical sensors on unmanned aerial vehicle (UAV) platforms. More specifically, this study investigates the potential of UAV-based cadastral mapping, where the ENVI feature extraction (FX) module has been used for data processing. The paper describes the workflow, which encompasses image pre-processing, automatic extraction of visible boundaries on the UAV imagery, and data post-processing. It shows that this approach should be applied when the UAV orthoimage is resampled to a larger ground sample distance (GSD). In addition, the findings show that it is important to filter the extracted boundary maps to improve the results. The results of the accuracy assessment showed that almost 80% of the extracted visible boundaries were correct. Based on the automatic extraction method, the proposed workflow has the potential to accelerate and facilitate the creation of cadastral maps, especially for developing countries. In developed countries, the extracted visible boundaries might be used for the revision of existing cadastral maps. However, in both cases, the extracted visible boundaries must be validated by landowners and other beneficiaries.

Keywords: land plot; land cadastre; cadastral boundaries; cadastral maps; UAV; image processing; image segmentation; feature extraction

1. Introduction

Establishing a complete land cadastre and keeping it up-to-date is a contemporary challenge for many developing and developed countries, respectively [1,2]. In this research, the distinction between ‘developing’ and ‘developed’ countries is considered from a land administration perspective. A developing country refers to a country with low cadastral coverage. A developed country refers to full coverage of a country’s territory with defined cadastral land plot boundaries and associated land rights. According to the International Federation of Surveyors (FIG) and the World Bank, only one-quarter of people’s land rights across the world are formally recognized by cadastral or other land recording systems [1]. Thus, in developing countries, initial efforts are directed to accelerating cadastral mapping as a basis for defining and recording land rights boundaries and formalizing land-related rights aiming to guarantee land tenure security [3,4]. In developed countries, beyond the initial adjudication stage or establishment of a cadastre, another challenge is the maintenance of person-right-land relation attributes and keeping the cadastral systems up-to-date [5,6]. In countries with a tradition and long history of developing a cadastral system, conventional ground-based cadastral surveying techniques and high positional accuracy of boundary surveying were required. Decades were needed to complete the process of cadastral surveying/mapping and registration [1,6]. Although land cadastres were established, some of the cadastral systems could not be maintained, which led to outdated cadastral maps. Person-right-land relationship is complex and dynamic. Keeping the cadastral system up-to-date

(continuous recording of person-right-land relation attributes, in any land related event, as close as possible to real-time) also requires a flexible and dynamic cadastral system [2,7]. Proposed cadastral surveying techniques are mostly indirect ones rather than ground-based. Ground-based techniques are often argued as being time-consuming and labor intensive [1,5,8].

Emerging tools are mapping techniques based on remote sensing data, in particular, data acquired with sensors on Unmanned Aerial Vehicles (UAVs) [9–18]. Cadastral maps are usually defined as a spatial representation of recorded land plot boundaries or other spatial units that the land rights concern [19]. In general, sensors on UAVs provide low-cost, efficient, and flexible high-resolution spatial data acquisition systems enabling the production of point clouds, Digital Surface Models (DSM) and orthoimages [20,21]. In cadastral applications, UAVs have gained increasing popularity due to the high cadastral mapping potential in a different setting, in rural and urban areas, for developing and developed countries [22]. In addition, UAVs are used for both the creation and updating of cadastral maps [22]. In developing countries, UAV-based cadastral mapping usually serves as a tool for the creation of a formal cadastral system [11–13]. In developed countries, the case studies focus on the assessment of UAVs' data positional accuracy estimation and its conformity with local positional accuracy requirements aiming to use the UAV data for updating existing cadastral maps [14–18]. Here, updating in most cases refers to the comparison of two cadastral maps—one representing the database state, the other recently acquired data. The term updating can be used as a synonym for a “revision” of existing cadastral maps [23]. However, in all case studies reported in [22], cadastral boundaries are manually delineated.

It is argued that a large number of cadastral boundaries are visible and coincide with natural or manmade physical object boundaries [2,24,25]. In the land administration domain, automatic extractions of visible cadastral boundaries have been a recent topic of investigation. The latest studies, though limited in number, assert that visible boundaries, such as hedges, land cover boundaries, etc., which might indicate cadastral boundaries, could be automatically extracted using methods such as algorithms that detect object boundaries in images [22,26–29]. In fact, not all visible cadastral boundaries can be automatically detected—certain boundaries would require a semi-automatic approach, especially in urban areas where the morphology of cadastral boundaries is complex [7]. Nevertheless, the potential of computer vision methods for automatic detection and extraction of visible objects in the images is promising for cadastral applications, especially due to the urgent global need for accelerating and facilitating cadastral mapping as a basis for registration of land rights and following the dynamics of land tenure and land use.

1.1. Visible Boundary Detection and Extraction for Cadastral Mapping

Automatic feature extraction methods from images acquired with high-resolution optical sensors have already proved to be useful for the extraction of boundaries of linear features such as roads and rivers [30–34], and to a much lesser degree, they have also been explored for the purpose of cadastral boundary delineation. A recent study from Crommelinck et al. [22] provides an overview of computer vision methods that might be applicable in the land administration domain for automatic detection and extraction of object boundaries from images acquired with high-resolution optical sensors. Additionally, the general workflow for automatic detection and extraction of visible object boundaries for UAV-based cadastral mapping is provided [22]. The general workflow consists of (i) image pre-processing, (ii) image segmentation, (iii) line extraction, (iv) contour or boundary generation, and (v) image and/or boundary post-processing. Image pre-processing usually includes image conversions, such as resampling or tiling, in order to fit the requirements of a chosen computer vision method. Image segmentation refers to the process of dividing a digital image into non-overlapping objects, which represent homogeneous areas [35]. The third workflow step is the extraction of lines or edges from the segmented images [36]. The next step, contour generation, refers to the extraction of a closed object outlines in the image. In computer vision, they are usually defined as object boundaries, which are derived from connecting edges or lines. An ‘object boundary’ should encompass an ‘object’ in an image,

and due to this, both terms are used synonymously in this study. In cadastral applications, objects are usually defined as polygon-based spatial units. The final step, post-processing, includes interventions on the image such as vectorization and/or simplification of automated extraction of objects [26,37]. However, only a limited number of studies have investigated the automatic extraction of objects from images acquired with high-resolution optical sensors for cadastral boundary delineation.

The work by Babawuro and Zou [38] tested Canny and Sobel edge-detection algorithms for the extraction of visible cadastral boundaries from high-resolution satellite imagery (HRSI). In addition, the Hough Transform feature extraction method was used to connect edges and to identify straight lines. The visual presentation of the results showed that the proposed approach can detect agricultural land boundaries, but there were no quantity measures on quality assessment. Kohli et al. [28,29] investigated the use of an object-based approach, namely the multi-resolution segmentation (MRS) and estimation of scale parameter (ESP) to extract visible cadastral boundaries from HRSI. An object-based approach refers to the extraction of object outlines based on a grouping of pixels with similar characteristics and is applied to high-level features which represent shapes in an image [22]. The accuracy assessment in Kohli et al. [28] was pixel-based, and the detection quality in terms of error of commission and omission for MRS were 75% and 38%, respectively. For ESP, the error of commission was 66% and the error of omission 58%. The localization quality for MRS was 71%, whereas it was 73% for ESP, within a 41–200 cm distance from the reference boundaries. Another case of the automatic extraction of visible boundaries based on HRSI is described in Wassie et al. [27]. The study explored the potential of mean-shift segmentation for the extraction of visible cadastral boundaries. The mean-shift segmentation algorithm is a QGIS open source plugin [27]. The object-based measures were applied for the accuracy assessment. Within a buffer distance of 2 m, the percentage indicated the correctness was 34%, while for the completeness it was 83% [27]. The extractions with mean-shift segmentation were closed object boundaries (polygon-based) in vector format and topologically correct. The mean-shift segmentation was applied to a full extent of satellite images. Accordingly, some of the automatic object extraction methods were applied also using UAV images.

The study from Crommelinck et al. [26] outlines the potential of the Global Probability of Boundary (gPb) contour detection method for an automatic boundary delineation based on UAV imagery. gPb is open-source and available as pre-compiled Matlab package. The method was found to be applicable only for processing images of fewer than 1000 × 1000 pixels due to the demanding computing process [26]. The contour map or detected objects were in raster format and required vectorization. Furthermore, Crommelinck et al. [37] discuss the interactive method of visible boundary extractions. The interactive method combines the gPb contour detection, simple linear iterative clustering (SLIC) super pixels and random forest classifier, which allow a semi-automatic approach for the delineation of visible boundaries. The interactive method was tested on visible road outlines based on UAV datasets. The results show that the approach is much more efficient than manual boundary delineation, and all road boundaries were delineated comprehensively.

All the case studies reviewed, both automatic boundary extractions from HRSI and UAV images, have been tested in rural areas since it is argued that most of the cadastral boundaries are visible in such areas [26]. However, not all computer vision automatic feature extraction methods suitable for visible cadastral boundary delineation have already been tested.

Another tool that is also referred to as the 'state-of-the-art' for automatic detection and extraction of features from images is the ENVI feature extraction (FX) module [39,40]. ENVI FX is an object-based module for detecting and extracting multiple object outlines from high-resolution multispectral or panchromatic digital images. The extraction is based on spectral (brightness and color), texture, and spatial characteristics [41]. To the best of the authors' knowledge, there have been no previous publications, nor evidence, that the ENVI FX module has been applied for detecting and extracting visible cadastral boundaries on UAV images.

The justification for using this method is based on Crommelinck et al. [22], in which general workflow and feature extraction methods appropriate for cadastral mapping are provided. The main aim

of this study is not to compare automatic feature extraction methods already used for cadastral mapping. Instead, the study focuses on the potential of a feature extraction method which has not been tested yet in cadastral applications. The study can be seen as an important contribution to land administration discussions focusing on cadastral mapping, as there have been a limited number of studies for automatic visible cadastral boundary delineation from imageries acquired using high-resolution optical sensors.

1.2. Objective of the Study

The study is based on the assumption that many cadastral boundaries are visible [2]. The study's main objective is to outline the potential of the ENVI FX module as well as its limitations for the automatic delineation of visible object boundaries for UAV-based cadastral mapping. It investigates which processing steps (scale level and merge level) using the ENVI FX module need to be applied for UAV-based cadastral mapping. The automatic delineated visible boundaries on UAV images, similarly as manual delineations, can be used for both the creation and updating/revision of cadastral maps.

Overall, the study addresses the whole of the UAV-based cadastral mapping workflow steps, which include image pre-processing, automatic detection and extraction of visible object boundaries on the UAV image, and post-processing of extracted boundaries to more closely approximate cadastral boundaries.

2. Materials and Methods

2.1. UAV Data

To achieve the objective of the study, a rural area in Slovenia was selected as the number of visible (cadastral) boundaries in such areas is higher compared to dense urban ones. In addition, the selected rural area includes roads, agricultural field outlines, fences, hedges, and tree groups, which are assumed to indicate cadastral boundaries [22]. The UAV images of the case study area were indirectly geo-referenced, using an even distribution of ground control points (GCP) within the field as criteria. The GCPs were surveyed with real-time kinematic (RTK) by using Global Navigation Satellite System (GNSS) receiver, Leica Viva, connected in the Slovenian GNSS network, SIGNAL. The signals were received from satellite constellations of GPS and GLONASS. The total number of GCPs was 12. The Position dilution of precision (PDOP) values ranged from 1.2 to 1.7. The flight altitude was 80 m and 354 images were taken to cover the study area. The images were captured on October 19th, 2018 in the noon time (good weather conditions, clear sky) at solar zenith angle of approximately 35 degrees. The study site had a coverage area of 25 ha. The planimetric accuracy assessment of the UAV orthoimage was based on comparison between GCPs coordinates surveyed with the GNSS receiver and the coordinates of GCPs on the UAV orthoimage. The estimated root-mean-square-error (RMSE) was 2.5 cm. Table 1 shows the specifications of data capture and Figure 1 shows the UAV orthoimage of the study area.

Table 1. Specification of unmanned aerial vehicle (UAV) dataset for the selected study area in Slovenia.

| Location | UAV Model | Camera/Focal Length [mm] | Overlap Forward/Sideward [%] | Flight altitude [m] | GSD [cm] | Pixels |
|----------------------|-------------------|--------------------------|------------------------------|---------------------|----------|-----------------|
| Ponova vas, Slovenia | DJI Phantom 4 Pro | 1" CMOS 20mp/24 | 80/70 | 80 | 2.0 | 35,551 × 31,098 |

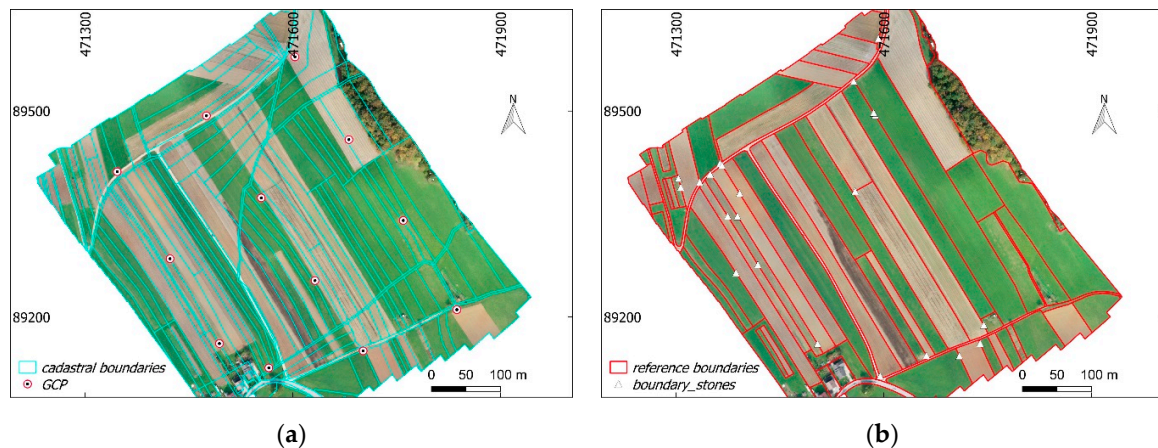


Figure 1. (a) Cadastral map and ground control points (GCPs). (b) Manually delineated object visible boundaries used as reference data to determine the detection/extraction quality. (a,b) Overlaid on UAV orthoimage of Ponoava vas, Slovenia (EPSG 3794).

2.2. Reference data

The current cadastral map for the selected area was retrieved from the e-portal of the Slovenian Surveying and Mapping Authority, which is an online platform for requesting official cadastral data [42]. The cadastral map was overlaid on the UAV orthoimage (Figure 1a). The visual interpretation of the combined dataset showed immediately that the cadastral map does not correspond with the visible objects that indicate land possession (land cover) boundaries (roads, agricultural field outlines) on the UAV orthoimage. From the initial analyses, it appeared that only 8% of cadastral boundaries correspond with the manually digitized visible boundaries (at 25 cm tolerance). This is because the current official cadastral map was created by digitizing previous analog cadastral maps whose origin goes back in the first half of 19th century. Due to the underestimated need for cadastral map updating as well as due to the land reforms in the 20th century (i.e., land nationalization and denationalization) the current possession land boundaries do not correspond with cadastral boundaries. Considering this, as reference data, manually digitized boundaries were used instead of the official cadastral data, as the aim of this research is to automatically delineate visible object boundaries from a UAV orthoimage and, at the same time, study the potential of the ENVI FX solution for the automatic detection of visible boundaries. Moreover, during the manual digitization of reference boundaries, some white stones considered as possession boundary signs were used as a guide for proper digitization (Figure 1b). The placement of white stones is a common practice in the selected study area, and for this reason, they were considered as reliable information during the manual digitization. In addition, the confidence in white stones as boundary signs is based on the authors' experiences in professional cadastral surveying.

2.3. Visible Boundary Delineation Method and Workflow

2.3.1. ENVI Feature Extraction (FX)

The investigated tool, ENVI FX, is a combined process of image segmentation and classification. The focus of this study is only at image segmentation and calculating spatial attributes for each segmented object [41]. In addition to spatial attributes, spectral and textural attributes are often used by users for further image classification analysis.

The first step, image segmentation, is based on the technique developed by Jin [43] and involves calculating a gradient map, calculating cumulative distribution function, modification of the gradient map by defining a scale level, and segmentation of a modified gradient map by using the Watershed Transform [44]. A gradient is calculated for each band of the image. The ENVI FX module uses two approaches: edge method and intensity. The edge method calculates a gradient map using the Sobel

edge detection algorithm [44]. The Intensity method converts each pixel to a spectral intensity value by averaging it across the selected image bands [44]. The edge method is used for detecting features with distinct boundaries and is considered in this study. In contrast, the Intensity method is suitable for digital elevation models, images of gravitational potential and images of electromagnetic fields [44]. After a gradient map is calculated, a density function of gradients over the whole map is calculated in the form of a cumulative relative histogram [43]. Once the cumulative distribution function has been calculated, it can be used along with the gradient map to calculate the gradient scale space [43]. The gradient map can be modified by changing the scale level. The scale level is the relative threshold on the cumulative relative histogram from which the corresponding gradient magnitude can be determined [43]. For example, at a scale level of 50, the lowest 50 percent of gradient magnitude values are discarded from the gradient image [44]. Increasing the scale level results in fewer segments and keeps objects with the most distinct boundaries [41]. Once the scale level is selected the Watershed Transform algorithm is applied to the modified gradient map. The Watershed Transform is based on the concept of hydrologic watersheds [22,35]. In digital imagery, the same process can be similarly explained as the darker a pixel, the lower its "elevation" (minimum pixel). The algorithm categorizes a pixel by increasing the greyscale value, then begins with the minimum pixels and "floods" the image, dividing the image into objects with similar pixel intensities. The result is a segmented image and each segmented object is assigned with a mean spectral value of all the pixels that belong to that object [44].

The second step is merging. This step aggregates over-segmented areas by using the ENVI FX default full Lambda schedule algorithm. The algorithm is meant to aggregate object outlines within larger, textured areas, such as trees and, fields, based on a combination of spectral and spatial information [41,45]. The merge level represents the threshold Lambda value. Merging occurs when the algorithm finds a pair of adjacent objects such that the merging cost is less than a defined threshold Lambda value—if the merge level is set to 20, it will merge adjacent objects with the lowest 20 percent of Lambda values [45]. When a merge level of 0 is selected no merging will be performed. In this step, the selection of Texture Kernel Size is optional, i.e., the size of a moving box centered over each pixel value. The ENVI FX default Texture Kernel Size is 3, and the maximum is 19 [45].

The final step is the export of object boundaries in a vector format and a segmented image in a raster format. Moreover, each extracted object consists of spatial, spectral, and texture information in the attribute table [41].

2.3.2. Visible Boundary Delineation Workflow

The visible boundary delineation workflow (Figure 2) consists of four main steps. In the following, each workflow step is described in detail with additional comments based on our own preliminary studies aiming to understand and justify the selection of the parameters and algorithms used. The first and second steps were implemented in ENVI 5.5 image analysis software [46] by using the ENVI FX [47] tool. The other steps were implemented using QGIS [48] and GRASS [49] functions.

1. *Image pre-processing*: The first step is resampling the UAV orthoimage. The UAV orthoimage was resampled from 2 cm to lower spatial resolutions—25 cm, 50 cm and 100 cm ground sample distances (GSD). The selected GSDs allowed the identification of the impact of different GSDs on the results of automatic boundary extractions. The pixel average method was used for resampling the UAV orthoimage as it provides a smoother image. In addition, further resampling methods (nearest neighbor and bilinear) were tested and did not provide significant differences in the number of automatic object boundary extractions—at higher scale and merge levels of the ENVI FX algorithm. The resampling step was also applied in [26], to make transferable the investigated method to a UAV orthoimage for cadastral mapping purposes. In addition, extracting objects from a UAV orthoimage of lower spatial resolution is computationally less expensive.
2. *Boundary detection and extraction*: The ENVI FX module was applied to each down-sampled UAV orthoimage. The detection and extraction of visible boundaries from the UAV orthoimage was based on the ENVI FX scale and merge level values. The texture kernel size was set to default,

i.e., 3. In addition, further object extractions were tested at the highest texture kernel size and no differences in the number and locations of extracted objects were identified. Scale level values ranged from 50 to 80 and merge level values from 50 to 99. The initial incremental value for both scale and merge levels was 10. In cases where a jump in the total number of extracted objects was detected the incremental value was dropped for both scale and merge levels. In order to identify the optimal scale and merge values for the detection and extraction of visible objects for cadastral mapping, all possible range values of scale and merge combinations were tested. For each extraction information about the total number of extracted objects and processing time was stored. This resulted in 50 boundary maps for each resampled UAV orthoimage. The boundary map consisted of extracted objects (polygon-based), which were in digital vector format.

3. *Data post-processing:* The process included two steps: (i) the filtering of extracted objects, and (ii) the simplification of extracted objects. (i) The minimum object area and the total number of objects identified in the reference data (Figure 1b) were used to determine optimal scale and merge levels. The minimum reference object area was 204 m², and the total number of objects was 68. All extracted objects that were smaller than the minimum object area from reference data were filtered out (removed). The total number of remaining objects was compared with the total number of objects from the reference data and the tolerance of +/- 10 objects was set—those parameters that produced numbers of objects that were closest to those found in the reference data, i.e., within defined tolerance, were deemed optimal. The boundary maps from which smaller objects were removed were labeled as filtered objects. The output of filtered objects consisted of holes, i.e., due to polygon-based geometry of objects, which were mostly present either in the forest or individual trees and are of less relevance for cadastral applications—a boundary between adjacent objects belongs to both. (ii) Extracted and filtered object boundaries were smoothed and simplified to be used for the interpretation of possession boundaries aiming to support a cadastral mapping (i.e., land plot restructuring in this case, as the situation requires a new cadastral survey or land consolidation). The smoothing of extracted/filtered object boundaries was done by using the Snakes algorithm [49]. The Douglas–Peucker algorithm was applied to the smoothed object boundaries in order to further simplify the object boundaries [22,49]. These objects both smoothed and simplified were labeled as simplified extracted/filtered objects.
4. *Accuracy assessment:* The accuracy assessment was object-based since the results were in vector format. The buffer overlay method was used for accuracy assessment. The method is described in detail in Heipke et al. [50]. The accuracy assessment was based on computing the percentages of extracted (or reference) boundary lengths which overlapped within a buffer polygon area generated around the reference (or extracted) boundaries (Figure 3) [50]. To determine the completeness, correctness, and quality of extracted boundaries, calculated boundary lengths of true positives (TP), false positives (FP), and false negatives (FN) were used. The completeness refers to the percentage of reference boundaries which lie within the buffer around the extracted boundaries (matched reference). The correctness refers to the percentage of extracted boundaries, which lie within the buffer around the reference boundaries (matched extraction). The accuracy assessment was performed on buffer widths of 25 cm, 50 cm, 100 cm, and 200 cm. The selection of buffer widths is in line with other studies and was based on the most common tolerances regarding boundary positions in land administration, especially for rural areas [26,27]. The percentage indicating the overall quality was generated from the previous two by dividing the length of the matched extractions with the sum of the length of extracted data and the length of unmatched reference [50]. The accuracy assessment was applied to automatic extracted objects, simplified extracted objects, filtered objects, and simplified filtered objects (Figure 2).

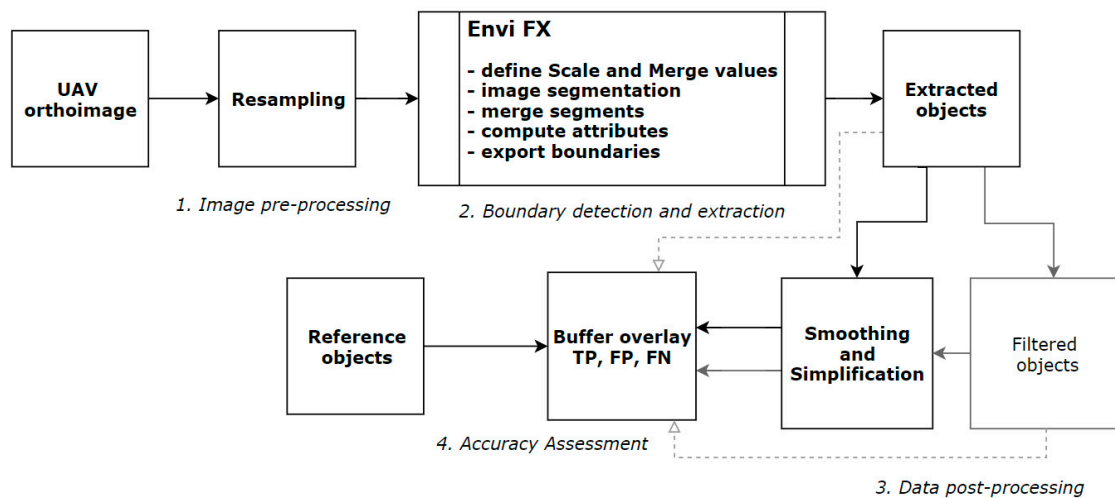


Figure 2. Cadastral mapping workflow based on the automatic detection and extraction of visible boundaries from UAV imagery.

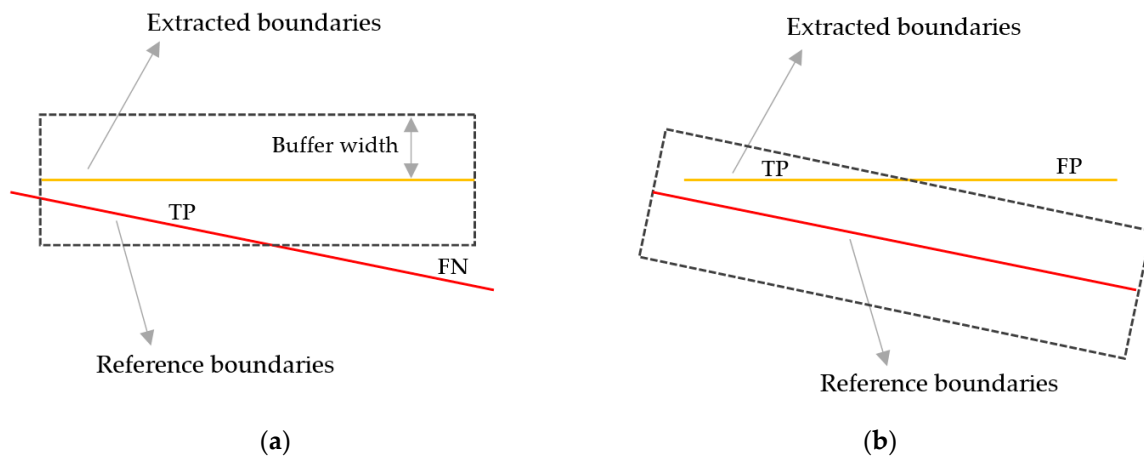


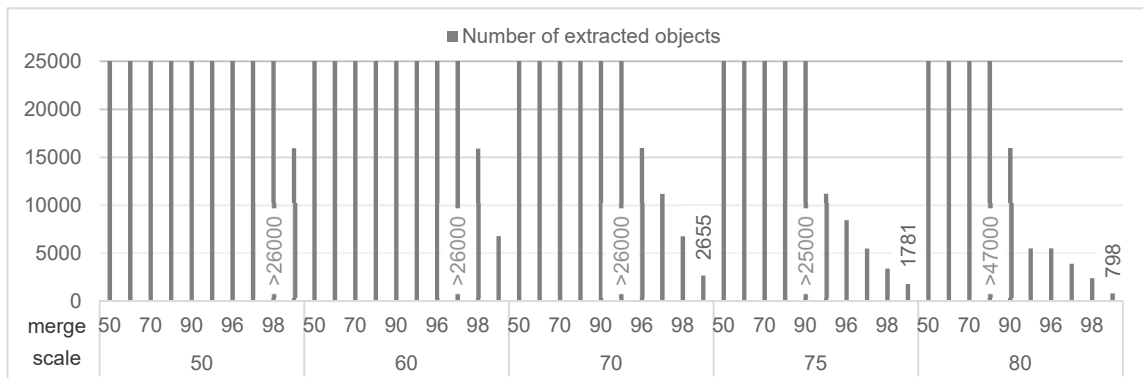
Figure 3. Object-based accuracy assessment method—buffer overlaying method. (a) Matched reference. (b) Matched extraction. (a,b) Calculation of boundary lengths of true positives (TP), false positives (FP) and false negatives (FN) (Adapted from [50]).

3. Results

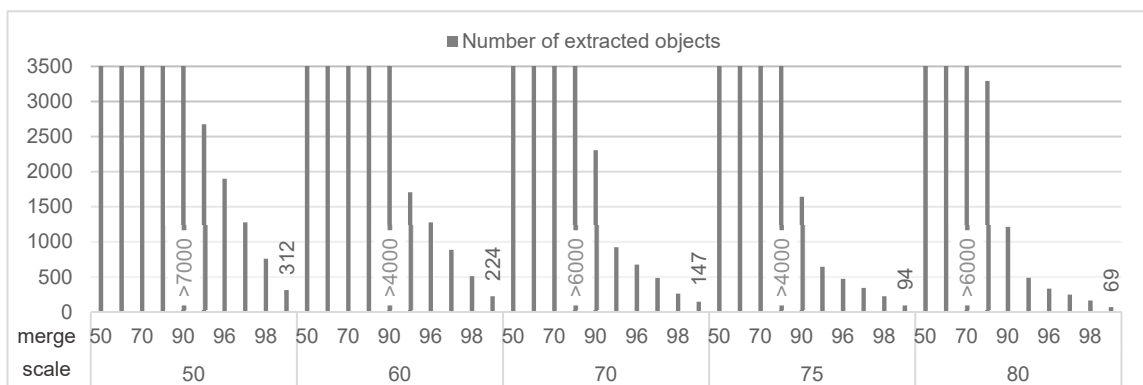
Resampling the UAV orthoimage to a lower spatial resolution, i.e., a larger value of GSD, resulted in fewer and faster extractions of object boundaries compared to the number of extracted object boundaries generated at the original size of the UAV orthoimage. The processing time for one boundary map was 1–2 min. A larger GSD, at the same scale and merge values, resulted in fewer boundary extractions (Table 2, Figures 4 and 5).

Table 2. Ground sample distance (GSD) and number of pixels after image pre-processing.

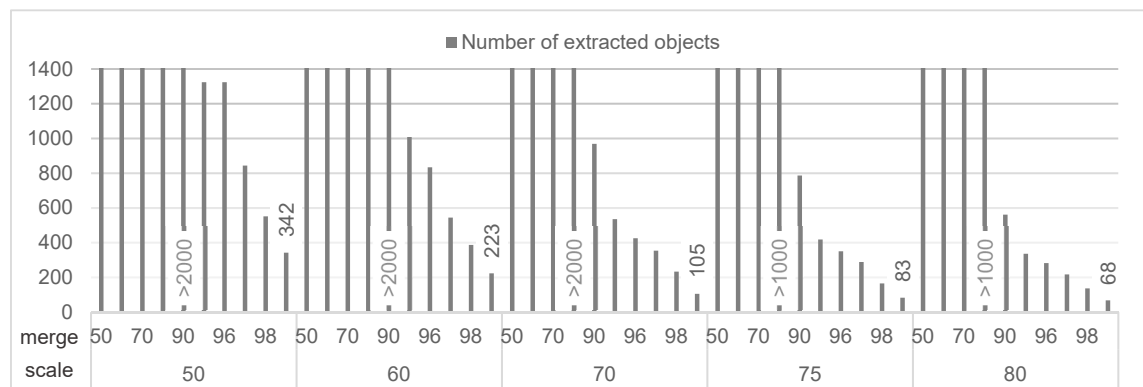
| GSD [cm] | Pixels | Resampling Method |
|----------|-------------|-------------------|
| 25 | 2856 × 2498 | Pixel average |
| 50 | 1428 × 1249 | Pixel average |
| 100 | 714 × 625 | Pixel average |



(a)



(b)



(c)

Figure 4. Scale/merge level and number of extracted objects from the resampled UAV orthoimages (a) ground sample distance (GSD) 25 cm, (b) GSD 50 c, and (c) GSD 100 cm. (a–c) Grey labels—number of extracted objects outside the range, black labels—the lowest number of extracted objects per scale and merge parameter value.

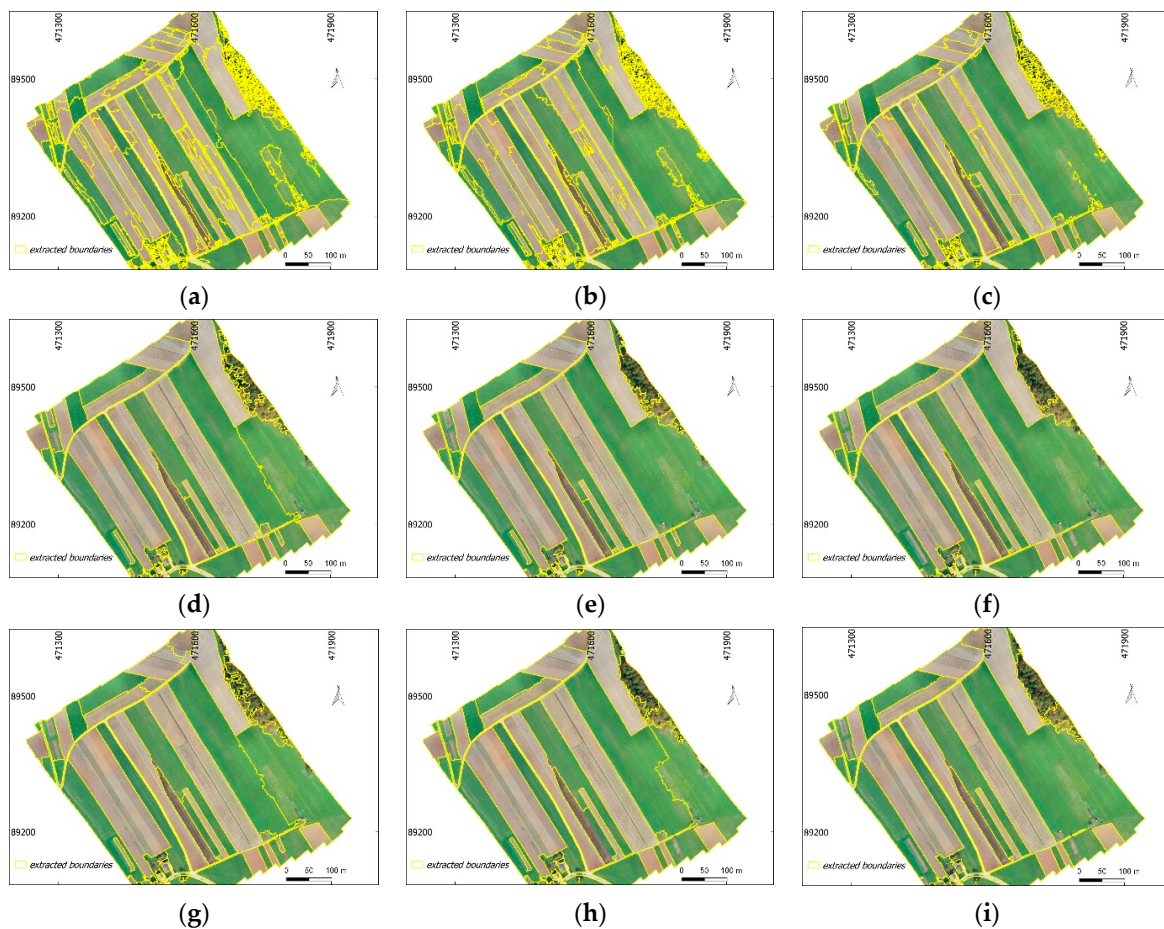


Figure 5. (a–i) Examples of extracted boundary maps. (a–c) GSD 25 cm; (d–f) GSD 50 cm, and (g–i) GSD 100 cm. (a,d,g) Extracted objects at scale 70 and merge 99. (b,e,h) Extracted objects at scale 75 and merge 99. (c,f,i) Extracted objects at scale 80 and merge 99.

A lower scale level and merge level resulted in a higher number of extracted object boundaries for each resampled UAV image. A higher scale and merge level resulted in fewer extracted boundaries (Figure 4). In general, for all resampling, the biggest drop in the number of extracted object boundaries was at scale level values within the range from 70 to 80, and merge level values within the range from 95 to 99 (Figure 4). The incremental value of 1, for merge level 95–99, turned out to be very sensitive in dropping the number of extracted object boundaries (Figure 4a–c).

The optimal scale and merge levels for an automatic boundary delineation were investigated by filtering out the total number of extracted objects with the minimum area of objects from the reference data. The results of this filtering approach are presented in Figure 6. The results showed that for the UAV orthoimages of higher spatial resolutions, namely a GSD of 25 cm, the optimal algorithm values for cadastral mapping resulted in 80 for scaling and from 95 to 99 for merging. In contrast, for the UAV orthoimages having a GSD of 50 cm and a GSD of 100 cm, the common optimal scale level values were 70–80 and merge level 95–98 (Figure 6). Some exceptions were observed for a GSD of 50 cm, where the scale level was 50, 60, and merge level to its maximum. In general, the results showed that the optimal scale and merge level values suitable for cadastral mapping range from 70 to 80 and from 95 to 99, respectively (examples in Figure 5). The optimal scale and merge level values appeared similar as in the investigation of the influence of different GSDs in extracting objects.

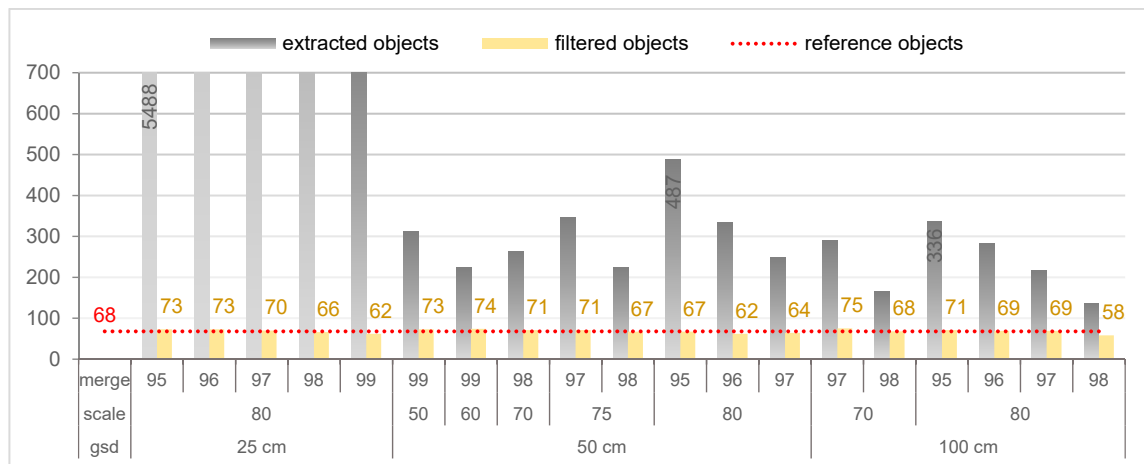


Figure 6. Comparison in the number of extracted and filtered objects using different scale and merge parameter values, to the number of objects identified in the reference data set.

For further analysis, optimal extracted objects with scale level 80 and merge level 95 for three GSDs of UAV orthoimages were selected (Figure 7a,c,e). The selection was based on common scale and merge levels for three GSDs as well on the highest number of filtered objects per GSD (Figure 6). The filtering approach was additionally applied to the selected optimal extracted objects, i.e., with scale level 80 and merge level 95, to remove objects under the minimum reference object area (Figure 7b,d,f).

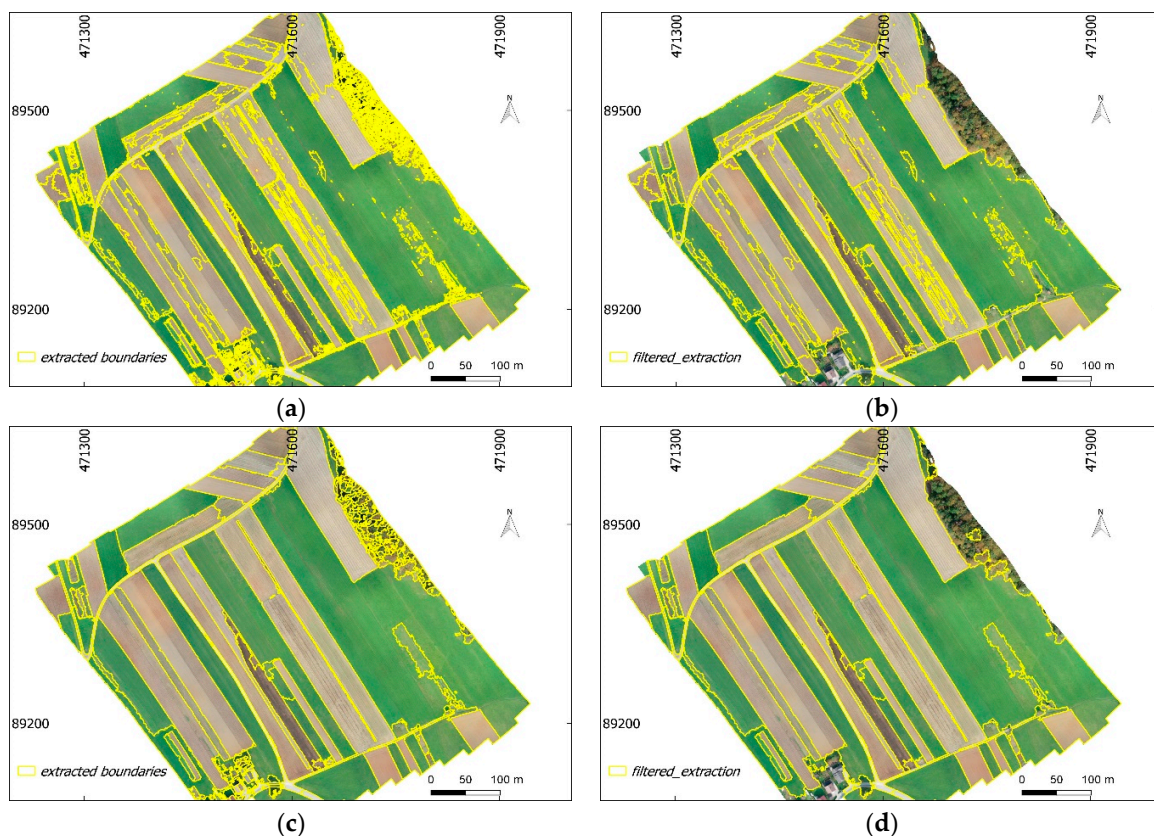


Figure 7. Cont.

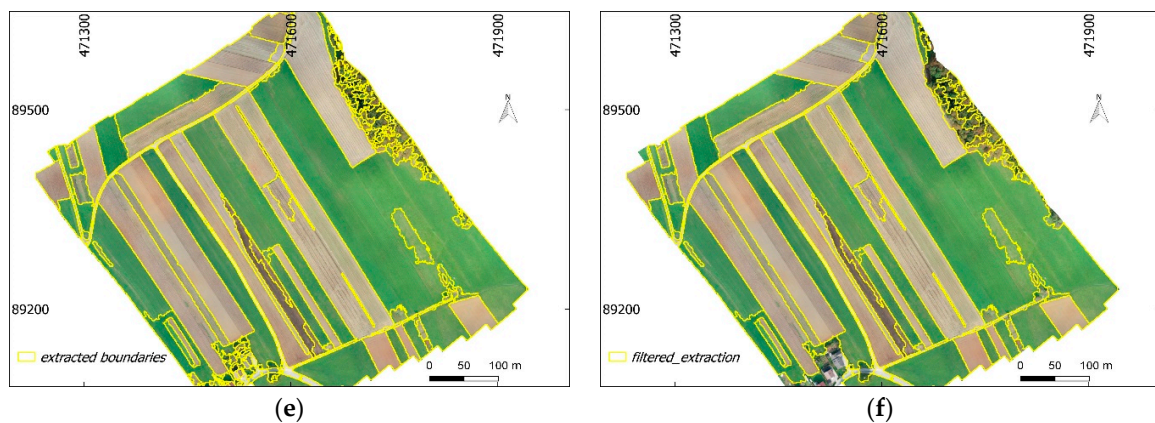


Figure 7. (a,c,e) Extracted objects at scale level 80 and merge level 95 for (a) GSD 25 cm, (c) GSD 50 cm, and (e) GSD 100 cm. (b,d,f) Filtered objects of scale level 80 and merge level 95 based on minimum object area from the reference data.

A simplification algorithm was applied to both extracted objects and filtered objects. The results showed that if extracted objects are smoothed and smoothed objects are later simplified, the localization of simplified objects is almost equal to that of the extracted ones (Figure 8). The initial tests show that possible shifts in location are possible when a direct implementation of the simplification algorithm to extracted visible objects is used.

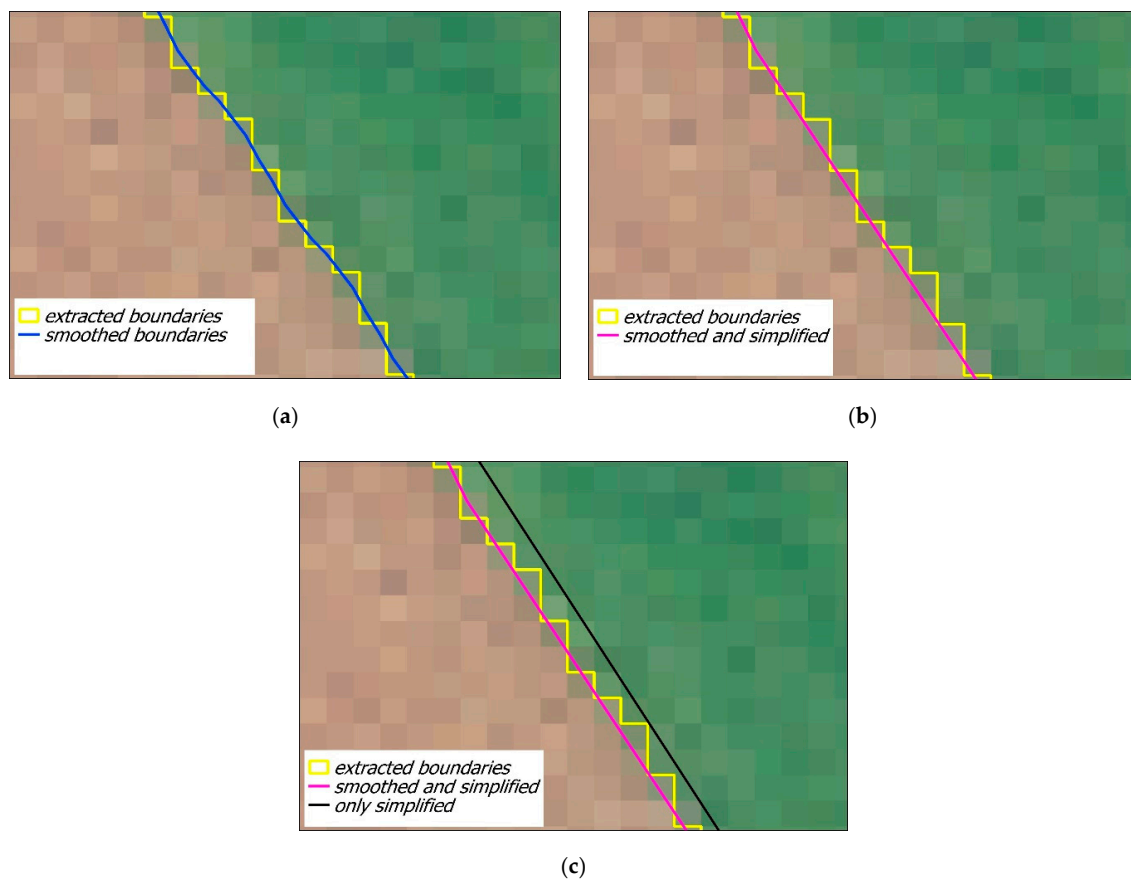


Figure 8. (a) Extracted objects smoothed by making use of the Snakes algorithm. (b) Simplification of extracted objects by making use of the Snakes smoothing algorithm and Douglas–Peucker simplification algorithm. (c) Extracted objects simplified with Douglas–Peucker algorithm (in black) and compared to object simplifications on (b).

The buffer overlay method was used for the accuracy assessment. The accuracy assessment method was applied to the extracted objects, simplified extracted objects, filtered objects and simplified filtered objects. The results show that there is no significant difference in accuracy assessment results when comparing extracted and simplified objects (Table 3, Table 4, and Table 5). At a buffer width of 2 m, a GSD of 50 cm and a GSD of 100 cm provide a higher percentage of correctly extracted objects compared to a GSD of 25 cm. The percentage of correctly extracted objects was 66% for both a GSD of 50 cm and a GSD of 100 cm (Tables 4 and 5). However, the filtering approach contributed to the increased correctness (decreased completeness) and overall quality, for all GSDs. From the filtered objects, the best results for correctness were recorded at a GSD of 50 cm (Figure 9). The percentage indicated the correctness was 77%, while for the completeness it was 67%.

Table 3. Accuracy assessment of boundary extractions for a GSD of 25 cm, scale 80, merge 95.

| Buffer width [cm] | Completeness [%] | | Correctness [%] | | Quality [%] | |
|----------------------|----------------------------|----------------------------|----------------------------|----------------------------|----------------------------|----------------------------|
| | Extracted | Filtered | Extracted | Filtered | Extracted | Filtered |
| 25 | 58 | 37 | 18 | 26 | 16 | 20 |
| 50 | 73 | 48 | 28 | 39 | 26 | 31 |
| 100 | 78 | 56 | 38 | 50 | 36 | 41 |
| 200 | 81 (81)¹ | 61 (62)¹ | 48 (49)¹ | 59 (61)¹ | 46 (46)¹ | 50 (48)¹ |

¹ Percentages of simplified boundaries.

Table 4. Accuracy assessment of boundary extractions for a GSD of 50 cm, scale 80, merge 95.

| Buffer width [cm] | Completeness [%] | | Correctness [%] | | Quality [%] | |
|----------------------|----------------------------|----------------------------|----------------------------|----------------------------|----------------------------|----------------------------|
| | Extracted | Filtered | Extracted | Filtered | Extracted | Filtered |
| 25 | 45 | 40 | 28 | 35 | 21 | 23 |
| 50 | 64 | 55 | 46 | 56 | 38 | 41 |
| 100 | 71 | 61 | 57 | 68 | 48 | 52 |
| 200 | 75 (74)¹ | 65 (67)¹ | 65 (66)¹ | 76 (77)¹ | 56 (53)¹ | 59 (56)¹ |

¹ Percentages of simplified boundaries.

Table 5. Accuracy assessment of boundary extractions for a GSD of 100 cm, scale 80, merge 95.

| Buffer Width [cm] | Completeness [%] | | Correctness [%] | | Quality [%] | |
|----------------------|----------------------------|----------------------------|----------------------------|----------------------------|----------------------------|----------------------------|
| | Extracted | Filtered | Extracted | Filtered | Extracted | Filtered |
| 25 | 31 | 27 | 21 | 24 | 14 | 15 |
| 50 | 53 | 47 | 39 | 43 | 29 | 30 |
| 100 | 67 | 59 | 58 | 64 | 47 | 47 |
| 200 | 73 (71)¹ | 63 (67)¹ | 66 (66)¹ | 72 (73)¹ | 55 (52)¹ | 55 (52)¹ |

¹ Percentages of simplified boundaries.

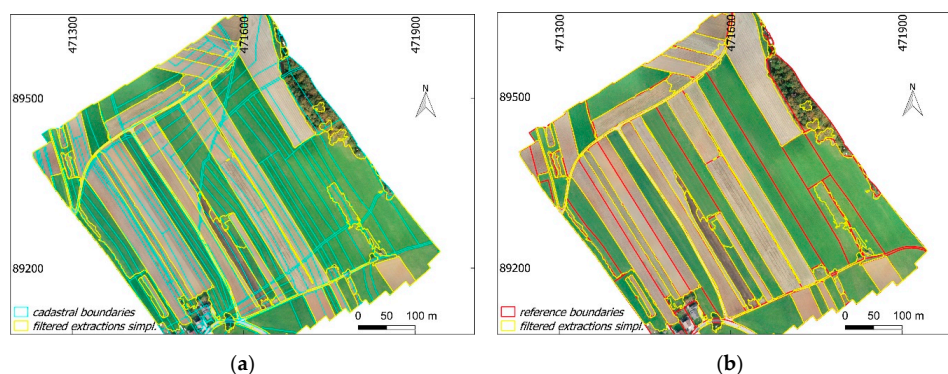


Figure 9. (a,b) Filtered objects of scale level 80 and merge level 95—simplified, compared with (a) cadastral map and (b) manually delineated visual object boundaries used as reference data.

4. Discussion

4.1. The Developed Workflow

The developed workflow aimed to provide a solution for UAV-based cadastral mapping using automatic visible boundary extraction with the ENVI FX module (Figure 2). The developed workflow consisted of four steps: (i) image pre-processing, (ii) boundary detection and extraction, (iii) data post-processing, and (iv) accuracy assessment.

The first workflow step includes resampling of a UAV orthoimage. Here, the results of our case study showed that larger GSDs provided faster and fewer extractions of visible object boundaries compared to the original GSD of a UAV orthoimage. For higher spatial resolutions, i.e., smaller GSDs, considering the selected Scale level and Merge level values, the total number of extracted objects was higher.

The second step, which includes object boundary detection and extraction, is dependent on the scale and merge level. The results, presented in Figure 4, showed that lower values of scale and merge levels resulted in a higher number of extracted objects, which led to over-segmentation by reaching thousands of extracted objects. Considering the total number of the reference objects, it is important to note that a scale and a merge level that provide object extractions close to the total number of objects from reference data are important for automatic delineation of visible cadastral boundaries.

The following step, data post-processing, aimed to investigate optimal scale and merge levels and to simplify the extracted objects. The optimal values based on a filtering approach showed that for all tested GSDs in this study, most suitable scale and merge level values for automatic delineation of visible cadastral boundaries were 70–80 and 95–99, respectively. These values can be considered as optimal scale and merge levels for rural areas in general or areas with characteristics similar to the study area of this research. However, to validate the proposed workflow and optimal Scale and Merge levels in areas with different characteristics, such as areas with a larger number of buildings or areas with trees covering parts of boundaries, further experiments are needed. Hence, the scale and merging levels appropriate for cadastral mapping have been determined and this step can be skipped from the workflow step of data post-processing (Figure 2). The use of the Snakes algorithm for smoothing and the Douglas–Peucker algorithm for simplifying has been shown to be very effective (Figure 8a,b). This approach, when combining both smoothing and simplification algorithms, gives better results in terms of a simplified boundary position compared to directly implementing the Douglas–Peucker simplification algorithm, where undesired shifting in boundary position was observed (Figure 8c). In [22], it was reported that the direct implementation of the Douglas–Peucker algorithm was used as a post-processing method in many papers to improve the output by optimizing the shape of objects. However, the simplification approach applied in this study was not examined in the previous papers.

The final step of the workflow was accuracy assessment (see also Section 4.2). The accuracy assessment was based on the buffer overlay method. By increasing the width of the buffer, more extracted boundaries appear to be within the buffer area, which impacts the completeness, correctness, and the overall quality—larger the buffer, the better the results. To have a uniform assessment for all tested GSDs the results were compared at a buffer distance of 2 m. From the reviewed publications presented in Section 1.2, a buffer width of 2 m was also applied in [26–28] as most suitable for the presentation of accuracy assessment results and to avoid uncertainties from resampling effects. However, for comparison to cadastral data, buffer widths should be based on local accuracy requirements [26].

The workflow developed, overall, is in accordance with the general workflow for the cadastral mapping based on suitable computer vision methods for automatic visible boundary extraction provided in [22]. In addition, it provides an additional step and method in data post-processing, such as filtering out irrelevant and small objects from the boundary map, which improves overall quality assessment. Furthermore, it suggests a combined approach for the simplification of extracted object boundaries.

4.2. Quality Assessment

Bringing the scale and merge levels to the maximum resulted in some unextracted and fewer visible objects for the whole extent of the image. Although some of the visible objects were left unextracted, the maximum scale and merge level enabled the detection of a group of objects such as a group of tree boundaries, especially at GSDs of 50 cm and 100 cm (Figure 5f,i). In both cases, the balance between completeness and correctness was hard to achieve. This issue was also reported in [26,28]. For this reason, the filtering approach was applied. It was based on the minimum object size as well as on the total number of the objects, both defined based on the reference data. This allowed us to reduce the risk that some of the visible object boundaries remained unextracted as well as over-segmented.

The optimal scale level of 80 and a merge level of 95, were chosen for all three GSDs, to investigate the impact of the same scale and merge level in different resampling. The selection was based on common scale and merge levels per GSD (Figure 6). However, this does not mean that the chosen scale and merge level provided the best object boundary extraction for each of the GSDs. For instance, for small GSDs, the correctness of extracted boundaries is higher at the maximum scale and merge levels (e.g., Figure 5c). For the same scale and merge level, the correctness grows significantly from a GSD of 25 cm to a GSD of 50 cm. The correctness for a GSD of 100 cm was almost equal to the one for a GSD of 50 cm. Considering that more optimal scale and merge levels were applicable for a GSD of 50 cm (Figure 6) and the difference insignificant when compared to the results obtained for a GSD of 100 cm, a GSD of 50 cm appeared to be better in detecting visible boundaries compared to the other two GSDs.

The quantitative method applied for accuracy assessment to automatically extracted objects, filtered objects and to their simplifications, showed that there was no significant difference between extracted objects and simplified objects. This result indicates that the method applied for simplification can be considered appropriate, i.e., the original location of extracted objects was maximally maintained. Although there was no difference in accuracy assessment, the simplification of extracted (or filtered) objects is significant for proper cadastral mapping. Cadastral boundaries usually are defined by straight lines with fewer vertices.

The percentage of suitable extracted boundaries (compared to reference data), for a scale level of 80 and a merge level of 95, resulted in 74% for the assessment of the completeness and 66% for the assessment of the correctness for the extracted object boundaries having a GSD of 50 cm. However, the filtering approach strongly influenced the accuracy assessment. For filtered extractions, the level of completeness was 67%, and the level of correctness was 77%. These results show that the filtering approach increased the correctness of automatically extracted boundaries, and it reaches almost 80% (Table 4). This was due to filtering out small object boundaries from the boundary map. The excluded small objects were mostly present in tree and built-up areas on the UAV orthoimage, i.e., only outlines of group objects were retained (Figure 7c,d). In road extractions, the achieved values for extractions are around 85% for correctness and around 70% for completeness to be of real practical importance [26,34]. Such percentages can hardly be achieved by the workflow developed for automatic delineation of all visible boundaries since the morphology of cadastral boundaries is usually more complex and not all cadastral boundaries are visible, unlike road boundaries.

The accuracy assessment was based on the manually delineated boundaries, which were defined as reference data (Figure 1b). The visible boundaries were manually delineated on the ground truth UAV orthoimage. It is argued that manually delineated boundaries influence the overall results of the accuracy assessment since different human operators might digitize differently [26]. However, in the selected case study, most of the object boundaries were sharp and the presence of white stones at outlines of the agricultural field contributed to the objectivity of manual digitalization. In addition, the real cadastral data could not be used since they did not correspond with the object boundaries on the image (Figure 1a) and it would not have been possible to outline the potential of the ENVI FX. However, the approach of automatic extraction of visible boundaries is case dependent. To reliably avoid the influence of manually digitized reference data, the following studies should consider a case study where the cadastral map is up to date.

4.3. Strengths and Limitations of the Automatic Extraction Method Used

The ENVI FX module handled the full extent of the resampled UAV orthoimages, and no additional image tiling or image conversions were required. ENVI FX provided closed object boundaries directly in vector format, topologically correct polygons. Therefore, no additional image post-processing step, such as vectorization of detected object boundaries, was needed (Figure 5). Thus, the visible object boundaries generated can be directly used for further processing and analysis within geographic information systems (GIS). Additionally, the final output consists of spatial, spectral and textural attributes which are assigned automatically to each extracted object and saved in the attribute table. The vectorized and geo-referenced visible object boundaries, as interpreted in this research, are crucial in cadastral applications especially for the purposes of land plot boundary delineations. Overall, ENVI FX has the potential to automatically delineate visible cadastral boundaries, especially in rural areas.

A comparison of the results regarding the accuracy assessment obtained in this study and the accuracies obtained in the studies [26–28] cannot be done at this time for a number of reasons. First, not all the reviewed feature extraction methods have been applied to UAV imagery. Second, different UAVs may provide different quality of orthoimages. Third, the nature, size, location, and the characteristics of the study objects are far too different. In order to make a reliable comparison on accuracy assessments of different feature extraction methods, first of all, each method has to be studied individually and later tested at the same study area(s). However, the image processing approach of different feature extractions methods may be comparable.

From the reviewed feature extraction methods that have already been applied for detection of visible cadastral boundaries, it can be seen that the MRS method, ESP method, and mean-segmentation method also do not require further image tiling and the final output of the boundary map was in vector format [27,28]. In contrast, vectorization of detected object boundaries was needed for the gPb contour detection method. In addition, it was reported that the method is inapplicable when processing UAV images of more than 1000 pixels in width and height [26]. Similar issues regarding the vectorization of detected object boundaries were reported in [38], where Canny and Sobel edge detection algorithms were used. In order to obtain topologically correct polygons, an additional feature extraction method was used aiming to connect the edges.

ENVI FX allowed some shadow areas in the UAV orthoimage to be extracted as boundaries; however, these do not represent real boundaries in the field. In order to minimize the influence of shadows on feature extraction, it is recommended to capture images in the local time where the solar zenith angle has the smallest possible value. However, the solar zenith angle depends on the geographic location of the study area. Additionally, some other factors such as weather conditions also influence the quality of captured images. To avoid such issues, it is preferable to capture images on a cloudy day without wind. Although ENVI FX has proved to be efficient, one of its limitations is that it is not an open-source tool like mean-shift segmentation, gPb contour detection, Canny, and Sobel, which might be a reason why it is not often used in the land surveyor community. In addition, the extracted objects from the resampled UAV orthoimages were following the pixel borders and further shape simplification was required to make them comparable to spatial units in cadastral applications.

Considering that the morphology of cadastral boundaries is complex [7], compared to physical boundaries, such as boundaries of roads or rivers, delineation of cadastral boundaries cannot be fully automated at this time, and additionally, the verification of the results has to be done with the participation of landowners and other land rights holders. The limitations on extracting only visible object boundaries lie in the fact that not all visible boundaries (land cover boundaries) represent cadastral boundaries (land right boundaries). For instance, when two agricultural cadastral units leased to the same farmer are farmed as one unit, and vice versa. However, visible object boundaries which coincide with the land right boundaries can be automatically detected and used in cadastral applications. In addition, the UAV-based spatial data acquisition is usually affected by special operational regulations that restrict the use of this technology, in particular in urban areas [18].

4.4. Applicability of the Developed Workflow

The developed workflow provided geo-referenced boundary maps in a format compliant with the formats that are used in GIS environments. This shows that the extracted objects can be easily transferable, and applicable in GIS for cadastral purposes. In cases where cadastral maps are rarely present and the concept of fit-for-purpose cadastre is in place, the workflow, with the selected method for automatic extraction of visible boundaries, shows the potential for the automation of the visible cadastral boundary delineation procedure [1]. Thus, the approach developed generally contributes to the acceleration and facilitation of the creation of cadastral maps (Figure 9b), especially in developing countries, where general boundaries are accepted, and positional accuracy is of lesser importance [25]. However, the approach is suitable for the areas where the boundaries of physical objects are visibly detectable on a UAV orthoimage, for instance, in rural areas. The workflow might be applicable for both the creation and updating/revision of cadastral maps, similar to the manual delineations of cadastral boundaries on a UAV orthoimage. In addition, the workflow developed might lower the costs and time compared to the manual delineation of cadastral boundaries, especially in rural areas [26].

Furthermore, in developed countries, the approach based on automatic extraction of visible boundaries might be used for a revision of current cadastral maps (Figure 9a). In this case, the extracted visible boundaries can be used as a basis for a new cadastral survey or land rearrangements, depending on the discrepancy between cadastral maps and land possession (as shown in the case study). Although the beneficiaries agree with the visible boundaries, if higher accuracy is required, the revised objects (spatial units) can later be manually delineated from a UAV orthoimage or re-surveyed with ground-based surveying techniques. It must be emphasized that the extracted visible boundaries, both for the creation of cadastral maps and updating, should be inspected by the local community and all beneficiaries (landowners, other land rights holders) in order to be legally validated.

5. Conclusions

The overall aim of this study was to provide an UAV-based cadastral mapping workflow based on the ENVI FX module for automatic detection of visible boundaries. The study first investigated, which processing steps are required for a cadastral mapping workflow following the potential and limitations of the ENVI FX for automatic visible boundary detection and extraction.

The results showed that more correct visible object boundaries, suitable for the interpretation of land cover (cadastral) boundaries, were extracted at larger values of GSD. In addition, the identified optimal scale and merge levels for detection and extraction of visible cadastral boundaries were between 70 and 80 and 95 and 99, respectively. The identification of the optimal parameters for cadastral mapping was based on the defined minimum object area and the total number of objects from the reference data using the so-called filtering approach. The filtering approach contributed to the increased correctness of automatically extracted boundaries. The best results were recorded at the resampled UAV orthoimage with a GSD of 50 cm, and the percentage of correctness indicated was 77%, while for the completeness it was 67%. It must be emphasized that the workflow developed is applicable mostly for rural areas where the number of visible boundaries is higher compared to complex urban areas.

The workflow can be used in developing countries to accelerate and facilitate the creation of cadastral maps aiming to formalize a land tenure system and guarantee legal security to land rights holders. In developed countries, the extracted visible boundaries based on this workflow might be used for efficient revision of existing cadastral maps. However, in both cases, the extracted visible boundaries have to be validated by landowners and other beneficiaries. The extraction of visible objects can be considered as only one step in the facilitation of cadastral mapping, as extracting these is not enough for complete and correct cadastral mapping. It is worth highlighting that cadastral boundaries may, in fact, be completely inside the property and that some boundaries between properties may not be clearly visible. In order to use the proposed workflow in the cadastral domain, the approach can be expanded. Additional steps should focus on methods for the possible involvement of current

landowners in the process of cadastral mapping. The extension of the current workflow is one of the aims of the authors' further research.

Author Contributions: Conceptualization, B.F. and A.L.; methodology, B.F., K.O. and A.L.; software, B.F.; validation, B.F., K.O. and A.L.; formal analysis and data processing, B.F.; investigation, B.F.; resources, B.F., A.L., K.O. and M.K.F.; writing—original draft preparation, B.F.; writing—review and editing, B.F., A.L., K.O. and M.K.F.; visualization, B.F.; supervision, A.L.

Funding: The authors acknowledge the financial support of the Slovenian Research Agency (research core funding No. P2-0406 Earth observation and geoinformatics).

Acknowledgments: We acknowledge Klemen Kozmus Trajkovski and Albin Mencin for capturing the UAV data and for the technical support during the fieldwork.

Conflicts of Interest: The authors declare no conflict of interest.

Abbreviations

The following abbreviations are used in this article:

| | |
|------|---------------------------------------|
| DSM | Digital Surface Model |
| ESP | Estimation of Scale Parameter |
| FIG | International Federation of Surveyors |
| FN | False Negative |
| FP | False Positive |
| FX | ENVI Feature Extraction |
| GCP | Ground Control Point |
| GIS | Geographic Information System |
| GNSS | Global Navigation Satellite System |
| gPb | Global Probability of Boundary |
| GSD | Ground Sample Distance |
| HRSI | High-Resolution Satellite Imagery |
| MRS | Multi-Resolution Segmentation |
| PDOP | Position Dilution of Precision |
| RMSE | Root-Mean-Square-Error |
| RTK | Real-Time Kinematic |
| SLIC | Simple Linear Iterative Clustering |
| TP | True Positive |
| UAV | Unmanned Aerial Vehicle |

References

1. Enemark, S. International Federation of Surveyors. In *Fit-For-Purpose Land Administration: Joint FIG/World Bank Publication*; FIG: Copenhagen, Denmark, 2014; ISBN 978-87-92853-10-3.
2. Luo, X.; Bennett, R.; Koeva, M.; Lemmen, C.; Quadros, N. Quantifying the Overlap between Cadastral and Visual Boundaries: A Case Study from Vanuatu. *Urban Sci.* **2017**, *1*, 32. [\[CrossRef\]](#)
3. Zevenbergen, J. A Systems Approach to Land Registration and Cadastre. *Nord. J. Surv. Real Estate Res.* **2004**, *1*, 11–24.
4. Simbizi, M.C.D.; Bennett, R.M.; Zevenbergen, J. Land tenure security: Revisiting and refining the concept for Sub-Saharan Africa's rural poor. *Land Use Policy* **2014**, *36*, 231–238. [\[CrossRef\]](#)
5. *Land Administration for Sustainable Development*, 1st ed.; Williamson, I.P. (Ed.) ESRI Press Academic: Redlands, CA, USA, 2010; ISBN 978-1-58948-041-4.
6. Zevenbergen, J.A. *Land Administration: To See the Change from Day to Day*; ITC: Enschede, The Netherlands, 2009; ISBN 978-90-6164-274-9.
7. Luo, X.; Bennett, R.M.; Koeva, M.; Lemmen, C. Investigating Semi-Automated Cadastral Boundaries Extraction from Airborne Laser Scanned Data. *Land* **2017**, *6*, 60. [\[CrossRef\]](#)
8. Enemark, S. Land Administration and Cadastral Systems in Support of Sustainable Land Governance—A Global Approach. In *Proceedings of the Re-Engineering the Cadastre to Support E-Government*, Tehran, Iran, 4–26 May 2009.

9. Maurice, M.J.; Koeva, M.N.; Gerke, M.; Nex, F.; Gevaert, C. A Photogrammetric Approach for Map Updating Using UAV in Rwanda. Available online: <https://bit.ly/2FyhbEi> (accessed on 25 June 2019).
10. Wayumba, R.; Mwangi, P.; Chege, P. Application of Unmanned Aerial Vehicles in Improving Land Registration in Kenya. *Int. J. Res. Eng. Sci.* **2017**, *5*, 5–11.
11. Ramadhani, S.A.; Bennett, R.M.; Nex, F.C. Exploring UAV in Indonesian cadastral boundary data acquisition. *Earth Sci. Inform.* **2018**, *11*, 129–146. [[CrossRef](#)]
12. Mumbone, M.; Bennet, R.; Gerke, M. Innovations in Boundary Mapping: Namibia, Customary Lands and UAVs. In Proceedings of the Linking Land Tenure and Use for Shared Prosperity, Washington, DC, USA, 23–27 March 2015; p. 22.
13. Volkmann, W.; Barnes, G. Virtual Surveying: Mapping and Modeling Cadastral Boundaries Using Unmanned Aerial Systems (UAS). In Proceedings of the FIG Congress 2014, Kuala Lumpur, Malaysia, 16–21 June 2014; p. 13.
14. Rijdsdijk, M.; van Hinsbergh, W.H.M.; Witteveen, W.; ten Buuren, G.H.M.; Schakelaar, G.A.; Poppinga, G.; van Persie, M.; Ladiges, R. Unmanned Aerial Systems in the process of Juridical verification of Cadastral borde. *ISPRS Int. Arch. Photogramm. Remote Sens. Spat. Inf. Sci.* **2013**, *XL-1/W2*, 325–331. [[CrossRef](#)]
15. Mesas-Carrascosa, F.J.; Notario-García, M.D.; Meroño de Larriva, J.E.; Sánchez de la Orden, M.; García-Ferrer Porras, A. Validation of measurements of land plot area using UAV imagery. *Int. J. Appl. Earth Obs. Geoinf.* **2014**, *33*, 270–279. [[CrossRef](#)]
16. Manyoky, M.; Theiler, P.; Steudler, D.; Eisenbeiss, H. Unmanned Aerial Vehicle in Cadastral Applications. *ISPRS Int. Arch. Photogramm. Remote Sens. Spat. Inf. Sci.* **2012**, *XXXVIII-1/C22*, 57–62. [[CrossRef](#)]
17. Kurczynski, Z.; Bakuła, K.; Karabin, M.; Kowalczyk, M.; Markiewicz, J.S.; Ostrowski, W.; Podlasiak, P.; Zawieska, D. The possibility of using images obtained from the UAS in cadastral works. *ISPRS Int. Arch. Photogramm. Remote Sens. Spat. Inf. Sci.* **2016**, *XLI-B1*, 909–915. [[CrossRef](#)]
18. Cramer, M.; Bovet, S.; Gültlinger, M.; Honkavaara, E.; McGill, A.; Rijdsdijk, M.; Tabor, M.; Tournadre, V. On the use of RPAS in National Mapping—The EuroSDR point of view. *ISPRS Int. Arch. Photogramm. Remote Sens. Spat. Inf. Sci.* **2013**, *XL-1/W2*, 93–99. [[CrossRef](#)]
19. Binns, B.O.; Dale, P.F. Cadastral Surveys and Records of Rights in Land. Available online: <http://www.fao.org/3/v4860e/v4860e03.htm> (accessed on 20 March 2019).
20. Watts, A.C.; Ambrosia, V.G.; Hinkley, E.A. Unmanned Aircraft Systems in Remote Sensing and Scientific Research: Classification and Considerations of Use. *Remote Sens.* **2012**, *4*, 1671–1692. [[CrossRef](#)]
21. Colomina, I.; Molina, P. Unmanned aerial systems for photogrammetry and remote sensing: A review. *ISPRS J. Photogramm. Remote Sens.* **2014**, *92*, 79–97. [[CrossRef](#)]
22. Crommelinck, S.; Bennett, R.; Gerke, M.; Nex, F.; Yang, M.; Vosselman, G. Review of Automatic Feature Extraction from High-Resolution Optical Sensor Data for UAV-Based Cadastral Mapping. *Remote Sens.* **2016**, *8*, 689. [[CrossRef](#)]
23. Heipke, C.; Woodsford, P.A.; Gerke, M. Updating geospatial databases from images. In *Advances in Photogrammetry, Remote Sensing and Spatial Information Sciences: 2008 ISPRS Congress Book*; Baltsavias, E., Li, Z., Chen, J., Eds.; CRC Press: London, UK, 2008.
24. Bennett, R.; Kitchingman, A.; Leach, J. On the nature and utility of natural boundaries for land and marine administration. *Land Use Policy* **2010**, *27*, 772–779. [[CrossRef](#)]
25. Zevenbergen, J.; Bennett, R. The visible boundary: More than just a line between coordinates. In Proceedings of the GeoTech Rwanda, Kigali, Rwanda, 18–20 November 2015; pp. 1–4.
26. Crommelinck, S.; Bennett, R.; Gerke, M.; Yang, M.; Vosselman, G. Contour Detection for UAV-Based Cadastral Mapping. *Remote Sens.* **2017**, *9*, 171. [[CrossRef](#)]
27. Wassie, Y.A.; Koeva, M.N.; Bennett, R.M.; Lemmen, C.H.J. A procedure for semi-automated cadastral boundary feature extraction from high-resolution satellite imagery. *J. Spat. Sci.* **2018**, *63*, 75–92. [[CrossRef](#)]
28. Kohli, D.; Crommelinck, S.; Bennett, R. Object-Based Image Analysis for Cadastral Mapping Using Satellite Images. In *Proceedings of the International Society for Optics and Photonics, Image Signal Processing Remote Sensing XXIII*; SPIE. The International Society for Optical Engineering: Warsaw, Poland, 2017.
29. Kohli, D.; Unger, E.-M.; Lemmen, C.; Koeva, M.; Bhandari, B. Validation of a cadastral map created using satellite imagery and automated feature extraction techniques: A case of Nepal. In Proceedings of the FIG Congress 2018, Istanbul, Turkey, 6–11 May 2018; p. 17.

30. Singh, P.P.; Garg, R.D. Road Detection from Remote Sensing Images using Impervious Surface Characteristics: Review and Implication. *ISPRS Int. Arch. Photogramm. Remote Sens. Spat. Inf. Sci.* **2014**, XL-8, 955–959. [[CrossRef](#)]
31. Kumar, M.; Singh, R.K.; Raju, P.L.N.; Krishnamurthy, Y.V.N. Road Network Extraction from High Resolution Multispectral Satellite Imagery Based on Object Oriented Techniques. *ISPRS Ann. Photogramm. Remote Sens. Spat. Inf. Sci.* **2014**, II-8, 107–110. [[CrossRef](#)]
32. Wang, J.; Qin, Q.; Gao, Z.; Zhao, J.; Ye, X. A New Approach to Urban Road Extraction Using high-resolution aerial image. *ISPRS Int. J. Geo-Inf.* **2016**, 5, 114. [[CrossRef](#)]
33. Paravolidakis, V.; Ragia, L.; Moirogiorgou, K.; Zervakis, M. Automatic Coastline Extraction Using Edge Detection and Optimization Procedures. *Geosciences* **2018**, 8, 407. [[CrossRef](#)]
34. Mayer, H.; Hinz, S.; Bacher, U.; Baltsavias, E. A test of Automatic Road Extraction approaches. *ISPRS Int. Arch. Photogramm. Remote Sens. Spat. Inf. Sci.* **2006**, 36, 209–214.
35. Dey, V.; Zhang, Y.; Zhong, M. A review of image segmentation techniques with remote sensing perspective. In Proceedings of the ISPRS TC VII Symposium, Vienna, Austria, 5–7 July 2010; Volume XXXVIII. Part 7a.
36. Mueller, M.; Segl, K.; Kaufmann, H. Edge- and region-based segmentation technique for the extraction of large, man-made objects in high-resolution satellite imagery. *Pattern Recognit.* **2004**, 37, 1619–1628. [[CrossRef](#)]
37. Crommelinck, S.; Höfle, B.; Koeva, M.N.; Yang, M.Y.; Vosselman, G. Interactive Cadastral Boundary Delineation from UAV data. *ISPRS Ann. Photogramm. Remote Sens. Spat. Inf. Sci.* **2018**, IV-2, 81–88. [[CrossRef](#)]
38. Babawuro, U.; Zou, B. Satellite Imagery Cadastral Features Extractions using Image Processing Algorithms: A Viable Option for Cadastral Science. *IJCSI Int. J. Comput. Sci. Issues* **2012**, 9, 30–38.
39. Wang, J.; Song, J.; Chen, M.; Yang, Z. Road network extraction: A neural-dynamic framework based on deep learning and a finite state machine. *Int. J. Remote Sens.* **2015**, 36, 3144–3169. [[CrossRef](#)]
40. Poursanidis, D.; Chrysoulakis, N.; Mitraka, Z. Landsat 8 vs. Landsat 5: A comparison based on urban and peri-urban land cover mapping. *Int. J. Appl. Earth Obs. Geoinf.* **2015**, 35, 259–269. [[CrossRef](#)]
41. *ITT Visual Information Solutions ENVI Feature Extraction User's Guide*; Harris Geospatial Solutions: Broomfield, CO, USA, 2008.
42. The Surveying and Mapping Authority of the Republic of Slovenia e-Surveying Data. Available online: <https://egp.gu.gov.si/egp/?lang=en> (accessed on 29 May 2019).
43. Jin, X. Segmentation-Based Image Processing System. U.S. Patent 8,260,048, 4 September 2012.
44. ENVI Segmentation Algorithms Background. Available online: <https://www.harrisgeospatial.com/docs/backgroundsegmentationalgorithm.html#Referenc> (accessed on 21 March 2019).
45. ENVI Merge Algorithms Background. Available online: <https://www.harrisgeospatial.com/docs/backgroundmergealgorithms.html> (accessed on 21 March 2019).
46. ENVI Development Team. *ENVI The Leading Geospatial Analytics Software*; Harris Geospatial Solutions: Broomfield, CO, USA, 2018.
47. Extract Segments Only. Available online: <https://www.harrisgeospatial.com/docs/segmentonly.html> (accessed on 25 March 2019).
48. QGIS Development Team. *QGIS a Free and Open Source Geographic Information System, Version 2.18*; Las Palmas de, G.C., Ed.; Open Source Geospatial Foundation: Beaverton, OR, USA, 2018.
49. GRASS GIS Development Team. *GRASS GIS Bringing Advanced Geospatial Technologies to the World, Version 7.4.2*; Open Source Geospatial Foundation: Beaverton, OR, USA, 2018.
50. Heipke, C.; Mayer, H.; Wiedemann, C. Evaluation of Automatic Road Extraction. *Int. Arch. Photogramm. Remote Sens.* **1997**, 32, 151–160.



APPENDIX D : Deep Learning for Detection of Visible Land Boundaries from UAV Imagery

B. Fetai, M. Račič, and A. Liseč (2021)

Remote sensing vol. 13, no. 11, p. 2077

doi: 10.3390/rs13112077



Article

Deep Learning for Detection of Visible Land Boundaries from UAV Imagery

Bujar Fetai *, Matej Račič and Anka Lisec

Faculty of Civil and Geodetic Engineering, University of Ljubljana, Jamova Cesta 2, 1000 Ljubljana, Slovenia; matej.racic@fgg.uni-lj.si (M.R.); anka.lisec@fgg.uni-lj.si (A.L.)

* Correspondence: bujar.fetai@fgg.uni-lj.si; Tel.: +386-1-4768629

Abstract: Current efforts aim to accelerate cadastral mapping through innovative and automated approaches and can be used to both create and update cadastral maps. This research aims to automate the detection of visible land boundaries from unmanned aerial vehicle (UAV) imagery using deep learning. In addition, we wanted to evaluate the advantages and disadvantages of programming-based deep learning compared to commercial software-based deep learning. For the first case, we used the convolutional neural network U-Net, implemented in Keras, written in Python using the TensorFlow library. For commercial software-based deep learning, we used ENVINet5. UAV imageries from different areas were used to train the U-Net model, which was performed in Google Collaboratory and tested in the study area in Odranci, Slovenia. The results were compared with the results of ENVINet5 using the same datasets. The results showed that both models achieved an overall accuracy of over 95%. The high accuracy is due to the problem of unbalanced classes, which is usually present in boundary detection tasks. U-Net provided a recall of 0.35 and a precision of 0.68 when the threshold was set to 0.5. A threshold can be viewed as a tool for filtering predicted boundary maps and balancing recall and precision. For equitable comparison with ENVINet5, the threshold was increased. U-Net provided more balanced results, a recall of 0.65 and a precision of 0.41, compared to ENVINet5 recall of 0.84 and a precision of 0.35. Programming-based deep learning provides a more flexible yet complex approach to boundary mapping than software-based, which is rigid and does not require programming. The predicted visible land boundaries can be used both to speed up the creation of cadastral maps and to automate the revision of existing cadastral maps and define areas where updates are needed. The predicted boundaries cannot be considered final at this stage but can be used as preliminary cadastral boundaries.



Citation: Fetai, B.; Račič, M.; Lisec, A. Deep Learning for Detection of Visible Land Boundaries from UAV Imagery. *Remote Sens.* **2021**, *13*, 2077. <https://doi.org/10.3390/rs13112077>

Academic Editors: Rohan Bennett, Claudio Persello and Mila Koeva

Received: 19 March 2021

Accepted: 24 May 2021

Published: 25 May 2021

Publisher's Note: MDPI stays neutral with regard to jurisdictional claims in published maps and institutional affiliations.



Copyright: © 2021 by the authors. Licensee MDPI, Basel, Switzerland. This article is an open access article distributed under the terms and conditions of the Creative Commons Attribution (CC BY) license (<https://creativecommons.org/licenses/by/4.0/>).

Keywords: land; cadastral mapping; visible boundary; UAV; deep learning

1. Introduction

Accelerating cadastral mapping to establish a complete cadastre and keeping it up-to-date is a contemporary challenge in the domain of land administration [1,2]. Cadastral mapping is considered the first step in establishing cadastral systems and serves as the basis for defining the boundaries of land units to which land rights refer [3]. Mapping the boundaries of land rights in a formal cadastral system helps to increase land tenure security [4]. More than 70% of land rights are unregistered globally and are not part of any formal cadastral system [1]. The challenge of accelerating the creation of cadastral maps is present mainly in developing regions with low cadastral coverage [5]. Cadastral maps are usually defined as spatial representations of cadastral records, showing the extent and ownership of land units [6]. An effective cadastral system should provide up-to-date land data [7]. In countries with complete cadastral coverage, this is considered one of the major challenges. To overcome the challenge of accelerating cadastral mapping while providing up-to-date land data, low-cost and rapid cadastral surveying and mapping techniques are required [5,8].

The proposed cadastral surveying techniques are indirect rather than direct surveying. Indirect cadastral surveying is based on the delineation of visible cadastral boundaries from high-resolution remote sensing imagery. In contrast, direct or ground-based surveying techniques are based on field survey and are often considered slow and expensive [1,5]. The application of image-based cadastral mapping is based on the recognition that many cadastral boundaries coincide with visible natural or man-made boundaries, such as hedgerows, land cover boundaries, building walls, roads, etc., and can be easily detected from remote sensing imagery [2,9]. The detection of such boundaries from data acquired with sensors on unmanned aerial vehicles (UAVs) has gained increasing popularity in cadastral applications [10–12].

In cadastral applications, UAVs have gained prominence as a powerful technology that can bridge the gap between slow but accurate field surveys and the fast approach of conventional aerial surveys [13]. Sensors on UAVs provide low-cost, efficient and flexible systems for high-resolution spatial data acquisition, enabling the production of orthoimages, digital surface models and point clouds [14]. Overall, UAVs have shown a high potential for detecting land boundaries in both rural and urban areas [8,15]. In addition, UAV-based orthoimages have been considered as base maps for the creation of cadastral maps and for updating or revising existing cadastral maps [10,12,16]. Besides the high visibility of cadastral boundaries on UAV imagery, manual delineations have been reported in many previous case studies [8]. The contemporary approach to cadastral mapping aims to simplify and speed up image-based cadastral mapping by automating the detection of visible cadastral boundaries from images acquired with high-resolution optical sensors [15,17,18].

1.1. Deep Learning for Cadastral Mapping

Only a limited number of studies have investigated the automatic approach to detect visible cadastral boundaries from UAV imagery. Mainly, tailored workflows using image segmentation and edge detection algorithms have been applied to automate cadastral mapping and thus provide more efficient approaches [8,15]. Multi-resolution segmentation (MRS) and globalized probability of boundary (gPb) are among the most popular segmentation and edge detection algorithms used in the cadastral mapping [15]. Early algorithms, such as Canny edge detection, extract edges by computing gradients of local brightness, which are then combined to form boundaries. However, the approach is characterized by the detection of irrelevant edges in textured regions [19]. Furthermore, gPb provides more accurate results compared to other approaches on edge detection (e.g., Canny detector and Prewitt, Sobel, Roberts operator) [20]. MRS, gPb and Canny are unsupervised techniques. Unsupervised techniques include methods that require segmentation parameters to be defined. The challenge is to define appropriate segmentation parameters for features that vary in size, shape, scale and spatial location. Then, the image is automatically segmented according to these parameters [19]. With respect to modern methods for automatic boundary detection in cadastral mapping, deep learning is becoming increasingly important—as a supervised technique [21]. However, the deeper understanding is challenging, so the abstraction of the process offers a solution.

Deep learning methods such as convolutional neural networks (CNNs) are very effective in extracting higher-level representations needed for classification or detection from raw input [22,23]. Moreover, recent studies indicate that deep learning ensures higher accuracy in delineating visible land boundaries than some object-based methods [15,17,24]. In the study by Crommelinck et al. [17], it was reported that CNNs, namely the VGG19 architecture, provide a more automated and accurate approach for detecting visible boundaries from UAV imagery than the machine learning approach random forest (RF). Furthermore, the study highlighted that the model based on VGG19 architecture provides more promising loss and accuracy metrics compared to other CNN architectures such as ResNet, Inception, Xception, MobileNet and DenseNet. The study conducted by Xia et al. [15] investigated the potential of fully CNNs for cadastral boundary detection in urban and

semiurban areas. The results showed that fully CNNs outperformed other state-of-the-art machine learning techniques, including MRS and gPb. The results indicated 0.37 in recall, 0.79 in precision and 0.50 in $F1$ score. The study by Park and Song [25] aims to identify the inconsistencies between the existing land use information from existing cadastral maps and the current land use in the field. The proposed method involves updating the existing land cover attributes of cadastral maps using UAV hyperspectral imagery classified with CNNs and then creating a discrepancy map showing the differences in land use. CNNs bring innovative capabilities to cadastral mapping that can facilitate and accelerate the delineation of visible cadastral boundaries. In line with these studies, improving the accuracy of automatic visible boundary detection remains a challenge in contemporary image-based cadastral mapping [15].

One CNN architecture that has not been satisfactorily investigated for visible boundary detection in cadastral applications is U-Net. U-Net was originally developed for biomedical image segmentation and is considered a revolutionary architecture for semantic segmentation tasks [26–30]. Generally, it is claimed that the main challenge in CNNs is a large amount of training data preparation and computational requirements [26]. Thus, providing thousands of UAV training data can be considered as a limitation for visible land boundary detection with CNNs, especially when a model is trained from scratch. However, the U-Net architecture is designed to work with fewer training images preprocessed by an intensive data augmentation procedure and still provide precise segmentation [26]. In addition, a software-based module, ENVI deep learning, has recently been developed to simplify and perform deep learning procedures with geospatial data. The number of studies that have tested its potential is very small [31]; in particular, it has not been sufficiently explored for the detection of visible cadastral boundaries from UAV imagery.

1.2. Objective of the Study

The main objective of this study is to investigate the potential of CNN architecture, namely U-Net, based on UAV imagery training samples, as a deep learning-based detector for visible land boundaries. In addition, we wanted to evaluate the advantages and disadvantages of programming-based, e.g., custom, deep learning compared to a commercial software-based solution. Here, we compared the results of U-Net with those of the recently released software-based ENVI deep learning by focusing on the boundary mapping approaches and their conformity in the land administration domain.

2. Materials and Methods

2.1. UAV Data

It is argued that the number of visible cadastral boundaries is higher in rural areas than in dense urban areas (an example of a visible cadastral boundary in Figure 1b). A rural area in Odranci, Slovenia, was selected for this study. UAV images were acquired at a flight altitude of 90 m, resulting in 997 images to cover the study area. The images were acquired in September 2020, at midday, under clear skies. The UAV images were indirectly georeferenced using a uniform distribution of 18 ground control points (GCPs). The GCPs were surveyed with real-time kinematic (RTK) using the global navigation satellite system (GNSS) receiver Leica GS18. In addition, the GCPs were also surveyed with RTK, using a multifrequency low-cost GNSS instrument (base and rover), namely ZED-F9P receiver with u-blox ANN-MB-00 antenna—as a cheaper alternative to geodetic GNSS receivers (Figure 1b). The differences were insignificant for 2D cadastral mapping ($RMSE_{x,y} = 0.019$ m). The obtained ground sampling distance (GSD) from the UAV orthoimage was 0.02 m. The study site had an area of 63.9 ha and was divided into areas for training and testing the CNNs (Figure 1a).

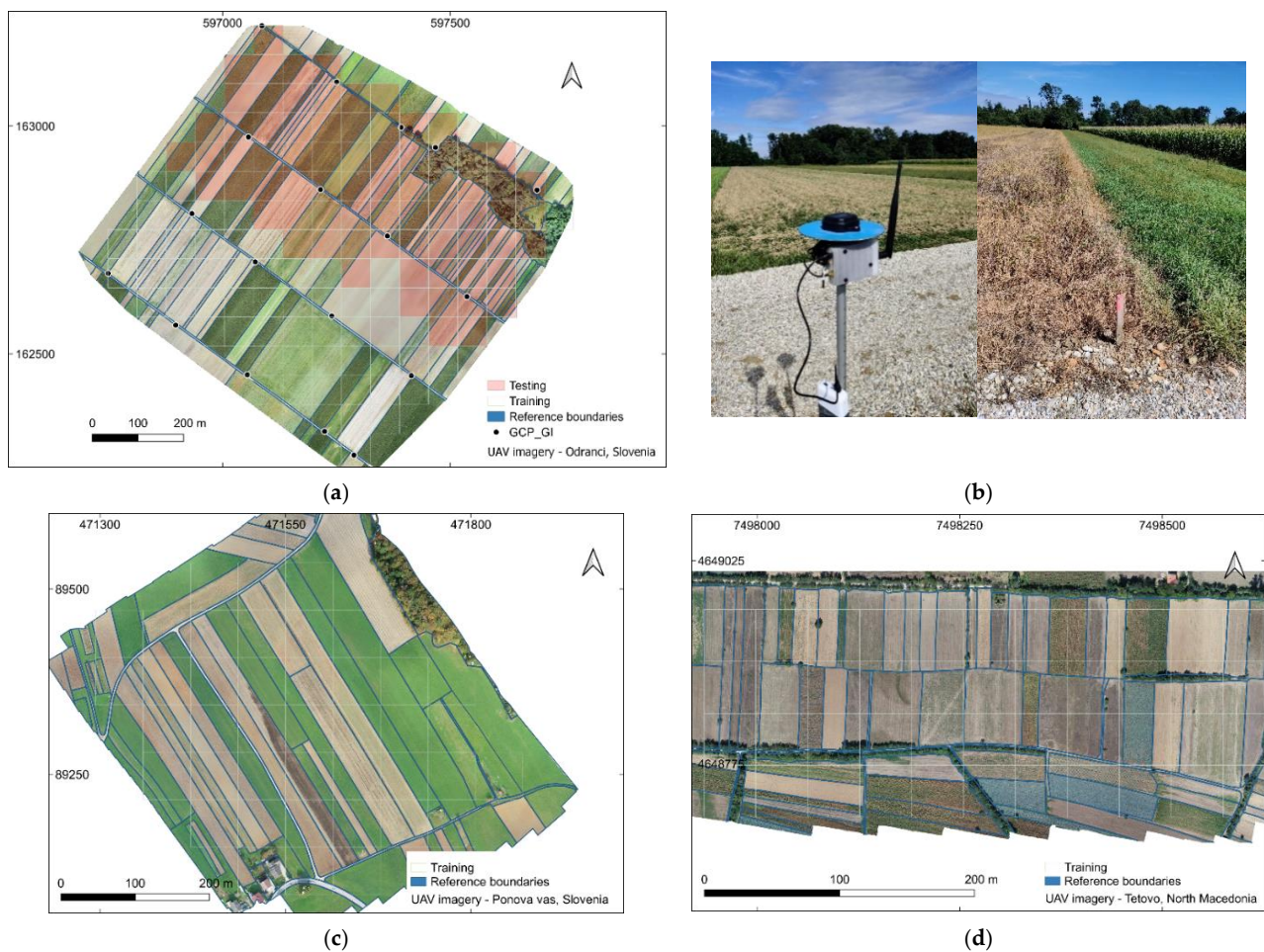


Figure 1. (a) UAV imagery of 0.25 ground sample distance (GSD) for Odranci–Slovenia, divided into areas for training and testing; (b) low-cost instrument ZED-F9P and example of visible cadastral boundaries. (c) UAV imagery of 0.25 (GSD) for Ponova vas—Slovenia, used for training; (d) UAV imagery of 0.25 (GSD) for Tetovo—North Macedonia, used for training.

With the aim of increasing the number and diversity of training data, additional UAV images with a rural scene from Ponova vas (Slovenia) and Tetovo (North Macedonia) were used (Figure 1c,d). The UAV data in Ponova vas was acquired at an altitude of 80 m and had a GSD of 0.02 m. The UAV data in Tetovo have a GSD of 0.03 m and were acquired at an altitude of 110 m. Figure 1a,c,d shows the UAV orthoimages of the study areas.

The selected areas contain agricultural fields, roads, fences, hedges and tree groups, which are assumed to represent cadastral boundaries [8]. The cadastral reference boundaries were derived from the UAV orthoimages by manual land delineation on-screen in all three study areas. All UAV images were acquired using a rotary-wing UAV, namely the DJI Phantom 4 Pro. Table 1 shows the specifications of the data acquisition.

Table 1. Specification of unmanned aerial vehicle (UAV) dataset for the selected study areas.

| Location | UAV Model | Camera/Focal Length (mm) | Overlap Forward/Sideward | Flight Altitude | GSD (cm) | Coverage Area (ha) | Purpose |
|-------------------------|-------------------|--------------------------|--------------------------|-----------------|----------|--------------------|----------------------|
| Odranci, Slovenia | DJI Phantom 4 Pro | 1" CMOS/24 mm | 80/70 | 90 m | 2.35 | 63.9 | Training and Testing |
| Ponova vas, Slovenia | | | | 80 m | 2.01 | 25.0 | Training |
| Tetovo, North Macedonia | | | | 110 m | 2.85 | 24.3 | Training |

2.2. Detection of Visible Land Boundaries

In general, the workflow of this study consists of three main parts, namely data preparation, visible land boundary detection and accuracy assessment. The specific steps for both the U-Net and ENVI deep learning boundary mapping approaches are described in the following subsections.

2.2.1. U-Net

In deep learning, CNNs can be trained in two approaches, from scratch or via transfer learning [17,32]. In our case, the U-Net model was trained from scratch based on UAV images.

The UAV orthoimages of the selected study areas (Figure 1a–c) were randomly tiled in 256 pixels \times 256 pixels. To increase the field of view for each tile, the original spatial resolution of the UAV orthoimages had to be converted to a larger GSD, from 2–3 to 25 cm. The results were 219 original tiles, namely 144 tiles for training and 75 tiles for testing (Figure 1a,c,d). In addition, corresponding label images (also called ground truth images) were created for each UAV image. The label images, with a size of 256 \times 256 \times 1, were created from the manually digitized reference boundaries, which were initially in the vector format. The reference boundaries were buffered to 50 cm and later rasterized using GRASS GIS tools [33]. Additionally, the UAV tiles were then rotated, flipped and scaled to improve generalization and increase the number of training samples. This technique is known in deep learning as data augmentation and is used to supplement original training data. Once the data preparation and augmentation were completed, the next step was to train the U-Net model.

The CNN based on U-Net is symmetric and contains encoding and decoding parts, which gives it the U-shaped form. U-Net is described in detail in [26]. The left part, the encoding path, is a typical convolutional network that contains repetitive usage of 3 \times 3 convolutions, each followed by a rectified linear unit (ReLU) and a max-pooling operation, i.e., 2 \times 2 convolutions. During the encoding path, the contextual information (depth) of the images was increased while the resolution of the images was reduced. The right part, the decoding path, merged the contextual and resolution information of the images through a sequence of 2 \times 2 up-convolutions. The goal of the decoding path is to provide precise localization using the contextual information from the encoding path. During the decoding path, the resolution of the image was upconverted to its original size. The U-Net architecture implemented in this study is shown in Figure 2.

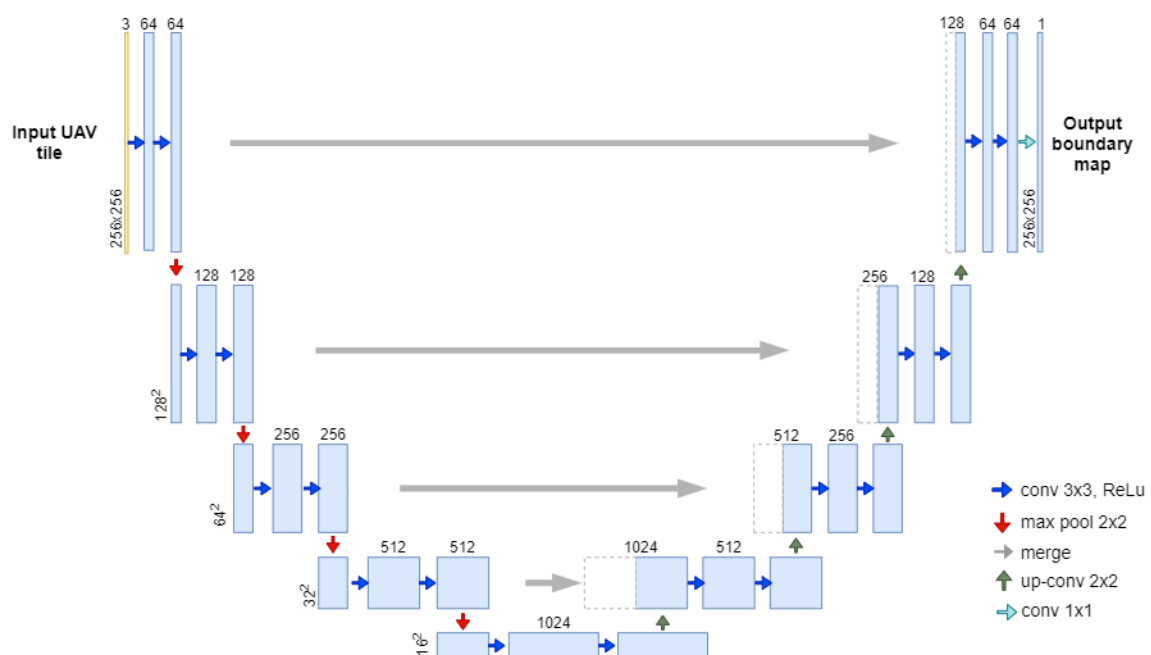


Figure 2. The implemented U-Net architecture (adapted from [26]).

Overall, training a CNN model requires a powerful graphics processing unit (GPU), lots of memory and efficient computations. To overcome this requirement while providing a cost-effective and fast approach for visible boundary detection and hence cadastral mapping, the training of U-Net was performed by Google Collaboratory [34]. U-Net was implemented in the high-level neural network API Keras [35]. The process was written in Python in combination with the TensorFlow library [36]. The implementation of the model in Keras was done by modifying and referencing to [37], which is an implementation for grayscale biomedical images. In this study, the U-Net model was adapted to work with three-band images, namely RGB UAV images, as input and produce a single band boundary map as output with the same image size as the input. However, the predicted boundary maps were not georeferenced.

Considering that georeferencing is the key component in cadastral mapping, further improvements were made. In this study, we considered two additional steps, namely georeferencing the predicted boundaries and merging the georeferenced tiles to obtain the boundary map for the entire extent of the test area. The processing and analysis were done using open-source modules, including Rasterio [38], GDAL [39] and Numpy [40]. The workflow and boundary mapping approach used in this study are shown in Figure 3.

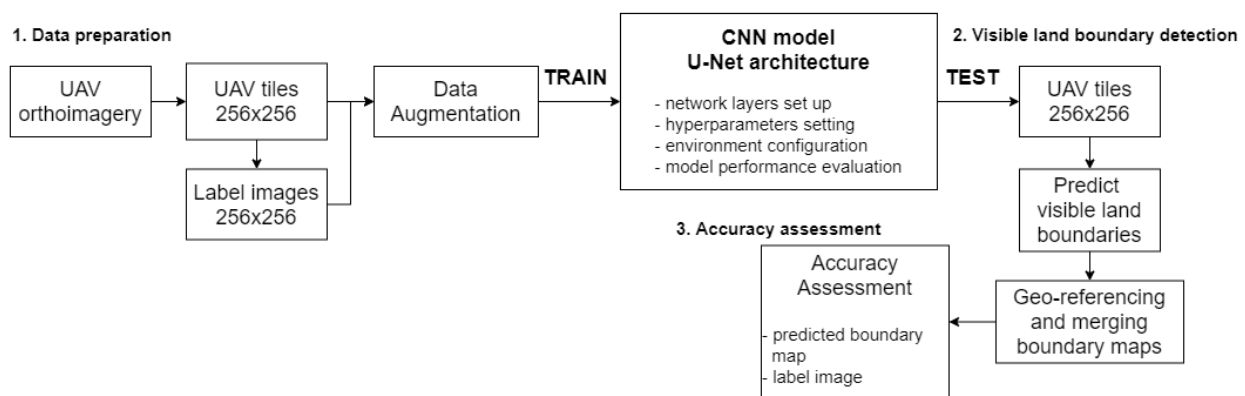


Figure 3. Workflow for the detection of visible land boundaries based on the U-Net model.

2.2.2. ENVI Deep Learning

ENVI deep learning [41] can be categorized as software-based deep learning technology that offers its own U-Net-like model. The model is called ENVINet5 and is described in detail in [42]. In this study, the ENVINet5 model was used to compare it with the U-Net model—both the results and the land boundary mapping approach.

The training approach is patch-based, i.e., the entire extent of the training UAV data can be used as input, and the model can learn based on the pixels specified in the patch. Considering this, a patch size of 256 pixels \times 256 pixels was used for training and validating the ENVINet5 as a single-class model. Moreover, the training of the ENVINet5 model is based on a labelled raster that should be created within the software. Generally, there are two approaches: by on-screen manual digitizing or by directly uploading features in vector format. In our case, we uploaded the shapefile (.shp) of reference cadastral boundaries (buffered to 50 cm), defined as the region of interest (ROI), from which the label raster was created. We used the recently released version of ENVI deep learning, i.e., version 1.1.2, which has an option for data augmentation, unlike the previous version where data augmentation was not possible. Data augmentation is performed by rotating and scaling the original UAV training data.

The training of the ENVINet5 model was done using the toolbox deep learning guide map. Before starting the training, it was necessary to initialize a TensorFlow model, which defines the structure of the model, including the architecture (ENVINet5 for a single class), the patch size (256 \times 256), and the number of the bands that are used for training (3 bands, RGB). After the model was initialized, the training data was uploaded. In the following,

the values for the training parameters are required, such as the number of epochs, the number of patches per epoch, the number of patches per batch, class weight, etc. For the number of patches per epoch and per batch, it is suggested to leave them blank so that ENVI automatically determines the most appropriate values. For saving the model and the trained weights (output model), ENVI uses the HDF5 (.h5) format. The generated land boundary maps were georeferenced, and no post-processing step was required. The boundary mapping approach and workflow used in this study are shown in Figure 4.

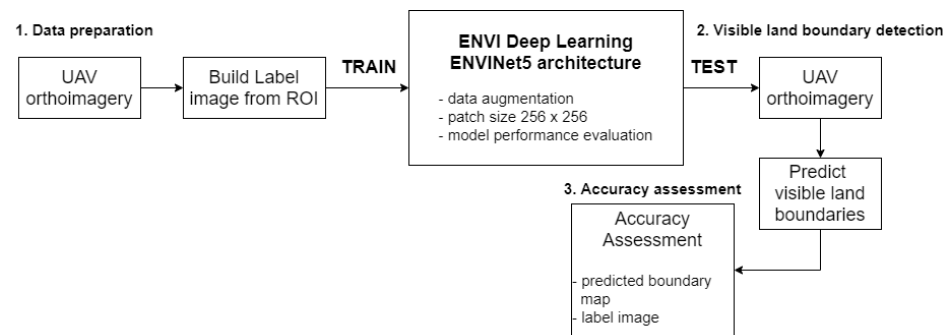


Figure 4. Workflow for the detection of visible land boundaries based on the ENVINet5 model.

However, there were some hardware and software requirements, such as NVIDIA GPU driver version 410.x or higher and NVIDIA graphics card with CUDA compute capability 3.5–7.5. Additionally, it is recommended to have at least 8 GB GPU memory to perform the training of the models with the GPU. If this requirement is not met, the training will be performed with the central processing unit (CPU), which is too slow for a large number of images.

2.3. Accuracy Assessment

The accuracy assessment in this study investigates two aspects—the evaluation of the two models U-Net and ENVINet5 and the evaluation of the detection quality of the visible land boundaries for the test UAV data (Figure 1a).

Both CNN models, U-Net and ENVINet5, were monitored with loss and accuracy during the training process. Loss is defined as the sum of errors for each sample in training between labels and predictions. To maximize the efficiency of the model, loss should be minimized. For this purpose, we used the cross-entropy loss expressed by the following formula:

$$\text{cross-entropy loss} = -(y_i \log(\hat{y}_i) + (1 - y_i) \log(1 - \hat{y}_i)) \quad (1)$$

where:

y_i —actual label value,
 \hat{y}_i —predicted value.

To assess the performance of the models, overall accuracy was used as the evaluation metric. The overall accuracy was calculated by summing the percentages of pixels correctly identified as land boundaries by the model compared to the labelled reference boundaries and dividing by all boundaries. Overall accuracy is expressed with the following equation:

$$\text{overall accuracy} = \frac{TP + TN}{TP + FP + FN + TN} \quad (2)$$

where true positive (TP), true negative (TN), false positive (FP) and false negative (FN) are shown in Table 2, which is the confusion matrix used to evaluate the detection quality of the visible land boundaries.

Table 2. Confusion matrix.

| | | Ground Truth | |
|------------|-------------|--------------|-------------|
| | | Boundary | No Boundary |
| Prediction | Boundary | <i>TP</i> | <i>FP</i> |
| | No boundary | <i>FN</i> | <i>TN</i> |

The detection quality of the visible land boundaries was evaluated by computing the F1 score derived from the confusion matrix. F1 score was calculated for test UAV data (not seen by the model during training) and represented the harmonic mean between recall and precision (Equations (3) and (4)). Larger values indicate higher accuracy.

$$recall = \frac{TP}{TP + FN} \quad (3)$$

$$precision = \frac{TP}{TP + FP} \quad (4)$$

The recall is the ratio of correctly predicted visible boundaries to all reference cadastral boundaries. The precision is the ratio of correctly predicted visible boundaries to all predicted positive visible boundaries. The F1 score combines precision and recall and is expressed with the following equation:

$$F1\ score = 2 * \frac{recall * precision}{recall + precision} \quad (5)$$

3. Results

3.1. CNN Architecture

In our study, the labelled images and RGB UAV images were used to train the deep CNN models.

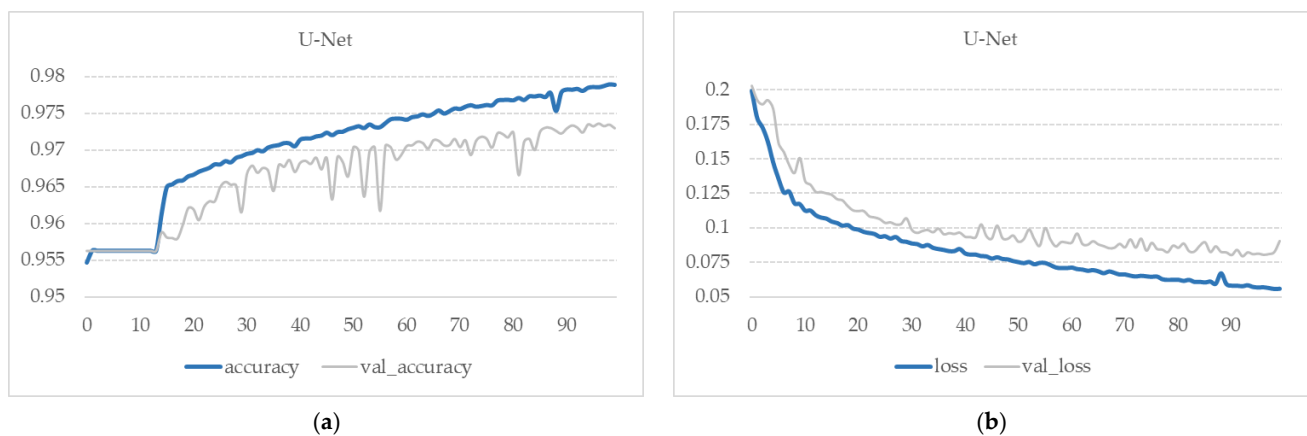
For the U-Net, the randomly cropped tiles (Figure 1a,c,d) were the candidate training datasets. The greater the variety of images used in the training data, the more robust the network and the better the detection of visible land boundaries. Data augmentation was applied to the provided images to increase the number of UAV images available for training the U-Net model. Of the data used for training, 30% was used for validation. Once the U-Net model was trained, we applied it to the test UAV images (Figure 1a).

The architecture was based on the original architecture of the U-Net, considering the number of layers (network depth) and the size of the convolutional filters. However, to avoid the resizing of the output image by the max-pooling operation, the padding was set to 'same'. In addition, a dropout rate of 0.8 was used as an optional function. The dropout rate aims to avoid overfitting the model, which means that the training and validation accuracy curves are less likely to diverge, then the model is more robust. To avoid under-fitting, the layer depth was set to 1024. The larger the layer size, the higher the probability that the curve for validation will be close to the training accuracy. We used sigmoid instead of softmax as the final activation layer to retrieve the predictions, which is good for binary classification. The main point is that when using sigmoid, the probabilities were independent and did not necessarily sum to one. This is because the sigmoid considers each raw output value separately. During training, the optimization algorithm stochastic gradient descent (SGD) was used as the optimizer, and the momentum was set to 0.9. The learning rate in the optimization defines the speed of learning, which makes the network training converge. We used an adjusted learning rate of 0.001. Table 3 shows the adjusted settings and parameters.

Table 3. Settings and adjusted parameters for our fine-tuned CNN based on the U-Net architecture.

| | Settings | Parameters |
|--------------------|---|---|
| Trainable layers | pooling layer | maxpooling 2D |
| | connected layer | layer depth = 1024 activation = ReLU |
| | dropout layer | dropout rate = 0.8 |
| | logistic layer | activation layer = sigmoid |
| Learning optimizer | SGD optimizer | learning rate = 0.001 momentum = 0.9 |
| Training | UAV images $256 \times 256 \times 3$, data augmentation, validation split 0.3 | number of epochs = 100 batch size = 32 steps per epoch = training samples/number of epochs |

The model was trained with a batch size of 32 for 100 epochs. An early stop function was also used to monitor validation loss. The number of steps per epoch was calculated by dividing the total number of training images by the batch size. Deep learning by the U-Net model was performed in Google Collaboratory, which provided a GPU with 25 GB of RAM. A total of 4768 samples, i.e., augmented images, were used for training and 2044 samples for validation. Training the model for 100 epochs took 4 h. The best model was saved at epoch 92 by achieving an overall accuracy of 0.978 and a loss of 0.058. The training performance of the U-Net is visualized in Figure 5.

**Figure 5.** Model performance: (a) accuracy and (b) loss for our fine-tuned U-Net.

In this study, we also used ENVI deep learning to compare the results obtained with the U-Net model. In this study, ENVI deep learning is considered a 'black box'. The information we had is that ENVINet5 is based on U-Net architecture, and it uses the same layer size and the same number of convolution layers.

The ENVINet5 model was trained with a patch size equal to the total extent of the training UAV data. In addition, the training data shown in Figure 1a,c,d were also processed as UAV images for validation. The adapted training parameters of ENVINet5, namely patch size of 256×256 , number of epochs 50 and class weights min. 1 and max. 2, data augmentation 'yes', resulted in a fine-tuned model for visible boundary detection. The values of the other parameters were automatically filled by ENVI deep learning as they are suggested to be left blank. The model with the best performance was saved at epoch 24, where the validation loss reached its lowest value. The overall accuracy of the model was 0.946 and with a loss of 0.234. The training performance of the CNN model ENVINet5 is shown in Figure 6.

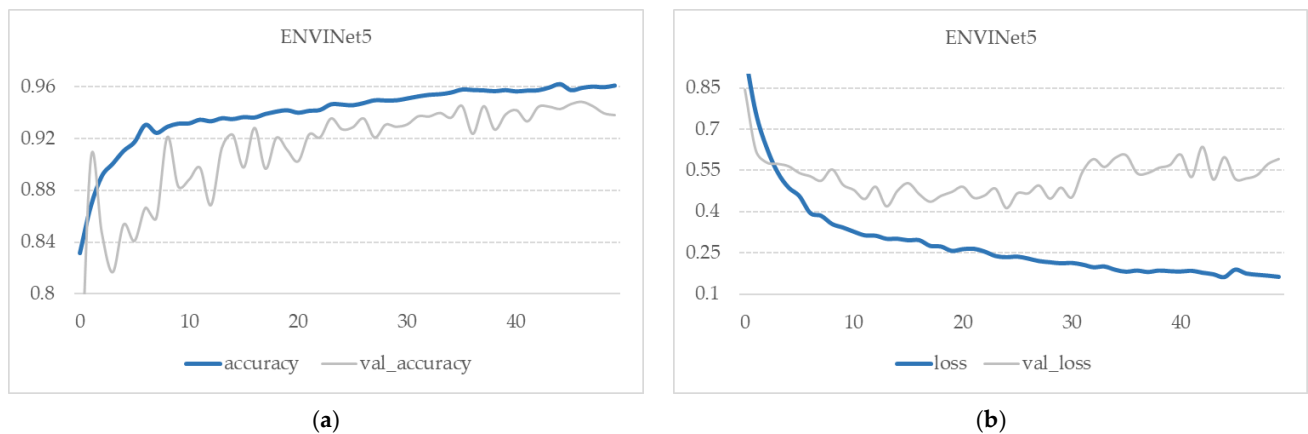


Figure 6. Model performance: (a) accuracy and (b) loss for our fine-tuned ENVINet5.

All experiments with ENVI deep learning were performed on an Intel® Core™ i7-4771 CPU 3.5 GHz machine with an NVIDIA GeForce GTX 650 GPU with 2 GB of RAM. The training time for 50 epochs was 6 h.

3.2. Detection of Visible Land Boundaries by U-Net

After training the CNN model, we evaluated its performance by applying it to the test area (Figure 1a). We applied the trained U-Net model to the test UAV tiles of size 256×256 to predict the visible land boundaries. Some results of the predicted boundary maps based on UAV tiles are shown in Figure 7.

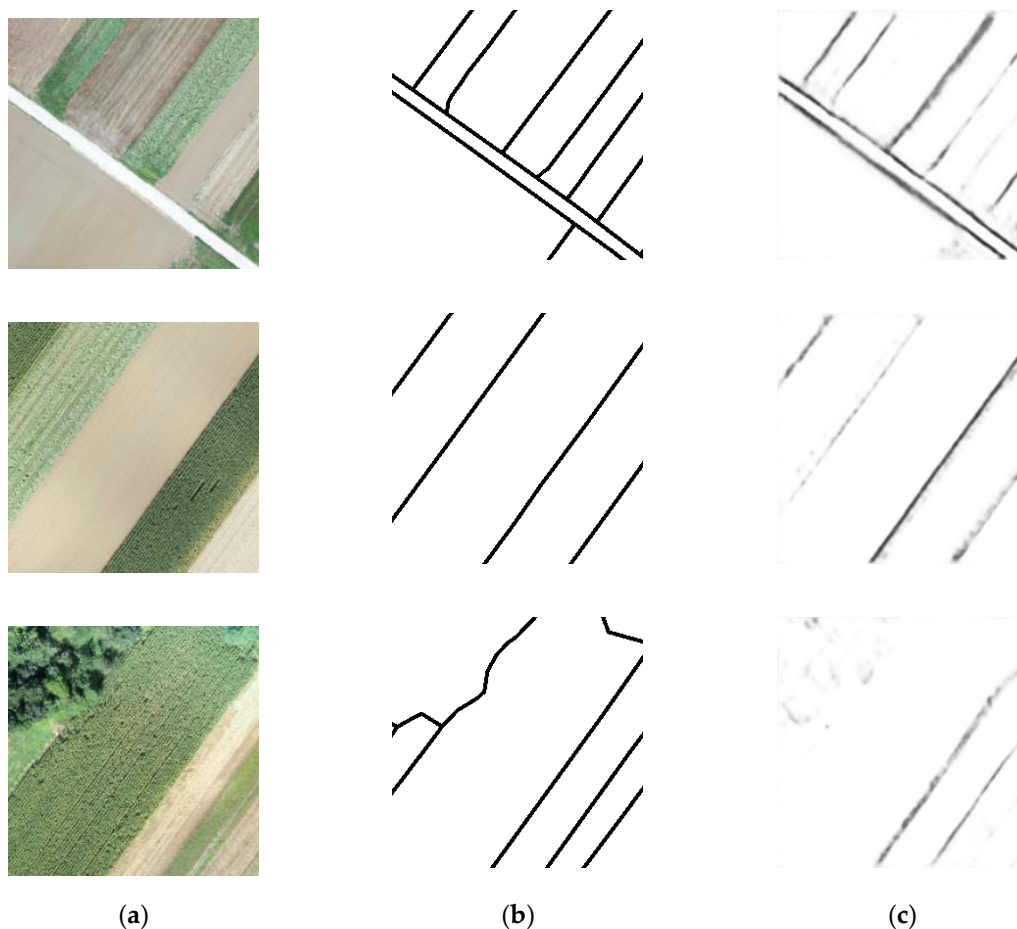


Figure 7. (a) Examples of UAV testing tiles; (b) label images; (c) predicted boundary maps with values 0–1.

The next step was to georeference the predicted visible land boundaries and merge them into a single land boundary map (Figure 8c). Considering that the predicted values were in the range of 0–1, in order to assess the accuracy and thus match the ground truth class values, it was necessary to reclassify the predicted values to 0 and 1, namely to ‘boundary’ and ‘no boundary’. In this study, few boundary map reclassifications were performed, e.g., ‘boundary’ ≤ 0.9 ; ‘boundary’ ≤ 0.7 ; ‘boundary’ ≤ 0.5 . The predicted boundary maps for the test area showed a good match with the labelling image (ground truth). The results of the georeferenced and merged predictions along with the reclassified boundary maps are shown in Figure 8c–f.

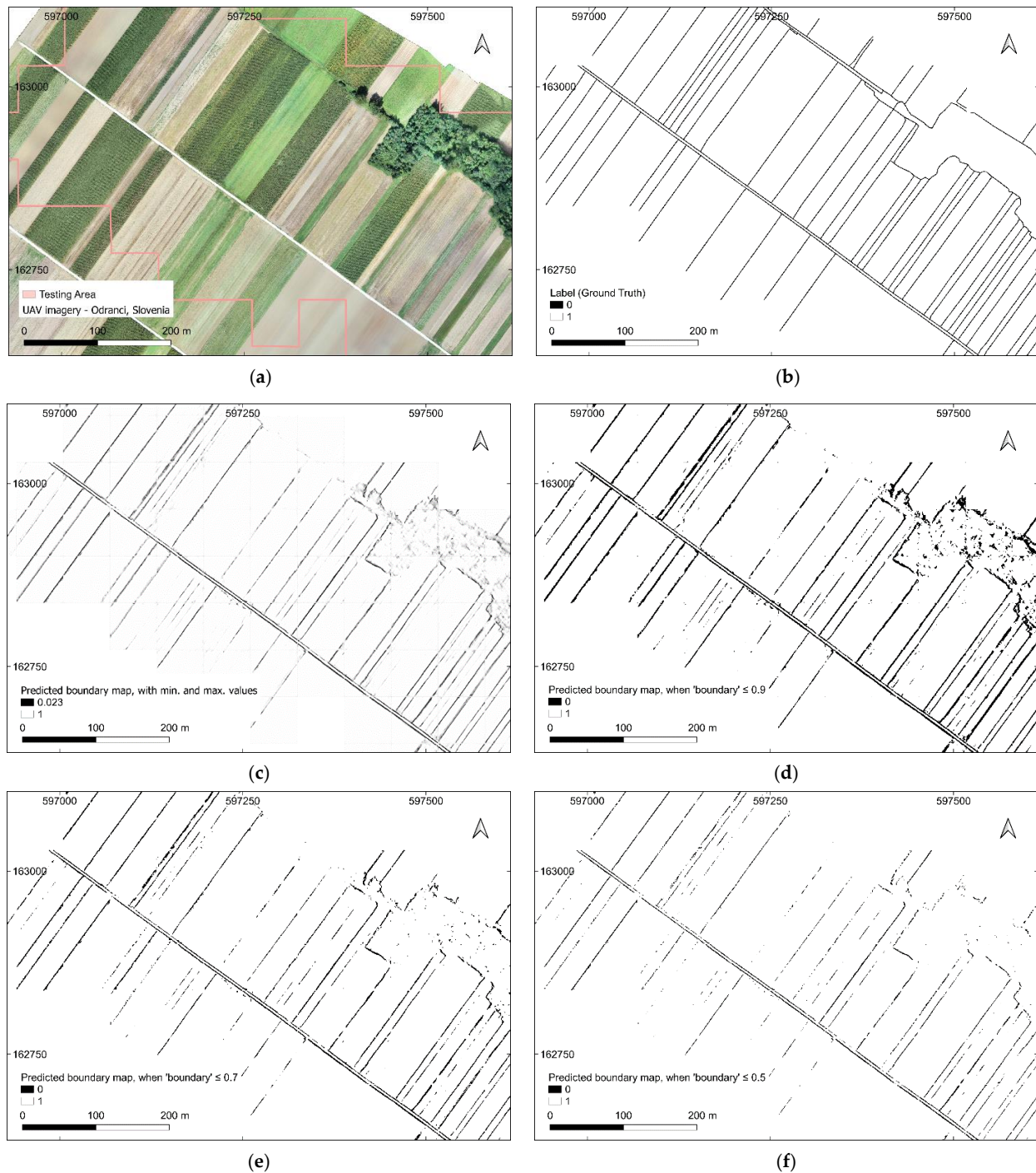


Figure 8. (a) Test UAV area; (b) label image; (c) predicted boundary map (0–1); reclassified boundary maps when (d) ‘boundary’ ≤ 0.9 ; (e) ‘boundary’ ≤ 0.7 ; (f) ‘boundary’ ≤ 0.5 .

For a quantitative description of the predicted boundary maps, overall accuracy, F1 score, recall and precision are summarized in Table 4. Overall accuracy represents a general metric by counting true positives/negatives and false positives/negatives, i.e., it considers both ‘boundary’ and ‘no boundary’ classes. All predicted boundary maps resulted in an overall accuracy of over 94%. To get a better insight into the detection quality, F1 score, recall and precision were calculated for the class ‘boundary’ or ‘0’ as a positive class. The results showed that more relevant visible land boundaries were detected when the predicted boundary map was reclassified with the threshold ‘boundary’ ≤ 0.9 , resulting in an F1 score of 0.51. More balanced scores were retrieved for the boundary map with ‘boundary’ ≤ 0.7 , resulting in an F1 score of 0.52. Higher precision was obtained for the boundary map with the reclassification threshold ‘boundary’ ≤ 0.5 , resulting in an F1 score of 0.46.

Table 4. Accuracy assessment of visible land boundary detection with U-Net.

| Predicted Boundary Map | Overall Accuracy (%) | Recall | Precision | F1 Score |
|------------------------|----------------------|--------|-----------|----------|
| Boundary ≤ 0.9 | 94.5 | 0.654 | 0.413 | 0.506 |
| Boundary ≤ 0.7 | 96.2 | 0.480 | 0.565 | 0.519 |
| Boundary ≤ 0.5 | 96.5 | 0.348 | 0.675 | 0.459 |

3.3. Comparison with ENVI Deep Learning—ENVINet5

The predicted land boundary map for the test area (Figure 8a) retrieved using ENVINet5 model was already georeferenced, so no further post-processing step was required. In addition, the retrieved boundary map contained predicted values of 0 and 1, and no additional reclassification step was performed to compare the results to the ground truth map and to assess accuracy. The predicted boundary is visualized in Figure 9b.

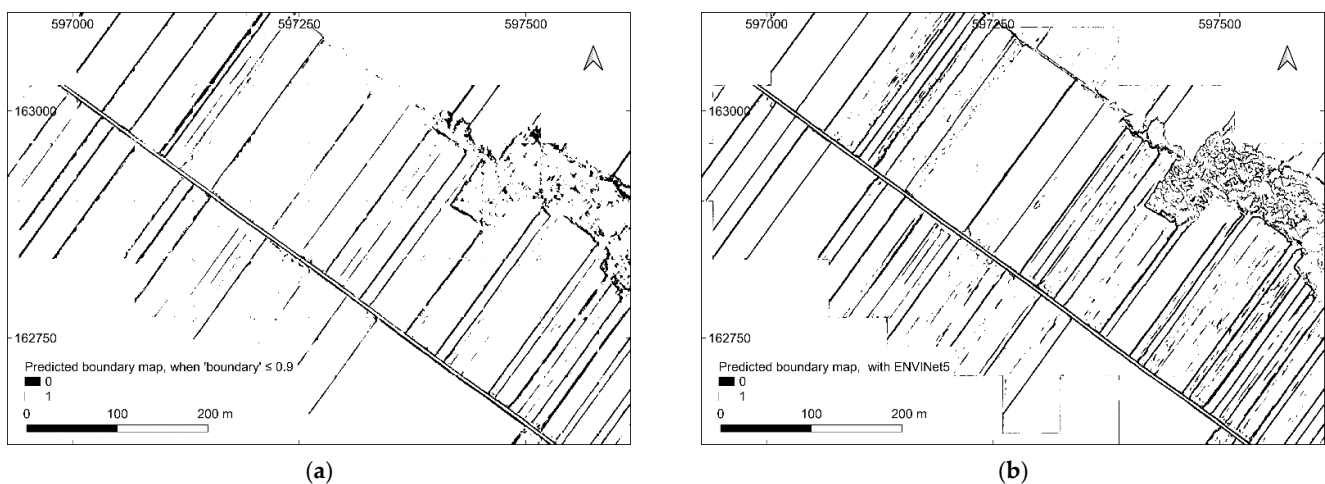


Figure 9. Comparison of predicted land boundary map: (a) predicted boundary map retrieved with U-Net, threshold ‘boundary’ ≤ 0.9 ; (b) predicted boundary map retrieved with ENVINet5.

Considering that all predictions retrieved with ENVINet5 were assigned the prediction value 0 for the class ‘boundary’, we selected the boundary map for the comparison of results with U-Net, where all predictions ≤ 0.9 , were reclassified as 0—‘boundary’. With this, we wanted to compare predictions from U-Net that were as close as possible to the predictions of ENVINet5. The overall accuracy was 94.5% for U-Net and 96.2% for ENVINet5. However, in terms of detection quality for the ‘boundary’ class, ENVINet5 showed higher recall and lower precision than U-Net. In short, F1 score showed a slightly higher value for U-Net, i.e., 0.51 compared to ENVINet5, where the value was 0.49. The confusion matrices are shown in Table 5 and the quantitative results in Table 6.

Table 5. Confusion matrices based on the number of pixels.

| | | Ground Truth | |
|----------|-------------|--------------|-------------|
| | | Boundary | No Boundary |
| U-Net | Boundary | 137,056 | 195,156 |
| | No boundary | 72,524 | 8,966,912 |
| ENVINet5 | Boundary | 175,559 | 325,076 |
| | No boundary | 34,021 | 8,836,992 |

Table 6. Accuracy assessment and comparison with ENVINet5.

| Predicted Boundary Map | Overall Accuracy (%) | Recall | Precision | F1 Score |
|------------------------|----------------------|--------|-----------|----------|
| U-Net | 94.5 | 0.654 | 0.413 | 0.506 |
| ENVINet5 | 96.2 | 0.838 | 0.351 | 0.494 |

4. Discussion

Deep learning is a relatively new research area and offers great potential for feature detection from remote sensing imagery [21,24]. The application of CNNs for detecting visible land boundaries is becoming increasingly important, especially for UAV-based cadastral mapping. In this work, we presented a deep learning application using Python with Keras to implement U-Net, and software-based ENVI deep learning for visible land boundary detection from UAV imagery. The research obtained encouraging and reasonable results that can help to automate the process of cadastral mapping.

4.1. CNN Architecture and Implementation

In both network models, the loss was constantly decreasing from the first epoch until the end. This indicated that the model was still learning on training samples. However, the training of the models was monitored with the validation loss to avoid overfitting. The training performance of the network models was shown in Figures 5 and 6. The validation loss for U-Net was decreasing until epoch 92 and for ENVINet5 until epoch 24. This was a good sign that the model did not lose the ability to generalize predictions for test datasets that were not seen by the model during training. The evaluation metric showed relatively high accuracies, 0.978 for U-Net and 0.946 for ENVINet5. The high accuracy of the network models, including the first epochs, is mainly due to the unbalanced pixels of the classes. The land boundaries occupy a minimal number of pixels compared to the background pixels.

In this study, we used a deep learning-based visible land boundary detector. Here, providing balanced pixels for 'boundary' and 'no boundary' is a bit challenging, especially for UAV imagery. UAV imagery usually has a small GSD (2–5 cm) and a limited coverage area beside the efficient and flexible data acquisition system [14]. Moreover, the number of background pixels in cadastral maps is always much higher than the number of pixels representing the course of the cadastral boundaries themselves (line-based). The imbalance of pixels per class is even more evident in randomly cropped tiles from UAV imagery. Resampling the original GSD to a larger GSD contributed somewhat to an increase in the field of view and balance between classes. However, the size of the GSD and the number of training tiles is limited by the coverage area. To increase the amount of training data, we applied data augmentation. Data augmentation has proven to be an efficient technique to supplement original UAV training data, especially when training the U-Net model from scratch. However, it remains a challenge to confirm what should be a sufficient variety of UAV training data to learn a robust network model for visible cadastral boundary detection.

The problem of unbalanced classes could be solved by rebalancing the class weights, using additional evaluation metrics besides overall accuracy, or performing deep learning with multiple classes for land cover (polygon-based). In addition, other remote sensing imagery can be used for the training data, e.g., aerial or satellite imagery; imageries can be cropped in a way to cover more balanced pixels for 'boundary' and 'no boundary' and may

not be limited with the coverage area. This can be applied if the deep learning model is to be trained using only cadastral data that requires manual data preparation, such as the creation of image tiles and corresponding ground truths. Instead, the CNN model could be trained via transfer learning, similar to [17]. To avoid ambiguity, the detection quality for UAV test data in this study was evaluated using recall, precision and *F1* score for the class 'boundary'. Thus, we had two indicators, overall accuracy, which includes both 'boundary' and 'no boundary' classes and one that is specific only to the 'boundary' class. Although both models performed well, there were significant differences in implementation and training, as one approach is customized, e.g., U-Net, and is offered as an API, while the other, e.g., ENVINet5, is software-based, where we have fewer parameters available but can still achieve good results.

Training a deep learning model requires more memory, a stronger GPU and efficient computation. Training of the U-Net model was performed in Google Collaboratory, which is open-source and can be considered as an alternative for the hardware costs to get more memory and a more powerful GPU. On the other hand, ENVI deep learning had some hardware and software requirements to perform the training of the network model. Google Collaboratory allowed faster training compared to our machine. For 100 epochs, the training time was 4 h with Google Collaboratory and three times the training time with ENVI deep learning since it was run on a local machine with less computational power. It should be emphasized that ENVI deep learning provided more stable training in terms of a training session interruption, which occasionally happened with Google Collaboratory.

4.2. Detection of Visible Land Boundaries

The network models, both U-Net and ENVINet5, generally performed well in detecting visible land boundaries, with some exceptions in the forest area. The results of the quality of visible land boundary detection are shown in Figures 8 and 9 and quantitatively in Tables 4 and 6. The results show that most visible land boundaries were correctly detected, which demonstrates the ability of the UAV imagery and network models to detect these types of land boundaries, especially in rural areas.

U-Net generated boundary maps with low recall and high precision when the threshold for 'boundary' was set ≤ 0.5 . This resulted in a recall of 0.35 and a precision of 0.68. More balanced results and a higher *F1* score were obtained when the threshold for 'boundary' was set ≤ 0.7 , namely a recall of 0.48, precision of 0.57 and *F1* score of 0.52. The boundary map with high recall and low precision was generated when the threshold was set almost to the maximum, namely 'boundary' ≤ 0.9 . This boundary map was used for comparison with the new map obtained with ENVINet5, since nearly all predictions were reclassified to the 'boundary' class, which is in accordance with the output of ENVINet5.

The results show an overall accuracy of 94% and 96% for U-Net and ENVINet5, respectively. However, for the 'boundary' class, U-Net gave 0.51 *F1* score and ENVINet5 0.49. This is mainly because U-Net provided more balanced scores, namely 0.65 in recall and 0.41 in precision. On the other hand, ENVINet5 provided higher recall (0.84) and lower precision (0.35), which means that the 'boundary' class is well detected, but the model also includes points of the background class in it.

U-Net provided boundary maps that were in the range of 0–1. This is due to the chosen sigmoid function as the activation function of the output layer, where the output values obtained are estimates of the probability that the input belongs to class 'boundary'. Then, we set a threshold to decide whether the input belongs to class 'boundary' or class 'no boundary'. The results maintain a balance; the lower the threshold, the lower the recall and the higher the precision. The significant point of the threshold is that the same can be used as a filtering method for boundary maps, depending on the need and purpose of the application. For example, a low threshold provided high precision, while a high threshold provided high recall. The recall is also referred to as completeness, while the precision is referred to as correctness [15]. Imbalanced classes are common in cadastral maps, and when it comes to specific use cases, more importance should be given to the metrics recall

and precision, and how a balance between them can be achieved—which in our case was supported by filtering the predicted boundary maps (Figure 8e). Unlike U-Net, ENVINet5 provided all predictions with values 0 and 1, and no further thresholding or filtering could be applied.

In cadastral mapping, it is desirable that the relevant or candidate boundaries are correctly extracted since the correct determination of the location of the cadastral boundaries is the core of the cadastre itself (correctness). On the other hand, increasing the number of possible boundaries increases the cadastral coverage (completeness). Considering this, a model that provides a balance between recall and precision is preferable. In short, a model that provides a high F1 score.

The comparison of the results obtained with U-Net with other studies, in particular [15,17,25], which deal with the automation of cadastral mapping using different CNN architectures, is not possible at this stage. This is mainly because the training approach of the network models along with the input training data differs from study to study. Thus, a reliable and qualitative comparison is not possible.

4.3. Boundary Mapping Approach

This section refers to the visible land boundary detection workflows applied in custom-based U-Net and software-based ENVI deep learning. In general, boundary mapping approaches are quite different, starting from data preparation to the final predicted boundary map. However, these differences provide advantages and disadvantages for each boundary mapping approach used in this study.

In general, programming-based deep learning is open-source and offers a more flexible but complex approach compared to software-based deep learning. Software-based deep learning, e.g., ENVI deep learning, is simpler but at the same time more rigid. For example, U-Net can be trained in a machine and in online platforms such as Google Collaboratory, where the hyperparameters can be configured individually. In contrast, ENVI deep learning has no implementation choices, but it also requires no additional configuration. The latter can be considered a very important aspect as not all land administrators are experts in programming, and this can be an option for them to perform deep learning. The main challenge with CNNs is the preparation of a large amount of training data [26], especially when the goal is to train the network only cadastral data [17]. In order to increase the amount of training data for the U-Net, it was necessary to decompose the UAV orthoimages in tiles before data augmentation. Moreover, for each UAV tile, a corresponding label image (ground truth) was manually created using additional software for rasterisation. In contrast, training in ENVI deep learning was patch-based, and the entire extent or a larger UAV tile can be used as input for training. In addition, the labelling images were created quite quickly within the software—directly by uploading reference boundaries as ROIs. The boundary maps retrieved using U-Net were the same size as the input but were not georeferenced. Considering that georeferencing is the key element in cadastral mapping, it was necessary to georeference and merge predicted boundary maps from the test UAV tiles. In ENVI deep learning, the prediction boundary map was already georeferenced, and the predictions had values of 0 and 1. Therefore, further filtering of the predicted boundary maps was not possible. The advantages and disadvantages of the U-Net and ENVI deep learning mapping approaches used in this study are summarized in Table 7.

Table 7. Summarized advantages (pros) and disadvantages (cons) for boundary mapping approaches used in this study.

| U-Net | | ENVI Deep Learning | |
|--|---|---|---|
| pros | cons | pros | cons |
| <ul style="list-style-type: none"> • open-source • impl. online or on machine • hyper-parameter configuration • prediction values in range; filtering of boundary maps | <ul style="list-style-type: none"> • programming • additional georeferencing step • label image manually | <ul style="list-style-type: none"> • no programming • georeferencing • label image by software | <ul style="list-style-type: none"> • commercial • impl. on machine only • hyper-parameter configuration • fixed predictions |

4.4. Application of Detected Visible Boundaries

Cadastral boundaries are often demarcated by objects visible in remote sensing imagery [2,8]. Automatic detection of cadastral boundaries based on remote sensing imagery, especially UAV imagery, has rarely been investigated. Automatic extraction of visible land boundaries, i.e., property boundaries, offers the potential to improve current approaches to cadastral mapping. The boundary mapping approaches investigated are based on deep learning and offer improvements in terms of time and cost.

Both boundary mapping approaches, i.e., U-Net and ENVI deep learning, can help to facilitate and accelerate cadastral mapping, especially in areas where large parts of the cadastral boundaries are continuous and visible. In terms of delineation effort per parcel, automatic delineation approaches (including post-alignments) require up to 40% less time in rural areas compared to manual delineation, based on [17]. However, in areas where cadastral boundaries are not visible in the image, manual delineation remains superior. Overall, it can be said that manual methods provide slower but more accurate delineations, while automatic methods are faster but less accurate (once the model is trained).

In countries with low cadastral coverage, deep learning-based mapping approaches can be used to produce cadastral maps. In countries with full cadastral coverage, the detected visible boundaries can be used to automate the process of revising the up-to-dateness of existing cadastral maps. In this way, areas requiring updating and improving cadastral boundary maps can be automatically identified. Notwithstanding the advances in cadastral mapping, the automation of cadastral boundary detection is still ongoing [15,17,18]. This is due to the nature of cadastral boundaries, which may have a simple geometry but are very complex to interpret. Consequently, automatically detected visible land boundaries should be considered as preliminary cadastral boundaries. Verification of automatically detected land boundaries should be aligned with the existing technical, legal and institutional framework of land administration. Moreover, not every cadastral boundary is demarcated with visible objects. In this study, boundary mapping approaches were tested in rural areas. It is argued that the number of visible cadastral boundaries is higher compared to urban areas [2].

Automating the detection of invisible cadastral boundaries remains a challenge in land administration, which has already been highlighted in [17]. Future work could investigate and analyze the applicability of deep learning for invisible cadastral boundaries that are marked prior to the UAV survey. It should be further investigated which type and size of land boundary markers are more appropriate for demarcating the invisible boundaries.

5. Conclusions

Deep learning is becoming increasingly important in cadastral applications as a state-of-the-art method for automatic boundary detection. The aim of this study was to investigate the potential of CNN architecture, namely U-Net, based on UAV imagery training samples—as a deep learning-based detector for visible land boundaries. The results and land boundary mapping approach using U-Net were compared with software-

based ENVI deep learning. The overall accuracy for both CNN models was higher than 95%. This indicates that deep learning-based land boundary detection usually faces an unbalanced distribution of pixels per class, namely for ‘boundary’ and ‘no boundary’.

Regarding the quality of recognition for the class ‘boundary’ in the case of U-Net, we obtained low recall and high precision when the threshold ‘boundary’ ≤ 0.5 was set. This resulted in a recall of 0.35 and a precision of 0.68. Prediction reclassification can be considered as a tool to filter the predicted boundary maps. For example, to compare the results with ENVINet5, the threshold had to be set almost to its maximum. Here, U-Net provided a recall of 0.65 and a precision of 0.41. For ENVI deep learning, we obtained a recall of 0.84 and a precision of 0.35. Based on the F1 score (U-Net 0.51 and ENVI deep learning 0.49), U-Net provided slightly better and more balanced results. The predicted land boundary maps obtained with U-Net were georeferenced and merged in an additional post-processing step. This was not an issue with ENVI deep learning—the output boundary maps were already georeferenced. Overall, U-Net is a programming-based solution and provides a more flexible boundary mapping approach in terms of hyperparameters and CNN model setting. On the other hand, it can be somewhat complex and demanding for the practice as not all land administrators are skilled in programming. In contrast, ENVI deep learning does not require any programming and deep learning is guided by the software process.

While programming-based deep learning is challenging due to the complexity of the processes and their control, commercial software-based deep learning brings some abstraction but at the same time has limitations in terms of influencing the processes flow. Both land boundary mapping approaches investigated in our study can be used to accelerate and facilitate cadastral mapping in rural areas. However, the automatically detected visible land boundaries should be considered as preliminary boundaries for cadastral map production and updating. The results should be further aligned with technical, legal and institutional framework of land administration.

Author Contributions: Conceptualization, B.F. and A.L.; methodology, B.F., M.R. and A.L.; software, B.F. and M.R.; validation, B.F., M.R. and A.L.; formal analysis, B.F.; investigation, B.F.; resources B.F., M.R. and A.L.; writing—original draft preparation, B.F.; writing—review and editing, B.F., M.R. and A.L.; visualization, B.F.; supervision, A.L. All authors have read and agreed to the published version of the manuscript.

Funding: This research was funded by Slovenian Research Agency, research core funding number P2-0406 Earth Observation and Geoinformatics. The APC was funded by P2-0406 and V2-1934 from the Slovenian Research Agency and the Surveying and Mapping Authority of the Republic of Slovenia.

Institutional Review Board Statement: Not applicable.

Informed Consent Statement: Not applicable.

Data Availability Statement: The data presented in this study are openly available in https://unilj-my.sharepoint.com/:f/g/personal/bfetai_fgg_uni-lj_si/EhZieqQdkc5EkrdfjPwo5AYBQI9n_GOE-yM3Yux-wjmfWA?e=5mTYrH (accessed on 25 May 2021).

Acknowledgments: We thank the anonymous reviewers for their valuable comments and suggestions. We acknowledge Klemen Kozmus Trajkovski for capturing the UAV data and for the support during the fieldwork.

Conflicts of Interest: The authors declare no conflict of interest.

References

1. Enemark, S.; Bell, K.C.; Lemmen, C.; McLaren, R. *Fit-For-Purpose Land Administration*; International Federation of Surveyors (FIG): Copenhagen, Denmark, 2014; ISBN 978-87-92853-11-0.
2. Luo, X.; Bennett, R.; Koeva, M.; Lemmen, C.; Quadros, N. Quantifying the Overlap between Cadastral and Visual Boundaries: A Case Study from Vanuatu. *Urban Sci.* **2017**, *1*, 32. [[CrossRef](#)]
3. Zevenbergen, J. A systems approach to land registration and cadastre. *Nord. J. Surv. Real Estate Res.* **2004**, *1*, 11–24.

4. Simbizi, M.C.D.; Bennett, R.M.; Zevenbergen, J. Land tenure security: Revisiting and refining the concept for Sub-Saharan Africa's rural poor. *Land Use Policy* **2014**, *36*, 231–238. [[CrossRef](#)]
5. Williamson, I.P. *Land Administration for Sustainable Development*, 1st ed.; ESRI Press Academic: Redlands, CA, USA, 2010; ISBN 9781589480414.
6. Binns, B.O.; Dale, P.F. *Cadastral Surveys and Records of Rights in Land*; Food and Agriculture Organization of the United Nations: Rome, Italy, 1995; ISBN 9251036276.
7. Grant, D.; Enemark, S.; Zevenbergen, J.; Mitchell, D.; McCamley, G. The Cadastral triangular model. *Land Use Policy* **2020**, *97*, 104758. [[CrossRef](#)]
8. Crommelinck, S.; Bennett, R.; Gerke, M.; Nex, F.; Yang, M.; Vosselman, G. Review of Automatic Feature Extraction from High-Resolution Optical Sensor Data for UAV-Based Cadastral Mapping. *Remote Sens.* **2016**, *8*, 689. [[CrossRef](#)]
9. Zevenbergen, J.; Bennett, R. The visible boundary: More than just a line between coordinates. In Proceedings of the GeoTech Rwanda, Kigali, Rwanda, 18–20 November 2015; pp. 1–4.
10. Manyoky, M.; Theiler, P.; Steudler, D.; Eisenbeiss, H. Unmanned Aerial Vehicle in Cadastral Applications. *Int. Arch. Photogramm. Remote Sens. Spat. Inf. Sci.* **2011**, 57–62. [[CrossRef](#)]
11. Puniach, E.; Bieda, A.; Ćwiakała, P.; Kwartnik-Pruc, A.; Parzych, P. Use of Unmanned Aerial Vehicles (UAVs) for Updating Farmland Cadastral Data in Areas Subject to Landslides. *ISPRS Int. J. Geo-Inf.* **2018**, *7*, 331. [[CrossRef](#)]
12. Koeva, M.; Muneza, M.; Gevaert, C.; Gerke, M.; Nex, F. Using UAVs for map creation and updating. A case study in Rwanda. *Surv. Rev.* **2018**, *50*, 312–325. [[CrossRef](#)]
13. Stöcker, C.; Nex, F.; Koeva, M.; Gerke, M. High-Quality UAV-Based Orthophotos for Cadastral Mapping: Guidance for Optimal Flight Configurations. *Remote Sens.* **2020**, *12*, 3625. [[CrossRef](#)]
14. Colomina, I.; Molina, P. Unmanned aerial systems for photogrammetry and remote sensing: A review. *ISPRS J. Photogramm. Remote Sens.* **2014**, *92*, 79–97. [[CrossRef](#)]
15. Xia, X.; Persello, C.; Koeva, M. Deep Fully Convolutional Networks for Cadastral Boundary Detection from UAV Images. *Remote Sens.* **2019**, *11*, 1725. [[CrossRef](#)]
16. Ramadhani, S.A.; Bennett, R.M.; Nex, F.C. Exploring UAV in Indonesian cadastral boundary data acquisition. *Earth Sci. Inf.* **2018**, *11*, 129–146. [[CrossRef](#)]
17. Crommelinck, S.; Koeva, M.; Yang, M.Y.; Vosselman, G. Application of Deep Learning for Delineation of Visible Cadastral Boundaries from Remote Sensing Imagery. *Remote Sens.* **2019**, *11*, 2505. [[CrossRef](#)]
18. Fetai, B.; Oštir, K.; Kosmatin Fras, M.; Liseč, A. Extraction of Visible Boundaries for Cadastral Mapping Based on UAV Imagery. *Remote Sens.* **2019**, *11*, 1510. [[CrossRef](#)]
19. Crommelinck, S.; Bennett, R.; Gerke, M.; Yang, M.; Vosselman, G. Contour Detection for UAV-Based Cadastral Mapping. *Remote Sens.* **2017**, *9*, 171. [[CrossRef](#)]
20. Arbeláez, P.; Maire, M.; Fowlkes, C.; Malik, J. Contour detection and hierarchical image segmentation. *IEEE Trans. Pattern Anal. Mach. Intell.* **2011**, *33*, 898–916. [[CrossRef](#)]
21. Ma, L.; Liu, Y.; Zhang, X.; Ye, Y.; Yin, G.; Johnson, B.A. Deep learning in remote sensing applications: A meta-analysis and review. *ISPRS J. Photogramm. Remote Sens.* **2019**, *152*, 166–177. [[CrossRef](#)]
22. Zhu, X.X.; Tuia, D.; Mou, L.; Xia, G.-S.; Zhang, L.; Xu, F.; Fraundorfer, F. Deep Learning in Remote Sensing: A Comprehensive Review and List of Resources. *IEEE Geosci. Remote Sens. Mag.* **2017**, *5*, 8–36. [[CrossRef](#)]
23. Persello, C.; Stein, A. Deep Fully Convolutional Networks for the Detection of Informal Settlements in VHR Images. *IEEE Geosci. Remote Sens. Lett.* **2017**, *14*, 2325–2329. [[CrossRef](#)]
24. Pan, Z.; Xu, J.; Guo, Y.; Hu, Y.; Wang, G. Deep Learning Segmentation and Classification for Urban Village Using a Worldview Satellite Image Based on U-Net. *Remote Sens.* **2020**, *12*, 1574. [[CrossRef](#)]
25. Park, S.; Song, A. Discrepancy Analysis for Detecting Candidate Parcels Requiring Update of Land Category in Cadastral Map Using Hyperspectral UAV Images: A Case Study in Jeonju, South Korea. *Remote Sens.* **2020**, *12*, 354. [[CrossRef](#)]
26. Ronneberger, O.; Fischer, P.; Brox, T. U-Net: Convolutional Networks for Biomedical Image Segmentation. 2015. Available online: <http://arxiv.org/pdf/1505.04597v1> (accessed on 24 February 2021).
27. Diakogiannis, F.I.; Waldner, F.; Caccetta, P.; Wu, C. ResUNet-a: A deep learning framework for semantic segmentation of remotely sensed data. *ISPRS J. Photogramm. Remote Sens.* **2020**, *162*, 94–114. [[CrossRef](#)]
28. Flood, N.; Watson, F.; Collett, L. Using a U-net convolutional neural network to map woody vegetation extent from high resolution satellite imagery across Queensland, Australia. *Int. J. Appl. Earth Obs. Geoinf.* **2019**, *82*, 101897. [[CrossRef](#)]
29. Zhao, X.; Yuan, Y.; Song, M.; Ding, Y.; Lin, F.; Liang, D.; Zhang, D. Use of Unmanned Aerial Vehicle Imagery and Deep Learning UNet to Extract Rice Lodging. *Sensors* **2019**, *19*, 3859. [[CrossRef](#)]
30. Alshaiikhli, T.; Liu, W.; Maruyama, Y. Automated Method of Road Extraction from Aerial Images Using a Deep Convolutional Neural Network. *Appl. Sci.* **2019**, *9*, 4825. [[CrossRef](#)]
31. Wierzbicki, D.; Matuk, O.; Bielecka, E. Polish Cadastre Modernization with Remotely Extracted Buildings from High-Resolution Aerial Orthoimagery and Airborne LiDAR. *Remote Sens.* **2021**, *13*, 611. [[CrossRef](#)]
32. Wani, M.A.; Bhat, F.A.; Afzal, S.; Khan, A.I. *Advances in Deep Learning*; Springer: Singapore, 2020; ISBN 978-981-13-6793-9.
33. GRASS Development Team. *GRASS GIS Bringing Advanced Geospatial Technologies to the World*; GRASS: Beaverton, OR, USA, 2020.
34. Google Colaboratory. Available online: <https://colab.research.google.com> (accessed on 29 April 2021).

35. Chollet, F.; et al. Keras. 2015. Available online: <https://keras.io> (accessed on 29 April 2021).
36. Martin, A.; Ashish, A.; Paul, B.; Eugene, B.; Zhifeng, C.; Craig, C.; Greg, S.C.; Andy, D.; Jeffrey, D.; Matthieu, D.; et al. TensorFlow: Large-Scale Machine Learning on Heterogeneous Systems. 2015. Available online: <https://www.tensorflow.org/> (accessed on 29 April 2021).
37. Zhixuhao. Unet for Image Segmentation. Available online: <https://github.com/zhixuhao/unet> (accessed on 24 February 2021).
38. Gillies, S. Rasterio: Geospatial Raster I/O for Python Programmers. 2013. Available online: <https://github.com/mapbox/rasterio> (accessed on 30 April 2021).
39. GDAL/OGR Contributors. GDAL/OGR Geospatial Data Abstraction Software Library. 2021. Available online: <https://gdal.org> (accessed on 30 April 2021).
40. Harris, C.R.; Millman, K.J.; van der Walt, S.J.; Gommers, R.; Virtanen, P.; Cournapeau, D.; Wieser, E.; Taylor, J.; Berg, S.; Smith, N.J.; et al. Array programming with NumPy. *Nature* **2020**, *585*, 357–362. [[CrossRef](#)]
41. Exelis Visual Information Solutions. In *ENVI Deep Learning*; L3Harris Geospatial: Boulder, CO, USA, 1977.
42. Exelis Visual Information Solutions. ENVI Deep Learning—Training Background. Available online: <https://www.l3harrisgeospatial.com/docs/BackgroundTrainDeepLearningModels.html> (accessed on 9 March 2021).

APPENDIX E : Revising Cadastral Data on Land Boundaries Using Deep Learning in Image-Based Mapping

B. Fetai, D. Grigillo, and A. Lisec (2022)

ISPRS International Journal of Geo-Information vol. 11, no. 5, p. 298

doi: 10.3390/ijgi11050298.

Article

Revising Cadastral Data on Land Boundaries Using Deep Learning in Image-Based Mapping

Bujar Fetai * , Dejan Grigillo and Anka Lisec 

Faculty of Civil and Geodetic Engineering, University of Ljubljana, Jamova Cesta 2, 1000 Ljubljana, Slovenia; dejan.grigillo@fgg.uni-lj.si (D.G.); anka.lisec@fgg.uni-lj.si (A.L.)

* Correspondence: bujar.fetai@fgg.uni-lj.si; Tel.: +386-1-4768629

Abstract: One of the main concerns of land administration in developed countries is to keep the cadastral system up to date. The goal of this research was to develop an approach to detect visible land boundaries and revise existing cadastral data using deep learning. The convolutional neural network (CNN), based on a modified architecture, was trained using the Berkeley segmentation data set 500 (BSDS500) available online. This dataset is known for edge and boundary detection. The model was tested in two rural areas in Slovenia. The results were evaluated using *recall*, *precision*, and the *F1 score*—as a more appropriate method for unbalanced classes. In terms of detection quality, balanced *recall* and *precision* resulted in *F1 scores* of 0.60 and 0.54 for Ponova vas and Odranci, respectively. With lower *recall* (completeness), the model was able to predict the boundaries with a *precision* (correctness) of 0.71 and 0.61. When the cadastral data were revised, the low values were interpreted to mean that the lower the *recall*, the greater the need to update the existing cadastral data. In the case of Ponova vas, the *recall* value was less than 0.1, which means that the boundaries did not overlap. In Odranci, 21% of the predicted and cadastral boundaries overlapped. Since the direction of the lines was not a problem, the low *recall* value (0.21) was mainly due to overly fragmented plots. Overall, the automatic methods are faster (once the model is trained) but less accurate than the manual methods. For a rapid revision of existing cadastral boundaries, an automatic approach is certainly desirable for many national mapping and cadastral agencies, especially in developed countries.

Keywords: land; visible boundary; cadastre; maintenance; UAV; deep learning



Citation: Fetai, B.; Grigillo, D.; Lisec, A. Revising Cadastral Data on Land Boundaries Using Deep Learning in Image-Based Mapping. *ISPRS Int. J. Geo-Inf.* **2022**, *11*, 298. <https://doi.org/10.3390/ijgi11050298>

Academic Editors: Wolfgang Kainz, Fabio Remondino, Joep Crompvoets and Norbert Haala

Received: 3 March 2022

Accepted: 30 April 2022

Published: 4 May 2022

Publisher's Note: MDPI stays neutral with regard to jurisdictional claims in published maps and institutional affiliations.



Copyright: © 2022 by the authors. Licensee MDPI, Basel, Switzerland. This article is an open access article distributed under the terms and conditions of the Creative Commons Attribution (CC BY) license (<https://creativecommons.org/licenses/by/4.0/>).

1. Introduction

Mapping the boundaries of land rights, creating a complete cadastre and being able to keep it up to date is a major concern for land administration. Considering that three-quarters of the world's land rights are not recognised and registered, it is necessary to speed up the process of cadastral mapping [1]. The challenge of creating a complete cadastre usually arises in developing countries—with low cadastral coverage [2,3]. Mapping and registering land rights in a formal cadastre is supposed to increase land tenure security [4,5]. However, an effective cadastre should also provide up-to-date information on people and land relationships beyond the adjudication stage [6,7]. Updating, in most cases, refers to the comparison of two datasets—one reflecting the state of the cadastral database and one newly acquired [8]. In view of this, the term “revision” is used as a synonym—since “updating” (as an act of formal change) is based on “revisions”.

In countries that already have a complete cadastre, providing up-to-date land data is a top priority [9]. It has taken decades for the cadastre to be complete in these countries, where conventional techniques such as ground-based surveying techniques or analogue aerial photogrammetry have typically been used [10]. Both methods are considered labour intensive and time-consuming [11,12]. The result was the creation of analogue cadastral maps and land records that later had to be digitised and integrated into a geographic information system (GIS) or broader land information systems. Although complete cadastral

were created, many national mapping and cadastral agencies (NMCAs) failed to properly maintain the cadastres [13]. The reality that cadastres attempt to depict is complex and dynamic [14,15], and underestimating the dynamics of the relationships between people and land, in reality, has led to outdated cadastral maps. Apart from the advances in surveying and mapping technologies, most of which have already been tested in developing countries [16–19], cadastral surveying and boundary data maintenance in developed countries continued to be carried out using ground-based techniques such as tacheometry and global navigation satellite systems (GNSS) methods [10,12]. This approach presents many challenges in terms of mapping efficiency, which can be overcome by low-cost and rapid cadastral surveying and indirect mapping techniques.

Indirect mapping techniques rely on delineating visible cadastral boundaries from high-resolution remote sensing imagery. The application of image-based cadastral mapping is based on the recognition that many cadastral boundaries coincide with natural or man-made structures that are readily visible on remote sensing imagery [3,17]. In cadastral applications, unmanned aerial vehicles (UAVs) have shown great potential for mapping land parcel boundaries in both rural and urban areas [18,20–22]. In addition, UAV-based orthoimagery has been considered as a basemap for the creation of cadastral maps and for the revision of existing cadastral maps [23–25]. Apart from the high visibility of spatial units on UAV imagery relevant to cadastral mapping, many previous case studies have reported the manual delineation of spatial units [16], but only a limited number of studies have investigated the automatic mapping approach. The innovative approaches aim to simplify and speed up image-based cadastral mapping by automating the delineation of visible boundaries. Mainly, customised image segmentation and edge detection algorithms have been used to automatically adjust cadastral mapping [23,26].

Modern methods for automatic boundary detection in cadastral mapping also include deep learning [27–30]. Recent studies indicate that deep learning such as convolutional neural networks (CNNs) ensure a higher accuracy in delineating visible land boundaries than some of the state-of-the-art machine learning or object-based techniques [27,28]. CNNs can be trained in two ways: from scratch or by transfer learning [31]. When training the model from scratch, remote sensing data have to be provided, i.e., images and labels. In transfer learning, the model is pre-trained, usually with a large amount of data with more abstract features, and the last convolutional layer is trained with the specific features of the new application. Crommelinck et al. [27] pre-trained the model using transfer-learning and reported that VGG19, i.e., 19 layers deep CNN, provides a more automated and accurate detection of visible boundaries from UAV imagery than random forest. The pre-training was based on aerial imagery, which also had to be provided. Furthermore, the study highlights that the model based on VGG19 provides more promising metrics than some other architectures (such as ResNet, MobileNet, and DenseNet). Xia et al. [28] investigated a fully CNN for cadastral boundary detection in urban and semi-urban areas. The model was trained from scratch using UAV tiles, and the results show that the approach outperformed object-based techniques, including global probability boundary (gPb) and multi-resolution segmentation (MRS). Park and Song [32] aimed to detect the changes between existing cadastral maps and current land use boundaries in the field. The model was trained from scratch using hyperspectral UAV imagery. However, providing thousands of UAV training data can be considered a limitation, especially when a model is trained from scratch, as highlighted in [29]. This can be overcome with a CNN architecture that requires less training data, for instance, U-Net, followed by data augmentation prior to processing [29,33]. The challenge here remains to confirm what should be a sufficient variety of UAV training data to learn a robust network model.

Objective of the Study

In general, it is argued that the main challenge with CNNs supporting cadastral mapping is the processing of a large amount of remote sensing training data and the computational requirements. Therefore, an important condition for any deep learning

method is that the total time required to detect the final boundaries, including pre- and post-processing, should not be longer than the total time of a manual method [10]. This serves as a justification and allows the objective of this study to be defined.

The main objective of this study was to develop an efficient and cost-effective approach for mapping visible land boundaries using CNN. The mapping approach is based on the detection of visible land boundaries that coincide with large parts of the cadastral boundaries—especially in rural areas. Automation of visible land boundary detection can be used to revise existing cadastral maps and to automatically identify areas where updates are needed. At this point, it should be emphasised that not all cadastral boundaries are visible and that some of them are difficult to detect on UAV imagery.

2. Materials and Methods

The workflow of this study was comprised of four core parts, i.e., the training approach, visible boundary detection, accuracy assessment, and vectorisation of boundary maps. The individual steps and details are described in the following subsections. The generalised workflow is shown in Figure 1.

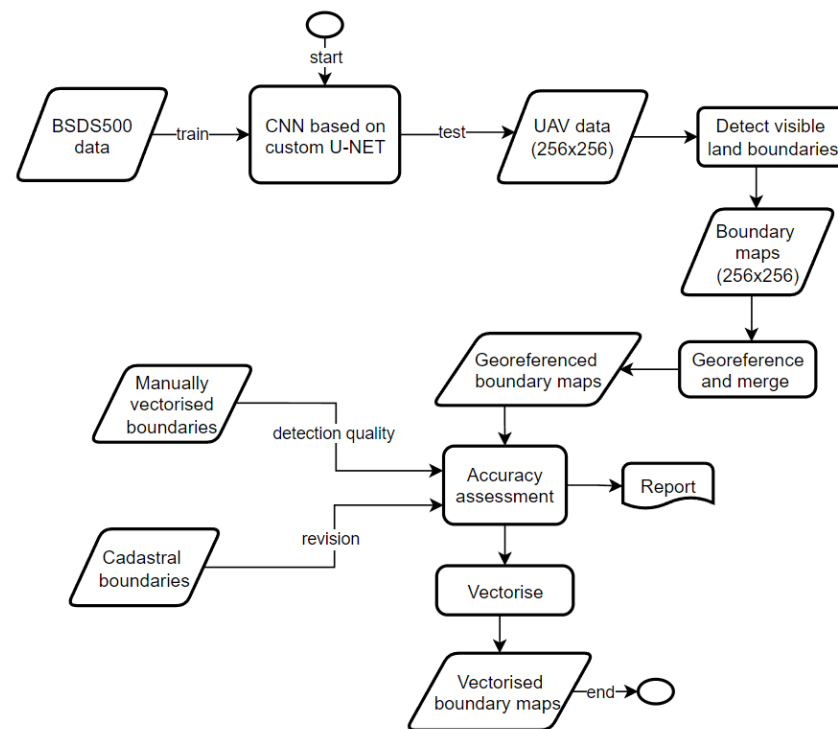


Figure 1. Generalised workflow applied in this study.

2.1. Training Approach and Dataset

Considering the main objective, a CNN that requires a smaller amount of training data is preferable. U-Net is a CNN architecture that provides fast and precise localisation of features from images. The U-Net consists of an encoding path and a decoding path, giving it a U-shape. The encoding path is a convolutional network consisting of repeated convolutions (3×3), each followed by a ReLU and max-pooling (2×2) operation. During the encoding path, spatial resolution is decreased while feature information is increased. The decoding path combines spatial and feature information through a sequence of up-convolutions (2×2) and merging with high-resolution features from the decoding path, where the size of the images is converted to their original size. A detailed description of the original U-Net architecture can be found in [33]. In this study, the U-Net was considered as a deep learning-based detector for visible boundaries.

Given the complexity of our domain problem, namely the detection of visible land boundaries to revise existing cadastral maps, the original architecture was customised

and is shown in Figure 2. The customisation included the removal of the first level of the original U-Net. This reduces the number of parameters that can be trained and was sufficient in terms of complexity for our domain problem.

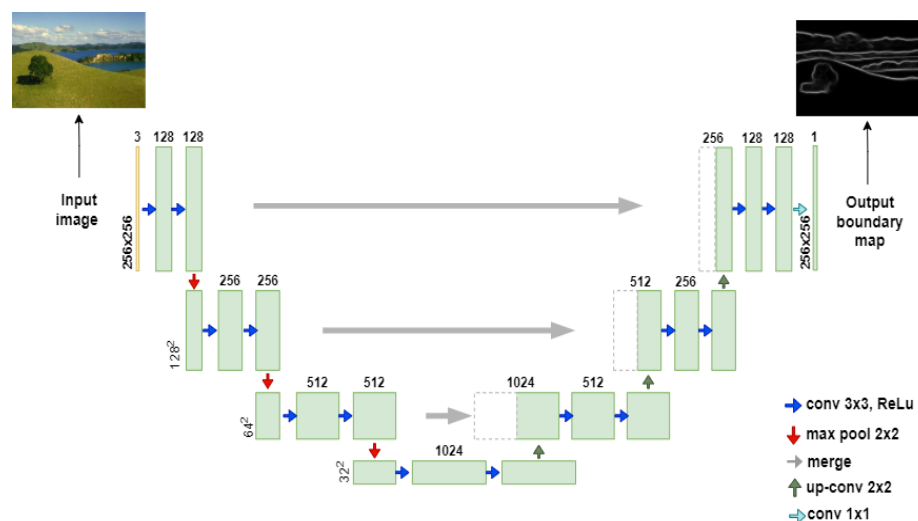


Figure 2. Convolutional neural network (CNN) based on customised U-Net architecture.

The model was trained using the Berkeley segmentation data set 500 (BSDS500) and is available at [34]. BSDS500 is an accessible dataset and a standard benchmark for image segmentation and edge or boundary detection tasks that can be used to train the CNN while matching the domain problem of this study. The dataset consists of 500 everyday images and their corresponding labels. The approach is intended to be transferable to images of other scenes and contexts—for example, UAV images. The data is organised in training, validation, and test subsets. Each image has hand-labelled boundaries that come from an average of five annotators, or about 2500 samples in total. To increase the number of training samples and to improve the flexibility of the validation split, the images of the training and validation subsets were merged into one. In addition, the target image size was set to 256×256 pixels.

Training a CNN requires a lot of memory and a powerful graphics processing unit (GPU) to perform efficient computations. To combat this, the training of the customised U-Net with the BSDS500 dataset was performed in Google Collaboratory [35]. The model was implemented in Keras [36], and the process was written in Python using the TensorFlow library [37]. The trained model was tested using UAV images with a size of 256×256 pixels.

2.2. Visible Boundary Detection from UAV Data

Two rural areas were selected to test the U-Net model, one in Ponova vas and the other in Odranci, both in Slovenia. The rural areas were chosen because the number of visible cadastral boundaries in these areas is higher than in dense urban areas.

In Ponova vas, the flight altitude was set to 80 m, and 354 images were acquired to cover the study area (Figure 3a). The UAV images were indirectly georeferenced using 12 ground control points (GCPs) evenly distributed over the field. The GCPs were surveyed with real-time kinematic (RTK) using the global navigation satellite system (GNSS) and Leica Viva receiver. The study area had an area of 25 ha, and an orthoimage with ground sampling distance (GSD) of 2.0 cm was produced from UAV images.



Figure 3. Manually delineated visible land boundaries; (a) UAV orthoimage with ground sampling distance (GSD) of 0.25 m Ponova vas, Slovenia; (b) UAV orthoimage with GSD of 0.25 m for Odranci, Slovenia; (a,b) (EPSG 3794).

In Odranci, UAV images were acquired at the altitude of 90 m, and 997 images were acquired to cover the study area (Figure 3b). A total of 18 GCPs were used to georeference the UAV images. The GCPs were surveyed using RTK with the Leica GS18 GNSS receiver. The GSD of the produced orthoimage was 2.3 cm, and the study area had an area of 63.9 ha.

All UAV data were acquired using a rotary-wing drone, the DJI Phantom 4 Pro. The selected rural areas included agricultural fields, roads, tree groves, and hedgerows. Table 1 shows the specifications of the UAV data.

Table 1. Specification of the unmanned aerial vehicle (UAV) dataset for the selected study areas.

| Location | UAV Model | Camera/Focal Length [mm] | Overlap Forward/Sideward | Flight Altitude | GSD [cm] | Coverage Area [ha] |
|----------------------|-------------------|--------------------------|--------------------------|-----------------|----------|--------------------|
| Ponova vas, Slovenia | DJI Phantom 4 Pro | 1" CMOS/24mm | 80/70 | 80 m | 2.01 | 25.0 |
| Odranci, Slovenia | | | | 90 m | 2.35 | 63.9 |

UAV orthoimages for Ponova vas and Odranci were randomly tiled in 256×256 pixels. To increase the field of view for each tile, the original spatial resolution of the UAV orthoimages had to be converted to a larger GSD, from 2 cm to 25 cm, using the nearest neighbour resampling method. In addition, corresponding ground truth images (also called label images) were created for each UAV image. The $256 \times 256 \times 1$ ground images were created from the manually digitised visible land boundaries, which were originally in the vector format (Figure 3a,b). Since the predicted boundary maps were in the raster format, the reference boundaries were buffered by 50 cm and later rasterised using tools from GRASS GIS [38]. Comparison of the predicted boundaries with the manually vectorised boundaries allowed the CNN model to be evaluated, i.e., the ability of the model to produce boundary maps for visible land boundaries.

In addition, cadastral boundaries were also used as reference data. The cadastral boundaries were rasterised using the same tool and buffer size as the manual boundaries. Unlike the manual approach, by comparing the predicted boundaries with the cadastral boundaries, the number of cadastral boundaries that overlap with the visible land boundaries can be determined. This approach allowed existing cadastral maps to be revised. The current cadastral boundaries were retrieved from the e-portal of the Slovenian NMCA, an online platform for requesting official cadastral data [39].

The predicted boundary maps were not georeferenced. Since georeferencing is a key component in cadastral mapping, further edits were made. First, the predicted boundary maps (for each UAV tile) were georeferenced. Second, the georeferenced tiles were merged to obtain the boundary map for the entire extent. The analysis and further processing were performed using GDAL [40], Rasterio [41], and Numpy [42]. After georeferencing, the merged boundary maps were used to evaluate the accuracy and to quantify the overlap between visible and cadastral boundaries.

2.3. Accuracy Assessment

The accuracy assessment refers to the evaluation of the CNN model and the evaluation of the detection quality of the visible land boundaries for the UAV data.

The CNN model, namely the customised U-Net model, was monitored with *accuracy* and *loss* during the training. The *loss* represents the difference between the boundaries predicted by the model and the reference boundaries. In this study, *cross-entropy loss* was used—the most common *loss* function used in CNNs. The performance of the model was measured using *overall accuracy*. *Overall accuracy* as an evaluation metric is defined as the sum of correctly predicted boundaries by the model divided by all predicted boundaries. The definitions and equations for *cross-entropy* and *overall accuracy* can be found in [43].

Boundary detection based on CNNs falls into the domain of binary classification. Here, it is a challenge to find balanced pixels for the classes “boundary” and “no boundary”. The reason is that the number of background pixels (class “no boundary”) in predicted boundary maps or cadastral maps is always much higher than the number of pixels representing the boundaries themselves. For this reason, detection quality (i.e., the degree of correctly detected visible boundaries compared to reference data) was evaluated by calculating the *F1 score*, *recall*, and *precision*—more appropriate metrics for unbalanced classes. In such a calculation, the “boundary” pixels were defined as a positive class since this was the focus of our study.

Table 2 shows the confusion matrix used to evaluate the detection quality of visible land boundaries and the overlap between visible and cadastral boundaries. The confusion matrix classifies pixels into true positive (TP), false positive (FP), true negative (TN), and false negative (FN).

Table 2. Confusion matrix.

| | | Ground Truth | | |
|------------|-------------|--------------|----------|-------------|
| | | Boundary | Boundary | No boundary |
| Prediction | Boundary | TP | FP | |
| | No boundary | FN | TN | |

Based on the number of pixels in the confusion matrix, *recall* and *precision* are calculated with the following equations:

$$recall = TP / (TP + FN) \quad (1)$$

$$precision = TP / (TP + FP) \quad (2)$$

Recall can be interpreted as completeness, while *precision* means correctness, and both are important for cadastral mapping. The *F1 score* is composed of *recall* and *precision* and is expressed by the following equation:

$$F1\ score = 2 * (recall * precision) / (recall + precision) \quad (3)$$

2.4. Vectorisation of Predicted Boundary Maps—Hough Transform

Current cadastral maps are in the vector format and are usually integrated into the GIS environment. To obtain cadastral compliant output data, an automatic vectorisation process was implemented. The predicted boundary maps were available in the raster

format, with pixel values from 0 to 1—for each UAV tile as the input. Once georeferenced, the predicted boundaries were automatically vectorised using the Hough transform [44,45]. Vectorisations were performed for binary predicted maps, with a threshold “boundary” ≥ 0.3 and “boundary” ≥ 0.5 . Thresholds were chosen based on an assessment of the accuracy of detected visible land boundaries.

The Hough transform extracts straight lines or curves from images and can be used for digitising cadastral maps [46], or for the extraction of land boundaries [47]. The feature extraction technique was implemented in Matlab. Here, the technique was designed to detect lines, using the parametric representation of a line:

$$\rho = x \cos\theta + y \sin\theta \quad (4)$$

where:

ρ —the distance from the origin to the line along a vector perpendicular to the line,

θ —the angle between the x -axis and this vector.

Various parameters for vectorisation were tested and empirically confirmed that the following parameters generally gave the best results: the resolution for ρ and θ was set to 2 and 0.05, respectively, and lines with a length of at least 10 pixels and filled gaps of 10 pixels between segments of a straight line were searched for. Vectorisation of relatively small tiles using Hough transform is not computationally demanding, which allowed us to implement it iteratively. After vectorising the straight line which corresponded to the highest value of Hough transform, the pixels in the binary image within a distance of 3 pixels from the vectorised line were set to 0. Then the Hough transformation was performed again. With the implemented method, the lines were simplified and avoided the vectorisation of doubly adjacent lines.

3. Results

3.1. CNN and Training Approach

Based on the custom U-Net architecture, the CNN was trained with the BSDS500 dataset, with the target size set to 256×256 pixels. The training images were in RGB, and 30% of the training data was used for validation. This resulted in 1505 samples for training and 645 samples for validation.

After some testing, the training parameters were adjusted to fine-tune the model. To avoid changing the size of the predicted boundary maps for each input image, a max-pooling method with equal padding was specified. In addition, a dropout rate of 0.5 was used. The dropout rate is used to ignore randomly selected neurons to avoid overfitting the model. The layer depth was set to 1024, and a sigmoid was used as the final activation layer. During training, the Adam optimiser was used with a learning rate of 10^{-4} .

The model was trained with a batch size of 16 for 50 epochs. The early stop function with the patience of 10 epochs was activated. This feature stops training when the performance of the model in a validation dataset stops improving. The number of steps per epoch was calculated by dividing the total number of training samples by the batch size. Training was performed in Google Collaboratory. The service provides access to different GPUs that affect the training time. In this study, the service provided a GPU with 12.7 GB RAM. The early stop ended the training at epoch 18, which took 1.5 h. With a more powerful GPU, e.g., 25 GB, training the model for 100 epochs took 82 min (with a batch size of 32 and without early stop). The training performance of the adapted U-Net is shown in Figure 4.

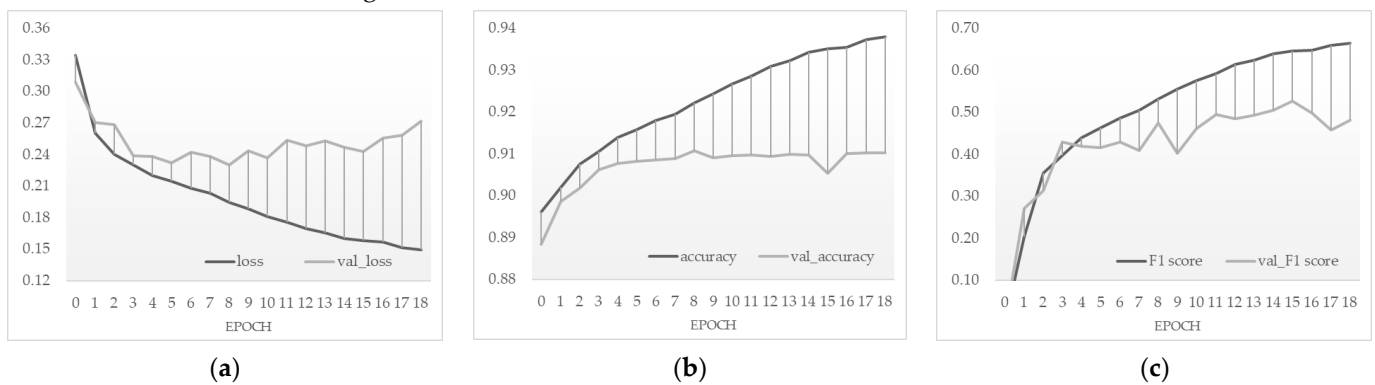


Figure 4. Performance of customised U-Net: (a) *loss*, (b) *accuracy*, and (c) *F1 score* for our fine-tuned model.

3.2. Visible Boundary Detection from UAV Imageries

Once the model was trained, it was applied to $256 \times 256 \times 3$ UAV images to detect visible land boundaries. A prediction boundary map was created for each UAV tile. The boundary maps were georeferenced and merged to determine the total extent of the test area. The results of the predicted boundary maps based on georeferenced and merged UAV tiles are shown in Figures 5 and 6. In addition, the results obtained with the customised CNN were compared with the original U-Net.

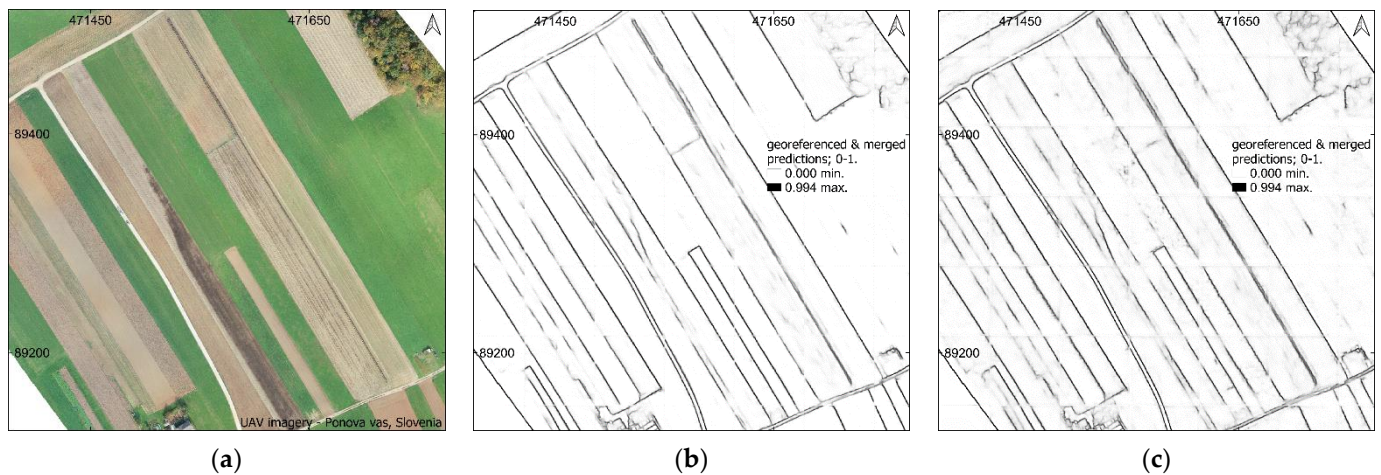


Figure 5. Georeferenced and merged boundary maps for the test area in (a) Ponova vas, Slovenia. Predicted boundary map with (b) customised CNN, and (c) original U-Net architecture.

The predicted boundary maps, shown in Figures 5 and 6, had pixel values ranging from 0 to 1. To evaluate the detection quality of the visible land boundaries, the predictions were compared to the ground truth data on land boundaries that had been manually digitised from the UAV imagery. The ground data consisted of two classes, i.e., “boundary” and “no boundary” with values of 1 and 0, respectively, so the predicted boundary maps were reclassified into two classes with threshold values of 0.3 and 0.5. The results of the reclassified boundary maps are shown in Figures 7 and 8.

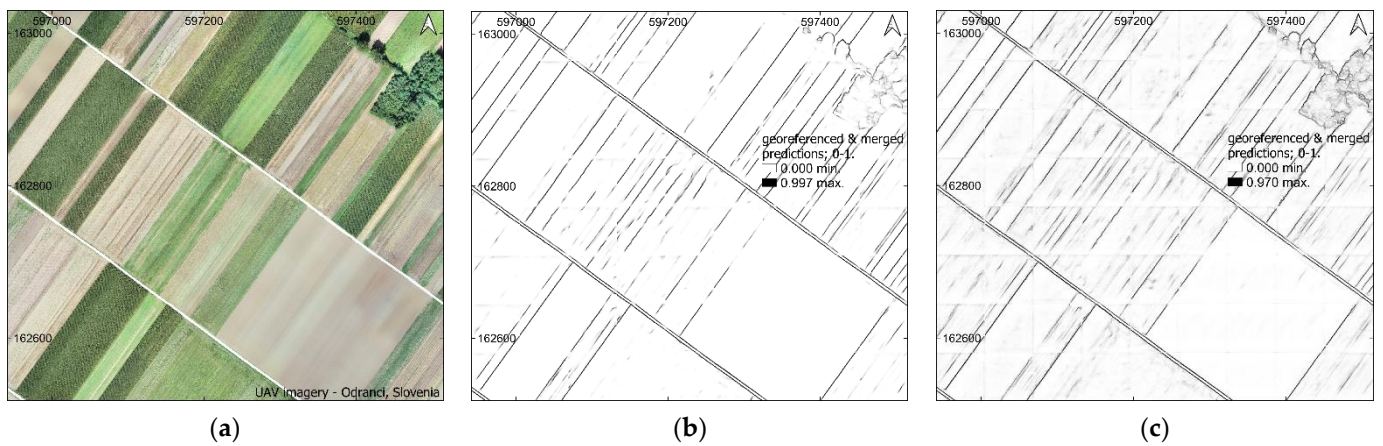


Figure 6. Georeferenced and merged boundary maps for the test area in (a) Odranci, Slovenia. Predicted boundary map with (b) customised CNN, and (c) original U-Net architecture.

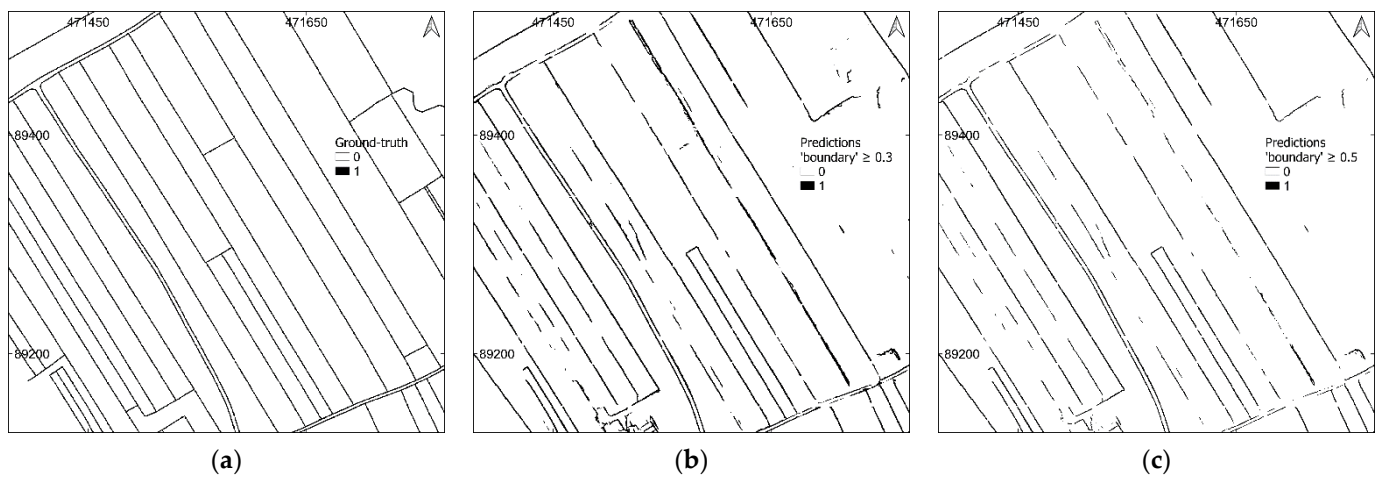


Figure 7. (a) Ground truth image for Ponova vas, Slovenia. (b,c) Reclassified boundary maps obtained with customised CNN: (b) with threshold “boundary” ≥ 0.3 , and (c) with threshold “boundary” ≥ 0.5 .

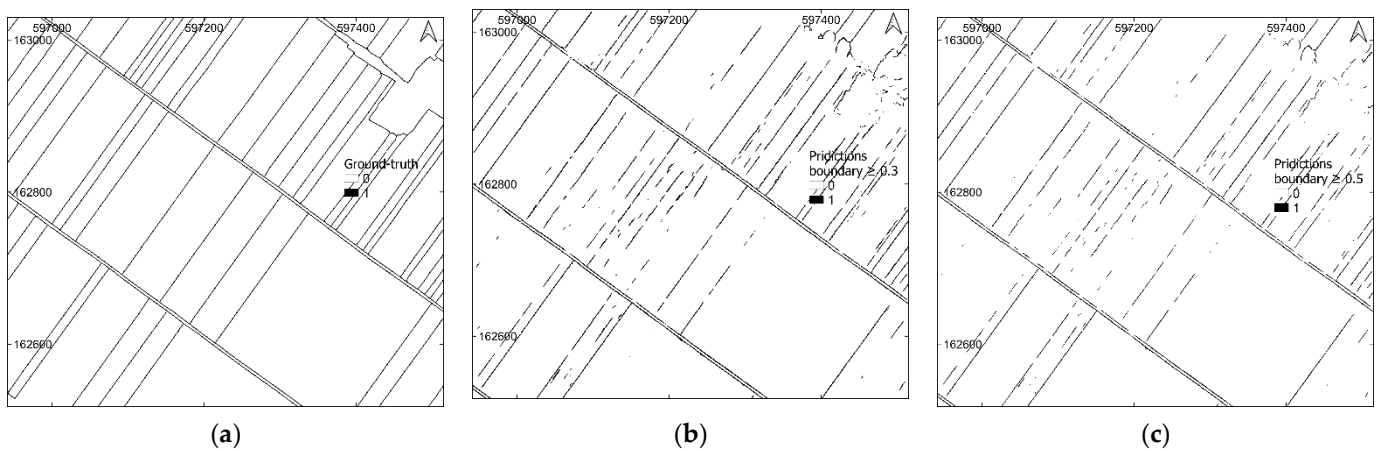


Figure 8. (a) Ground truth image for Odranci, Slovenia. (b,c) Reclassified boundary maps obtained with customised CNN: (b) with threshold 0.3, and (c) with threshold 0.5.

Next, we evaluated the accuracy of the reclassified boundaries for both models, i.e., the customised model and the original U-Net model. The results of the accuracy evaluation are shown in Tables 3 and 4.

Table 3. Assessment of the detection quality of visible land boundaries and comparison of approaches—Ponova vas.

| Test Area | Predictions | Customised U-Net (CNN) | | | Original U-Net (CNN) | | |
|------------|-------------|------------------------|------------------|-----------------|----------------------|------------------|-----------------|
| | | <i>recall</i> | <i>precision</i> | <i>F1 score</i> | <i>recall</i> | <i>precision</i> | <i>F1 score</i> |
| Ponova vas | threshold | | | | | | |
| | 0.3 | 0.600 | 0.597 | 0.598 | 0.565 | 0.520 | 0.542 |
| | 0.5 | 0.454 | 0.714 | 0.555 | 0.412 | 0.624 | 0.496 |

Table 4. Assessment of the detection quality of visible land boundaries and comparison of approaches—Odranci.

| Test Area | Predictions | Customised U-Net (CNN) | | | Original U-Net (CNN) | | |
|-----------|-------------|------------------------|------------------|-----------------|----------------------|------------------|-----------------|
| | | <i>recall</i> | <i>precision</i> | <i>F1 score</i> | <i>recall</i> | <i>precision</i> | <i>F1 score</i> |
| Odranci | Threshold | | | | | | |
| | 0.3 | 0.534 | 0.549 | 0.598 | 0.495 | 0.494 | 0.494 |
| | 0.5 | 0.438 | 0.615 | 0.511 | 0.355 | 0.592 | 0.444 |

3.3. Revision of Existing Cadastral Data on Land Boundaries

The predicted land boundary maps with the highest *F1 score*, obtained with customised CNN (Tables 3 and 4), were used to further revise the existing cadastral maps for the two test areas, Ponova vas and Odranci. In addition, the manually vectorised visible boundaries were compared with the existing cadastral data on land boundaries to obtain reference values for the overlap of the two geospatial data layers. The revision of the existing cadastral maps was based on the same metrics used to evaluate accuracy in the previous section. The existing cadastral maps were compared to the automatically detected visible boundaries, as shown in Figures 9 and 10. The accuracy assessment is shown in Tables 5 and 6.

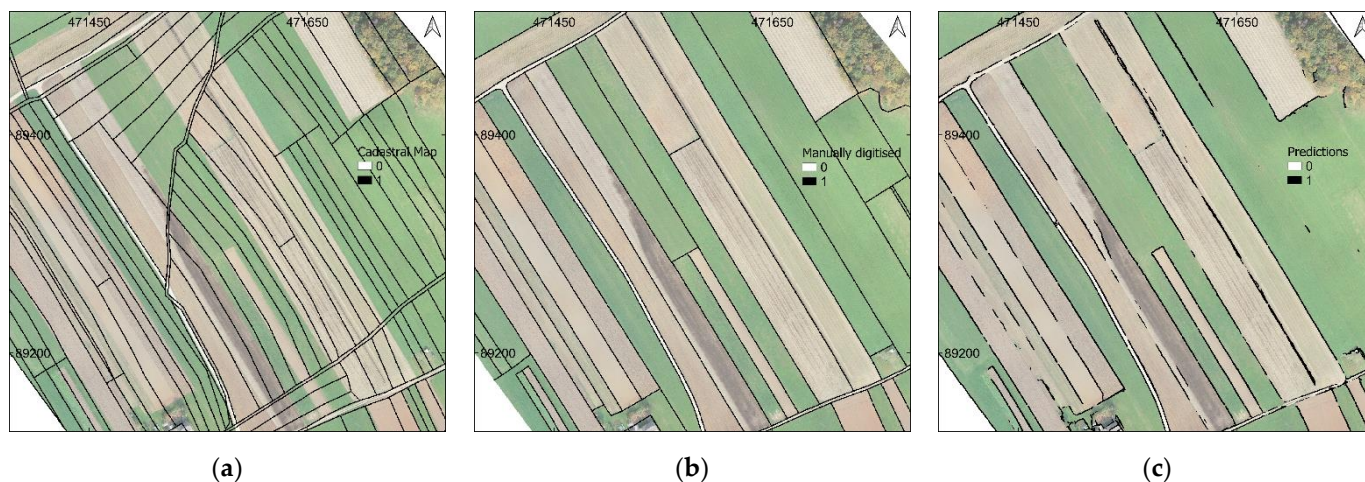
**Figure 9.** Revision of the cadastral map in Ponova vas: (a) Cadastral boundaries; (b) manually vectorised visible boundaries; and (c) predicted visible boundaries with customised CNN; (a–c) overlaid on UAV imagery.



Figure 10. Revision of cadastral map in Odranci: (a) Cadastral boundaries; (b) manually vectorised visible boundaries; and (c) predicted visible boundaries with customised CNN; (a–c) overlaid on UAV imagery.

Table 5. Assessment of the overlap between cadastral boundaries and land visible boundaries—Ponova vas.

| | | Cadastral Map | | |
|------------|--------------|---------------|------------------|-----------------|
| | Boundary Map | <i>recall</i> | <i>precision</i> | <i>F1 score</i> |
| Ponova vas | Manually | 0.051 | 0.090 | 0.065 |
| | Predicted | 0.055 | 0.095 | 0.070 |

Table 6. Assessment of the overlap between cadastral boundaries and land visible boundaries—Odranci.

| | | Cadastral Map | | |
|---------|--------------|---------------|------------------|-----------------|
| | Boundary Map | <i>recall</i> | <i>precision</i> | <i>F1 score</i> |
| Odranci | Manually | 0.372 | 0.627 | 0.467 |
| | Predicted | 0.207 | 0.491 | 0.291 |

The predicted boundaries were vectorised to match the format of the current cadastral data. Vectorisation was performed using the Hough transform. The fill gap of 10 was applied because it was considered more appropriate, and we thus avoided the possibility of bias in the predicted boundaries. This approach not only vectorised the pixels defined as the “boundary” but also produced straight lines, which are crucial for cadastral mapping. This can be considered a vectorisation and simplification step. Once the vectorisation was complete, we also created an overlapping (discrepancy) map, which can be seen in Figure 11.

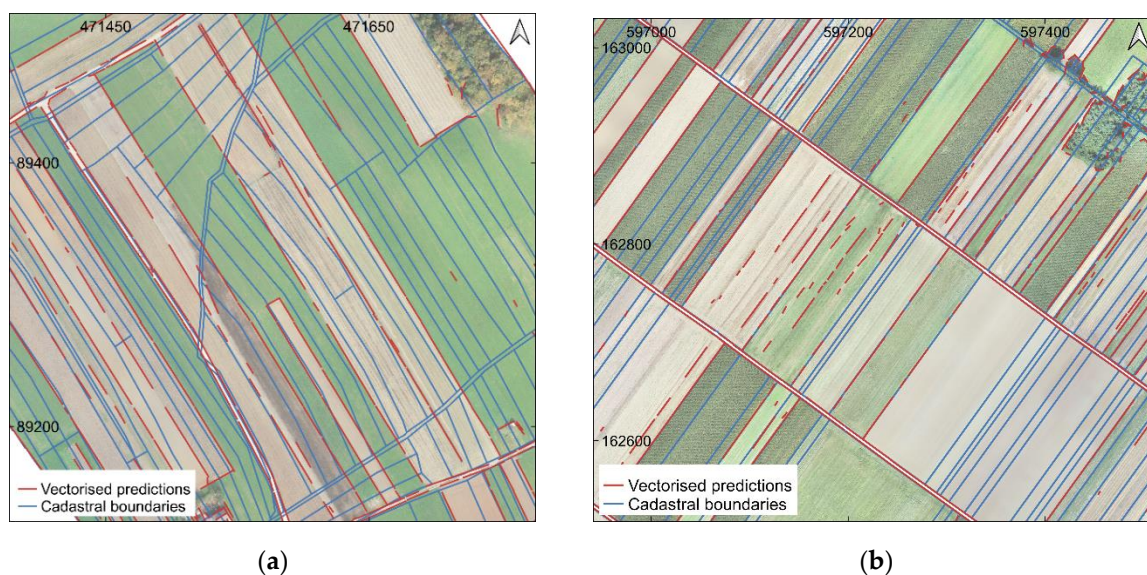


Figure 11. Vectorised predictions overlaid with cadastral boundaries: (a) discrepancy map for Ponovavas; (b) discrepancy map for Odranci.

4. Discussion

The discussion is divided into three parts: (i) CNN and training approach for visible land boundary mapping; (ii) detection of visible land boundaries using UAV imagery and deep learning and (iii) revision of existing cadastral maps based on the detected and digitised visible land boundaries, addressing the objectives of our study.

4.1. CNN and Training Approach

In general, deep learning is a relatively new research area in the geospatial domain and offers great potential for feature recognition from remote sensing imagery [30]. The up-scaling deep learning solutions, including CNNs, for visible land boundary detection is becoming increasingly important, especially for UAV-based cadastral mapping [27,29]. Deep learning requires processing a large amount of training data and powerful computations. In this study, an efficient and cost-effective deep learning approach was developed that provides reasonable results and helps to further automate the cadastral mapping process.

The CNN model is based on the U-Net architecture [33]. Since our research problem was binary classification, the original U-Net architecture was simplified (Figure 2) to reduce the number of training parameters and training time. This led to a more efficient and, at the same time, more accurate result compared to the original architecture (Figures 5 and 6 and Tables 3 and 4).

Training of the CNN model was based on the BSDS500 dataset [34]. This dataset is well known for edge or boundary detection tasks and already fitted the purpose of the study. The CNN model was trained from scratch, and no additional preparation of the training data was completed since the dataset contained both images and labels. Typically, CNNs are trained from scratch or by transfer learning. Both approaches require the preparation of custom training data, including images and labels, which usually takes some time and has already been highlighted in [27–29]. However, the amount of training data depends on the type of CNN architecture used. For example, the U-Net is an architecture that requires less training data and still provides accurate localisations [33]. In this study, the model was trained with 1505 samples, which can be considered a small amount of training data, but the model still provided satisfactory results. In addition, the model was trained for 18 epochs and required a total of 1.5 h to complete the training, which can also be considered a fast approach. The CNN model was trained in Google Collaboratory [35]. This approach reduces the cost of strong GPUs and RAM and can be considered a low-cost approach. The only bottleneck is the provided RAM memory, which varies from 12.7 GB to 25 GB. These

variations also affect the training time. In addition, there were some interruptions during the training, so a local computer is beneficial in this area and can be considered a more stable solution.

Model performance during training was monitored by *loss*, *overall accuracy*, and *F1 score* (Figure 4). The *loss* decreased steadily from the first epoch to the end of training. The early stop function monitored the *validation loss* to stop the training before the model was over-fitted. The *overall accuracy* had high values from the beginning of the training, mainly due to the unbalanced pixels for the “boundary” and “no boundary” classes. In addition, the *F1 score* was applied. At this point, it should be emphasised that the *overall accuracy* cannot be considered as a suitable metric to monitor the performance of the model during training. The reason is that the main problem in boundary detection tasks is the unbalanced number of pixels per class. Normally, the boundary pixels occupy a small number of pixels compared to the background pixels. For this reason, the model was additionally monitored with the *F1 score*, which was calculated only for pixels of the class “boundary”.

4.2. Visible Boundary Detection from UAV Imageries

In this study, deep learning was used as a detector for visible land boundaries. Once the model was trained, it was applied to the UAV test data. First, the original UAV orthoimages were resampled from 2 cm to 25 cm GSD. This was performed to increase the field of view for each test UAV tile with a size of 256×256 pixels. A map of visible land boundaries was created for each tile. Second, the predicted boundary maps were georeferenced and later merged, as this is essential for cadastral mapping.

To evaluate the quality of the predicted boundary maps, they were compared with manually digitised boundaries from UAV orthoimagery. The evaluation was based on *recall*, *precision*, and *F1 score*, as this is considered a reasonable and unambiguous approach. Boundary maps were buffered (with 50 cm) and rasterised, and a value of 0 was set for the “no boundary” class and a value of 1 for the “boundary” class. The boundary maps generated by the CNN model originally ranged from 0 to 1. Therefore, the boundary maps were reclassified with a threshold value where “boundary” ≥ 0.3 and “boundary” ≥ 0.5 .

Boundary maps with a threshold of 0.3 generated more balanced values for *recall* and *precision* (and at the same time a higher *F1 score*) compared to predictions with a threshold of 0.5 (Tables 3 and 4). For Pono vas, we obtained an *F1 score* of 0.60 for a threshold of 0.3 and an *F1 score* of 0.55 for a threshold of 0.5. In the case of Odranci, the results showed an *F1 score* of 0.54 and 0.51 for a threshold of 0.3 and 0.5, respectively. It is worth highlighting here that the higher the threshold for the “boundary” class, the higher the *precision* and the lower the *recall*. For cadastral mapping, both values can be considered relevant since *recall* represents completeness (the number of detected boundaries compared to the reference data), while *precision* represents the correctness of the detected boundaries. Considering this, an *F1 score* as high as possible would have been desirable. The threshold can be used as an aid or balance between *recall* and *precision* and can be used depending on the purpose or requirement. In short, the higher the completeness or the detected boundaries, the lower the correctness and vice versa.

Boundary maps created using a customised CNN (basically a simplified U-Net) were additionally compared to a CNN based on the original U-net architecture [33]. This was used to evaluate our adapted approach. The results obtained with the original U-Net for both thresholded boundary maps showed worse results compared to our adapted model. The best results were obtained for reclassified boundary maps with a threshold of 0.3, namely an *F1 score* of 0.54 for Pono vas and an *F1 score* of 0.49 for Odranci.

What would be a perfect *F1 score* for cadastral mapping is not easy to determine. First of all, not all cadastral boundaries are visible. Second, it depends on the area where the CNN model is tested and the scenes it covers, for example, rural, urban, or mixed. This is also true when comparing the results of one study to another, as methods and case studies differ, thus making reliable comparison impossible [27,28]. However, for further analyses,

such as revising existing cadastral boundaries, an *F1 score* of 60 is considered sufficient for rapid analysis, especially in rural areas.

4.3. Revision of Existing Cadastral Data on Land Boundaries

Predicted visible land boundaries were compared with official data, i.e., cadastral boundaries, to revise current cadastral maps [39]. The cadastral boundaries were buffered and rasterised in the same manner as the manually delineated boundaries. The boundary maps that provided a higher *F1 score* were selected to revise the existing cadastral maps in Ponova vas and Odranci, both in Slovenia. The revision was based on the same metrics, namely *recall*, *precision*, and *F1 score*. Before comparing the predicted boundaries with the cadastral boundaries, reference values were generated by comparing the cadastral boundaries to the manually delineated visible land boundaries on the same UAV imagery (Tables 5 and 6). This was undertaken because the manually digitised boundaries were assumed to have complete and correct data and were defined as ground truth data.

In the case of Ponova vas, it was obvious even from visual interpretation that the cadastral map was outdated (Figure 9a). The currently visible land boundaries (the boundaries that define the use of the land on site) did not match the cadastral boundaries. This was also confirmed by the accuracy assessment. The results presented in Table 5 showed very low values, namely a *recall* of 0.06, a *precision* of 0.10 and an *F1 score* of 0.07 compared to the predicted boundaries. Almost the same results were obtained when comparing with the ground truth data (*recall*: 0.05, *precision*: 0.09, *F1 score*: 0.07). In this case, very low metrics, specifically low *recall*, can be interpreted as an indicator of the identification of specific areas where cadastral updates are needed. In addition, the metrics generated when compared to the predictions also did not indicate any overlap between the visible and cadastral boundaries (regardless of the fact that not all visible boundaries were automatically generated). A very low *recall* indicates that there must also be a problem with the directions of the cadastral boundaries and that they do not correspond to the situation on the ground. In order to align the land possession and (legal) cadastral data, a complex revision of cadastral data is required in Ponova vas, using legal cadastral instruments, such as the setting up cadastral data or restructuring of land parcels through complex land consolidation. For these purposes, the provided data on visible land boundaries can serve as important input data, for creating or updating cadastral maps [16,20].

In the case of Odranci, the situation is a little different since the direction of the cadastral boundaries matched the direction of the visible land boundaries (Figure 10a). The results yielded a *recall* of 0.21, a *precision* of 0.49, and an *F1* of 0.29, compared to reference values of 0.37, 0.63, and 0.47. From these metrics, 37% of the visible land boundaries overlapped with the cadastral boundaries, which corresponded to a correctness of 63% (based on ground truth data). Our CNN provided a lower *F1 score*, which was to be expected, but at the same time, it was sufficient to determine boundary overlaps [3]. The values of *recall* and *precision* indicated that the direction and location of the cadastral boundaries were consistent with the visible boundaries. The low values for overlap could be due to excessive fragmentation. Many parcels were fragmented into small pieces while they were shown under the same land cover in the UAV imagery. This was also evident from the visual interpretation. A simplified land consolidation merging land units would have been preferable in Odranci, where, again, the provided data on visible land boundaries can serve as important input data.

For both study areas, the predicted boundary maps were also vectorised using the Hough transform (Figure 11). In addition to vectorisation, the Hough transform provided straight lines and filled some gaps—this can also be considered a simplification approach. In this study, a filling gap of 10 was used so as not to bias the predicted results. Moreover, increasing the value for filling the gaps sometimes led to undesirable results. Vectorisation is crucial for cadastral mapping because it allows for further analysis. In this study, the evaluation of accuracy was performed on a pixel basis. Further studies could focus on comparing pixel-based methods with object-based methods to evaluate accuracy, such as

the buffer overlay method [48], once the predicted boundaries are vectorised. In the buffer overlay method, the buffer can be increased around the cadastral data, which is called a tolerance in cadastral applications; this may not affect the assessment of completeness because the approach is based on the length that falls within the buffer. In the pixel-based method, if the width or buffer of the reference data is increased while the predictions are thinner, this would lead to a bias in completeness and correctness.

5. Conclusions

In the last decade, much attention has been given to the creation of cadastral maps and the establishment of cadastral systems, including innovative surveying and mapping techniques, but less to the maintenance and sustainability of the cadastral systems. This article focused on data maintenance by revising existing cadastral maps using deep learning. The whole workflow was developed and presented, starting with training the CNN, detecting the visible land boundaries, georeferencing, evaluating the model and vectorising the predicted boundary maps, and revising the existing cadastral maps. The model was tested with UAV imagery, but the developed approach could also be used for satellite or aerial imagery.

The approach can be considered efficient and cost-effective in automatically identifying areas where updates of cadastral maps are needed. In addition, the identified visible land boundaries could be used as input data for updating cadastral data or other cadastral procedures that can be applied for cadastral mapping, including for land parcel restructuring. The identified visible land boundaries did not represent final cadastral boundaries. They can be considered as preliminary boundaries for quick analysis and public presentations of the current state of the art.

One of the main land administration problems in developed countries is to keep the cadastral system up to date. Here, an automated approach that identifies the areas where such updates are needed would highlight and narrow down this challenge for NMCAs. Overall, it can be said that automatic methods are faster but less accurate (once the model is trained), while manual methods provide slower but more accurate boundary delineations. Combining automatic methods with manual corrections can reduce the user effort and still provide high accuracy. However, when revising existing cadastral boundaries, an automatic approach is certainly desirable for many NMCAs. It should also be reiterated that not all cadastral boundaries are visible in remote sensing imagery and not all can be automatically detected or extracted. Therefore, automating invisible cadastral boundaries by tagging them prior to UAV or satellite imagery acquisition could be an interesting and challenging task for further research.

Author Contributions: Conceptualisation, Bujar Fetai and Anka Lisec; methodology, Bujar Fetai; software, Bujar Fetai and Dejan Grigillo; validation, Bujar Fetai, Dejan Grigillo and Anka Lisec; formal analysis, Bujar Fetai and Anka Lisec; investigation, Bujar Fetai; resources, Bujar Fetai and Anka Lisec; data curation, Bujar Fetai and Anka Lisec; writing—original draft preparation, Bujar Fetai; writing—review and editing, Bujar Fetai, Dejan Grigillo and Anka Lisec; visualisation, Bujar Fetai; supervision, Anka Lisec. All authors have read and agreed to the published version of the manuscript.

Funding: This research and APC were funded by the Slovenian Research Agency (research core funding Earth observation and geoinformatics grant number P2-0406) and by the Slovenian Research Agency and Surveying and Mapping Authority of the Republic of Slovenia (research project grant number V2-1934).

Institutional Review Board Statement: Not applicable.

Informed Consent Statement: Not applicable.

Data Availability Statement: The data presented in this study are openly available in link (https://unilj-my.sharepoint.com/:f/g/personal/bfetai_fgg_uni-lj_si/ErN_s1uLnidMmdyGk2ZPk8oBKEyFDzbT7wQ6PpS2yr9k-Q?e=mnxPJO, accessed on 2 March 2022); the training data in [34]; and official cadastral data in [39].

Acknowledgments: This research is part of the Ph.D. thesis of the corresponding author. We thank the anonymous reviewers for their insightful comments and suggestions. We acknowledge Klemen Kozmus Trajkovski for capturing the UAV data and Matej Račić for the technical support.

Conflicts of Interest: The authors declare no conflict of interest. The funders had no role in the design of the study; in the collection, analyses, or interpretation of data; in the writing of the manuscript, or in the decision to publish the results.

References

1. Enemark, S.; Bell, K.C.; Lemmen, C.; McLaren, R. *Fit-For-Purpose Land Administration: Joint FIG/World Bank Publication*; FIG: Copenhagen, Denmark, 2014; ISBN 978-87-92853-10-3/978-87-92853-11-0.
2. Williamson, I.P. *Land Administration for Sustainable Development*, 1st ed.; ESRI Press Academic: Redlands, CA, USA, 2010; ISBN 9781589480414.
3. Luo, X.; Bennett, R.; Koeva, M.; Lemmen, C.; Quadros, N. Quantifying the Overlap between Cadastral and Visual Boundaries: A Case Study from Vanuatu. *Urban Sci.* **2017**, *1*, 32. [\[CrossRef\]](#)
4. Enemark, S. Land Administration and Cadastral Systems in support of Sustainable Land Governance: A global approach. In Proceedings of the 3rd Land Administration Forum for the Asia and Pacific Region, Tehran, Iran, 24–26 May 2009; pp. 53–71.
5. Simbizi, M.C.D.; Bennett, R.M.; Zevenbergen, J. Land tenure security: Revisiting and refining the concept for Sub-Saharan Africa's rural poor. *Land Use Policy* **2014**, *36*, 231–238. [\[CrossRef\]](#)
6. Grant, D.; Enemark, S.; Zevenbergen, J.; Mitchell, D.; McCamley, G. The Cadastral triangular model. *Land Use Policy* **2020**, *97*, 104758. [\[CrossRef\]](#)
7. Enemark, S.; McLaren, R.; Lemmen, C. Fit-for-Purpose Land Administration—Providing Secure Land Rights at Scale. *Land* **2021**, *10*, 972. [\[CrossRef\]](#)
8. Heipke, C.; Woodsford, P.A.; Gerke, M. Updating geospatial databases from images. In *Advances in Photogrammetry, Remote Sensing and Spatial Information Sciences: 2008 ISPRS Congress Book*; Baltsavias, E., Li, Z., Chen, J., Eds.; CRC Press: London, UK, 2008; ISBN 978-0-415-47805-2/978-0-203-88844-5.
9. Kocur-Bera, K.; Fraszcak, H. Coherence of Cadastral Data in Land Management—A Case Study of Rural Areas in Poland. *Land* **2021**, *10*, 399. [\[CrossRef\]](#)
10. Bennett, R.M.; Koeva, M.; Asiama, K. Review of Remote Sensing for Land Administration: Origins, Debates, and Selected Cases. *Remote Sens.* **2021**, *13*, 4198. [\[CrossRef\]](#)
11. Koeva, M.; Stöcker, C.; Crommelinck, S.; Chipofya, M.; Kundert, K.; Schwering, A.; Sahib, J.; Zein, T.; Timm, C.; Humayun, M.; et al. Innovative Geospatial Solutions for Land Tenure Mapping. *RJESTE* **2020**, *3*, 34–49. [\[CrossRef\]](#)
12. Stöcker, C.; Bennett, R.; Koeva, M.; Nex, F.; Zevenbergen, J. Scaling up UAVs for land administration: Towards the plateau of productivity. *Land Use Policy* **2022**, *114*, 105930. [\[CrossRef\]](#)
13. Zevenbergen, J. Proceedings of the Land Administration: To See the Change from Day to Day: Inaugural Address by Jaap Zevenbergen, Professor of Land Administration Systems, Enschede, The Netherlands, 22 April 2009; ITC: Enschede, The Netherlands, 2009. ISBN 978-90-6164-274-9.
14. Luo, X.; Bennett, R.M.; Koeva, M.; Lemmen, C. Investigating Semi-Automated Cadastral Boundaries Extraction from Airborne Laser Scanned Data. *Land* **2017**, *6*, 60. [\[CrossRef\]](#)
15. Zevenbergen, J. A systems approach to land registration and cadastre. *Nord. J. Surv. Real Estate Res.* **2004**, *1*, 11–24.
16. Crommelinck, S.; Bennett, R.; Gerke, M.; Nex, F.; Yang, M.; Vosselman, G. Review of Automatic Feature Extraction from High-Resolution Optical Sensor Data for UAV-Based Cadastral Mapping. *Remote Sens.* **2016**, *8*, 689. [\[CrossRef\]](#)
17. Kohli, D.; Bennett, R.; Lemmen, C.; Morales, A.; Pinheiro, A.; Zevenbergen, J. A Quantitative Comparison of Completely Visible Cadastral Parcels Using Satellite Images: A Step towards Automation. In Proceedings of the FIG Working Week 2017, Helsinki, Finland, 29 May–2 June 2017; pp. 1–14.
18. Ramadhani, S.A.; Bennett, R.M.; Nex, F.C. Exploring UAV in Indonesian cadastral boundary data acquisition. *Earth Sci. Inform.* **2018**, *11*, 129–146. [\[CrossRef\]](#)
19. Casiano Flores, C.; Tan, E.; Crompvoets, J. Governance assessment of UAV implementation in Kenyan land administration system. *Technology in Society* **2021**, *66*, 101664. [\[CrossRef\]](#)
20. Koeva, M.; Muneza, M.; Gevaert, C.; Gerke, M.; Nex, F. Using UAVs for map creation and updating. A case study in Rwanda. *Surv. Rev.* **2018**, *50*, 312–325. [\[CrossRef\]](#)
21. Stöcker, C.; Nex, F.; Koeva, M.; Gerke, M. High-Quality UAV-Based Orthophotos for Cadastral Mapping: Guidance for Optimal Flight Configurations. *Remote Sens.* **2020**, *12*, 3625. [\[CrossRef\]](#)
22. Rijdsdijk, M.; van Hinsbergh, W.H.M.; Witteveen, W.; Buuren, G.H.M.; Schakelaar, G.A.; Poppinga, G.; van Persie, M.; Ladiges, R. Unmanned Aerial Systems in the process of Juridical verification of Cadastral borde. *Int. Arch. Photogramm. Remote Sens. Spatial Inf. Sci.* **2013**, *XL-1/W2*, 325–331. [\[CrossRef\]](#)
23. Crommelinck, S.; Bennett, R.; Gerke, M.; Yang, M.; Vosselman, G. Contour Detection for UAV-Based Cadastral Mapping. *Remote Sens.* **2017**, *9*, 171. [\[CrossRef\]](#)

24. Puniach, E.; Bieda, A.; Ćwiakała, P.; Kwartnik-Pruc, A.; Parzych, P. Use of Unmanned Aerial Vehicles (UAVs) for Updating Farmland Cadastral Data in Areas Subject to Landslides. *IJGI* **2018**, *7*, 331. [[CrossRef](#)]
25. Manyoky, M.; Theiler, P.; Steudler, D.; Eisenbeiss, H. Unmanned Aerial Vehicle in Cadastral Applications. *Int. Arch. Photogramm. Remote Sens. Spatial Inf. Sci.* **2011**, XXXVIII-1/C22, 57–62. [[CrossRef](#)]
26. Wassie, Y.A.; Koeva, M.N.; Bennett, R.M.; Lemmen, C.H.J. A procedure for semi-automated cadastral boundary feature extraction from high-resolution satellite imagery. *J. Spat. Sci.* **2018**, *63*, 75–92. [[CrossRef](#)]
27. Crommelinck, S.; Koeva, M.; Yang, M.Y.; Vosselman, G. Application of Deep Learning for Delineation of Visible Cadastral Boundaries from Remote Sensing Imagery. *Remote Sens.* **2019**, *11*, 2505. [[CrossRef](#)]
28. Xia, X.; Persello, C.; Koeva, M. Deep Fully Convolutional Networks for Cadastral Boundary Detection from UAV Images. *Remote Sens.* **2019**, *11*, 1725. [[CrossRef](#)]
29. Fetaj, B.; Račić, M.; Lisec, A. Deep Learning for Detection of Visible Land Boundaries from UAV Imagery. *Remote Sens.* **2021**, *13*, 2077. [[CrossRef](#)]
30. Ma, L.; Liu, Y.; Zhang, X.; Ye, Y.; Yin, G.; Johnson, B.A. Deep learning in remote sensing applications: A meta-analysis and review. *ISPRS J. Photogramm. Remote Sens.* **2019**, *152*, 166–177. [[CrossRef](#)]
31. Garcia-Gasulla, D.; Parés, F.; Vilalta, A.; Moreno, J.; Ayguadé, E.; Labarta, J.; Cortés, U.; Suzumura, T. On the Behavior of Convolutional Nets for Feature Extraction. *Jair* **2018**, *61*, 563–592. [[CrossRef](#)]
32. Park, S.; Song, A. Discrepancy Analysis for Detecting Candidate Parcels Requiring Update of Land Category in Cadastral Map Using Hyperspectral UAV Images: A Case Study in Jeonju, South Korea. *Remote Sens.* **2020**, *12*, 354. [[CrossRef](#)]
33. Ronneberger, O.; Fischer, P.; Brox, T. U-Net: Convolutional Networks for Biomedical Image Segmentation. 2015. Available online: <http://arxiv.org/pdf/1505.04597v1> (accessed on 22 February 2022).
34. Arbeláez, P.; Fowlkes, C.; Martin, D. The Berkeley Segmentation Dataset and Benchmark. Available online: <https://www2.eecs.berkeley.edu/Research/Projects/CS/vision/bsds/> (accessed on 2 March 2022).
35. Google Colaboratory. Available online: <https://colab.research.google.com> (accessed on 6 December 2021).
36. Chollet, F.; others. *Keras*. 2015. Available online: <https://keras.io> (accessed on 29 April 2021).
37. Abadi, M.; Agarwal, A.; Barham, P.; Brevdo, E.; Chen, Z.; Citro, C.; Corrado, G.S.; Davis, A.; Dean, J.; Devin, M.; et al. TensorFlow: Large-Scale Machine Learning on Heterogeneous Systems. 2015. Available online: <https://www.tensorflow.org/> (accessed on 10 December 2021).
38. GRASS Development Team. *GRASS GIS Bringing Advanced Geospatial Technologies to the World, Version 7.8*; Open Source Geospatial Foundation: Beaverton, OH, USA, 2020.
39. The Surveying; Mapping Authority of the Republic of Slovenia. *e-Surveying Data. e-Surveying Data*. Available online: <https://egp.gu.gov.si/egp/?lang=en> (accessed on 17 January 2022).
40. GDAL/OGR Contributors. *GDAL/OGR Geospatial Data Abstraction Software Library*. 2021. Available online: <https://gdal.org> (accessed on 20 January 2022).
41. Gillies, S. *Rasterio: Geospatial Raster I/O for Python Programmers*. 2013. Available online: <https://github.com/mapbox/rasterio> (accessed on 4 February 2022).
42. Harris, C.R.; Millman, K.J.; van der Walt, S.J.; Gommers, R.; Virtanen, P.; Cournapeau, D.; Wieser, E.; Taylor, J.; Berg, S.; Smith, N.J.; et al. Array programming with NumPy. *Nature* **2020**, *585*, 357–362. [[CrossRef](#)]
43. Loss vs Accuracy. Available online: <https://kharshit.github.io/blog/2018/12/07/loss-vs-accuracy> (accessed on 3 February 2022).
44. Duda, R.O.; Hart, P.E. Use of the Hough transformation to detect lines and curves in pictures. *Commun. ACM* **1972**, *15*, 11–15. [[CrossRef](#)]
45. Hough, P.V.C. Method and Means for Recognising Complex Patterns. U.S. Patent No. 3.069.654, 18 December 1962.
46. Kim, N.W.; Lee, J.; Lee, H.; Seo, J. Accurate segmentation of land regions in historical cadastral maps. *J. Vis. Commun. Image Represent.* **2014**, *25*, 1262–1274. [[CrossRef](#)]
47. Hong, R.; Park, J.; Jang, S.; Shin, H.; Kim, H.; Song, I. Development of a Parcel-Level Land Boundary Extraction Algorithm for Aerial Imagery of Regularly Arranged Agricultural Areas. *Remote Sens.* **2021**, *13*, 1167. [[CrossRef](#)]
48. Heipke, C.; Mayer, H.; Wiedemann, C. Evaluation of Automatic Road Extraction. *Inter. Arch. Photogramm. Remote Sens.* **1997**, *32*, 1–10.